

# **Modeling of Short Circuit Fault Arc in 150 kV System and Its Influence on the Performance of Distance Protection**

Handy Wihartady

## **Msc Thesis Committee**

Dr. ir. M. Popov

Prof. ir. L. van der Sluis

Prof. Dr. J.J. Smit

Prof. Dr. V. Terzija – The University of Manchester, School of Electrical and Electronic Engineering

**Delft University of Technology**

**Faculty of Electrical Engineering, Mathematics and Computer Science**

**Electrical Power Systems**

## **ABSTRACT**

*The short circuit arc is the most dominant fault in the power system that leads to single phase to ground fault. South Sumatera 150 kV system in Indonesia consists of two different string insulator types in the transmission line, with and without arching horn. In this study, some fault situations in that system is reconstructed by using ATP Draw – EMTP software. As the main part of the simulation, the fault arc is represented in the MODELS language form. The voltage and current terminal results are compared with the measurements to obtain the primary and secondary arc parameter for two types of string insulator. At the end, the fix arc models are used in different simulation cases to evaluate existing distance protection setting by using impedance extraction in ISA TDMS software and recursive DFS in MODELS.*

## Table of Content

Abstract.....	ii
Table of content.....	iii
<b>Chapter 1 : Introduction.....</b>	<b>6</b>
1.1. Overhead Transmission Line, Fault and Protection.....	6
1.2. Problem Definition.....	7
1.3. Objective of This Study.....	8
1.4. Thesis Layout.....	8
<b>Chapter 2 : Fault Arc.....</b>	<b>10</b>
2.1. Fault Arc.....	10
2.2. Lightning Impulses as a Source of Fault Arc.....	10
2.3. Streamer Mechanism Breakdown Initiated.....	12
2.4. An Unconstrained Long Fault Arc in Air.....	14
2.4.1. Black Box Model.....	15
2.4.2. Fault Arc Model.....	16
<b>Chapter 3 : Distance Protection and Discrete Fourier Series (DFS).....</b>	<b>19</b>
3.1. Distance Protection.....	19
3.1.1. Distance Protection Setting.....	20
3.1.2. Impedance ( $R - X$ ) Diagram.....	22
3.1.3. Distance Protection Characteristic.....	23
3.1.3.1. Mho Characteristic.....	24
3.1.3.2. Quadrilateral Characteristic.....	25
3.1.4. Impedance Measuring Principle.....	26
3.1.4.1. Phase-to-Phase Fault.....	27
3.1.4.2. Phase-to-Ground Fault.....	28
3.1.5. Distance Protection Application Problems.....	31
3.1.5.1. Double Infeed Line (from Both Sides) without Load Transfer.....	31
3.1.5.2. Double Infeed Line (from Both Sides) with Load Transfer.....	32
3.1.5.3. Intermediate Infeed.....	33
3.1.5.4. Parallel Lines.....	34
3.1.5.5. Tower Footing Resistance.....	36

3.1.6. Distance Protection Signaling Scheme.....	37
3.1.6.1. Permissive Underreach Transfer Trip (PUTT).....	38
3.1.6.2. Permissive Overreach Transfer Trip (POTT).....	39
3.1.6.3. Blocking Overreaching Scheme.....	39
3.1.6.4. Zone 1 Extension Scheme.....	40
3.1.6.5. Weak Infeed Scheme.....	41
3.2. Recursive Discrete Fourier Series.....	41
3.2.1. The Fourier Series.....	42
3.2.2. The Full and Half Cycle Window Fourier Algorithms.....	43
3.2.3. The Recursive Form.....	45
<b>Chapter 4 : Fault Arc and Impedance Extraction Model and Simulation.....</b>	<b>47</b>
4.1. The Fault Arc Modeling.....	47
4.2. The Impedance Extraction Modeling.....	48
4.3. Simulation of The 20 kV Synthetic Test Circuit and Fault Arc Analysis.....	50
4.4. The Arc Parameters in 150 kV System.....	56
4.4.1. Arcing Fault on 15 February 2007, Type A String Insulator.....	58
4.4.1.1. The Transmission Line Model.....	59
4.4.1.2. The Generator Voltage Source Model.....	61
4.4.1.3. The Circuit Breaker Model.....	61
4.4.1.4. The Impedance Model.....	61
4.4.1.5. Simulation Results.....	62
4.4.2. Arcing Fault on 3 March 2006, Type B String Insulator.....	66
4.4.2.1. Simulation Models.....	67
4.4.2.2. Simulation Results.....	68
4.5. Conclusion.....	70
<b>Chapter 5 : Fault Arc Simulation Condition in 150 kV System and Distance Protection</b>	
<b>Performance Evaluation.....</b>	<b>72</b>
5.1. General.....	72
5.2. Design Quadrilateral Characteristic in Ohm-phase Domain.....	74
5.3. Radial Single Circuit Case (Talang Kelapa – Betung).....	76
5.4. Radial Double Circuit Case (Keramasan – Mariana).....	78
5.5. Non-radial Double Source Double Circuit Case (Prabumulih – Bukit Asam).....	81
<b>Chapter 6 : Conclusion and Recommendation.....</b>	<b>85</b>
6.1. Conclusion.....	85

6.2. Recommendation.....	87
Reference.....	88
Acknowledgement.....	90

## I. INTRODUCTION

### 1.1. Overhead Transmission Line, Fault and Protection

High voltage (HV), between 60 and 345 kV, and extra high voltage (EHV), above 345 kV, overhead transmission lines have an important role since they serve as a “freeway” to transfer electricity from the generating power plant to the load centre. Although they are equipped with overhead ground wires to eliminate direct lightning stroke incidents, overhead transmission lines are still prone to disturbances caused by direct and indirect lightning that strike the lines or the branches of tree. Statistics show that more than 70% of all faults in overhead transmission lines are temporary single phase-to-ground arc faults caused by direct or indirect lightning stroke.

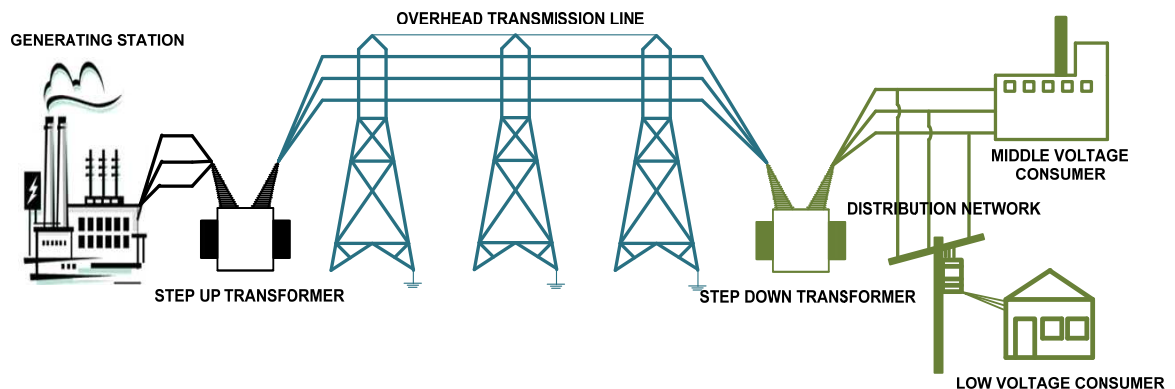


Figure 1.1: Overhead transmission line as a part of power system.

Faults in overhead lines must be localized as soon as possible in order to prevent the widespread effects that can largely influence the continuity of supply to the consumer. To fulfill that condition, each section of the line is provided by relay protection which automatically switches off the circuit breaker on each side when the fault occurs and isolates the faulted line. System protection in HV and EHV transmission lines is divided by two types according to their function, main protection and back-up protection. Main protection usually is related to distance relay or current differential relay, and back up protection is related to distance relay and current differential relay for redundant system protection, or an overcurrent relay. The implementation of distance relay as a main form of protection is more challenging than current differential relay because distance relay also serves as back up protection for the subsequent section. Besides, the setting and coordination between distance relays in each section are important for achieving the best performance in line protection. In this research, distance protection is seen as the main type of protection for HV overhead lines.

Single Phase Auto Reclosure (SPAR) completes the main protection in HV and EHV power systems with earthed neutral points that will reclose the open pole circuit breaker after the short circuit arc fault to the ground has been entirely removed. SPAR is an effective way to clear the fault while retaining system stability and taking out outage duration when temporary single phase-to-ground faults arise in overhead lines. On the basis of the open-close conditions of the faulted phase, arcing faults can be divided in primary and secondary arcs. The primary arc is a strong arc developed by a high short circuit current; the length of the arc is steady and an arc elongation rarely occurs. The secondary arc evolves from a small current that still flows in the arc built through inductive and capacitive coupling to the sound (healthy) phases after the ground fault has been isolated by main protection. The length of the secondary arc can be more than 10 times the length of the primary arc. However, unlike the primary arc, the random variation of the arc parameters significantly influences the secondary arc. After the secondary arc has eventually extinguished, the fault condition ends and the SPAR can safely reclose the former faulted phase. So, it is important to know the duration of the secondary arc for correct operation of the SPAR.

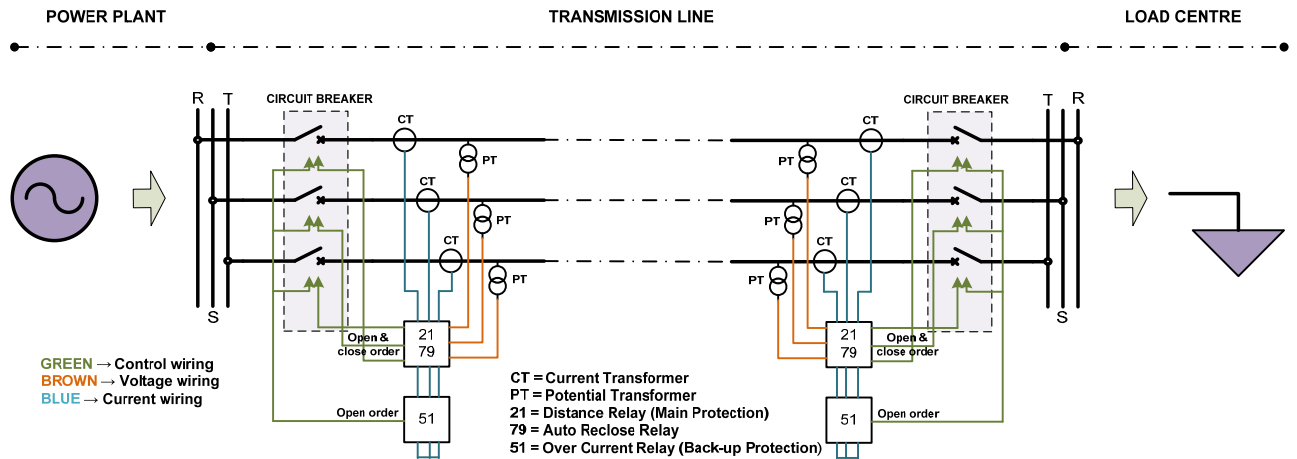


Figure 1.2: Main and back-up protection in transmission line.

## 1.2. Problem Definition

As described above, the single phase-to-ground arc fault is the most frequent fault in overhead lines. The definition of fault arc discussed in this thesis is the short circuit fault from phase to ground that is caused by a direct or an indirect lightning stroke. The arc usually takes the form of a sparkover in the arcing horn in parallel with string insulator or as a flashover on the surface of the string insulator. Previous power arc test research [8] presented the pattern of primary arc parameters ( $u_0$ ,  $r_0$  and  $\tau_0$ ) in 20, 110 and 220 kV systems in relation to the length of the arc fitting and the short circuit current. In another paper [6], the secondary arc attitude is modeled to determine the unpredictable extinction phenomenon. Interaction between dynamic fault arc

and power system networks is important in relation to system protection relaying. From the transmission line system protection point of view, the primary arc is important for the correct, fast operation of the distance protection and for the precise fault locator, while the secondary arc is important for the dead time setting of SPAR.

In this research, the 150 kV solidly grounded system network of South Sumatera in Indonesia is used as a study case. It is necessary to know arc parameters and the random extinction phenomenon of fault arc in 150 kV system for distance relay protection evaluation. To accomplish this work, three different types of software are used; Alternative Transient Program (ATP) Draw – Electromagnetic Transient Program (EMTP) software with its MODELS language program for modeling the fault arc, modeling recursive Discrete Fourier Series (DFS) and simulating power system networks; Digsilent software to calculate the short circuit impedance of the existing system and ISA TDMS software for distance protection design characteristics as well as post-processing terminal impedance plotting.

### **1.3. Objective of This Study**

The objectives of this study are:

- to model the primary and the secondary arc by applying the MODELS function in ATPDraw-EMTP.
- to compare the current and the voltage during arcing fault in the simulation results with the measurements taken from distance protection disturbance records, and to find arc parameters in 150 kV systems with and without arc fitting in the string insulator.
- to evaluate the dead time setting of the SPAR according to the secondary arc incidents.
- to determine the arc impedance during an arcing fault along a line by applying the recursive Discrete Fourier Series (DFS) algorithm.
- To plot the terminal impedance and distance protection characteristic in the impedance diagram by applying comtrade TDMS ISA software to establish the behavior and the influence of a non-linear arc in distance relay performance.
- To analyze the distance protection performance by simulating arcing faults for different location and cases

### **1.4. Thesis Layout**

This thesis is divided in several chapters that discuss the research topic in detail starting from Chapter 1 that highlights the problem definition and the objective of this study. Chapter 2 explains the fault arc; how the arc is formed and how can be modeled. Chapter 3 discusses



distance protection and recursive DFS theory. Chapter 4 presents the implementation of the fault arc model and how the fault arc impedance can be extracted by using ATPDraw-EMTP software. In the same chapter, the arc parameters of 150 kV systems are obtained by performing several fault arc incidents in the South Sumatera network based on disturbance records of the distance protection for an actual case. Chapter 5 talks about the simulation and the evaluation of the system protection performance during arc fault incidents at different locations and examined cases in the South Sumatera network. And finally, in Chapter 6, all conclusions and recommendations arising from this research are presented.

## II. FAULT ARC

### 2.1. Fault Arc

A fault arc is a short circuit fault current from a phase to ground through the air that is caused predominantly by a direct or an indirect lightning stroke which usually occurs between the arcing horns or on the surface of the string insulator as described below.

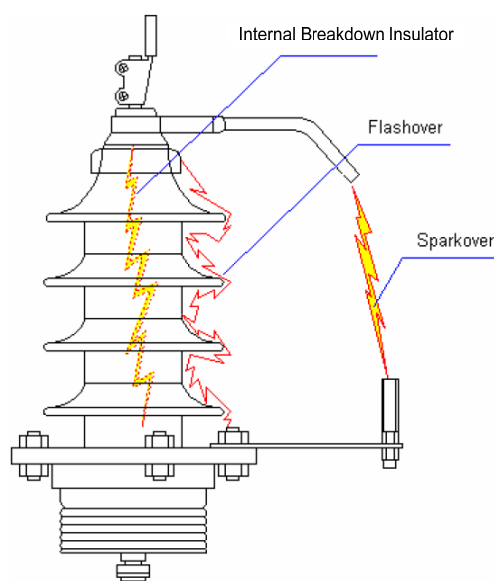


Figure 2.1: A fault arc occurrence (primary arc) in a string insulator.

If an arc fitting in the form of an arcing horn exists, then the fault arc will completely over bridge the insulation in an air (a gaseous) medium, this situation is known as sparkover. Furthermore, when the string insulator as a dielectric is not accompanied by a pair of arcing horn, the arc fault will connect the phase wire to the ground over the surface of the dielectric in the air (the gaseous) medium. This is called a flashover.

### 2.2. Lighting Impulse as a Source of Fault Arc

A fault arc in the air is usually caused by a lightning impulse overvoltage which travels in the ground or phase wire (traveling wave) as a result of a lightning stroke. When the voltage impulse magnitude exceeds the breakdown voltage of the air between arc fittings, the air as an insulating medium will become fully conductive and it will no longer be sufficient to insulate the voltage. Consequently, a breakdown in the air appears in the form of a flashover or sparkover.

Generally, lightning impulses are evoked by:

- A direct lightning stroke in the power line. This condition arises from shielding failure where the protection angle of the ground wire does not fully cover the striking area of the phase wire. That is why the fault arc is in this case called a shielding failure flashover. Together with the characteristic impedance of the line  $Z$ , this kind of stroke results in a peak voltage magnitude:

$$V = \frac{1}{2} \times I \times Z \quad (2.1)$$

$I$  is the lightning current amplitude. At a moderate current of 20 kA and characteristic impedance about 300  $\Omega$  result in a voltage around 3 MV.

- An indirect lightning stroke in the tower or in the overhead ground wire. After hitting the tower or ground wire, the lightning current will pass the impedance of the tower to earth and cause a high voltage at the top of the tower. The condition can be even worse when the foot grounding tower resistance is higher than the standard resistance. Consequently, it will result in back flashover to the power line.
- A lightning stroke in the vicinity of a line or a tower. The charge induced by the thunderclouds is suddenly released into the phase or ground wire giving rise to the travelling wave of a high voltage level (induced overvoltage). This kind of a lightning surge is importance for the medium voltage networks only.

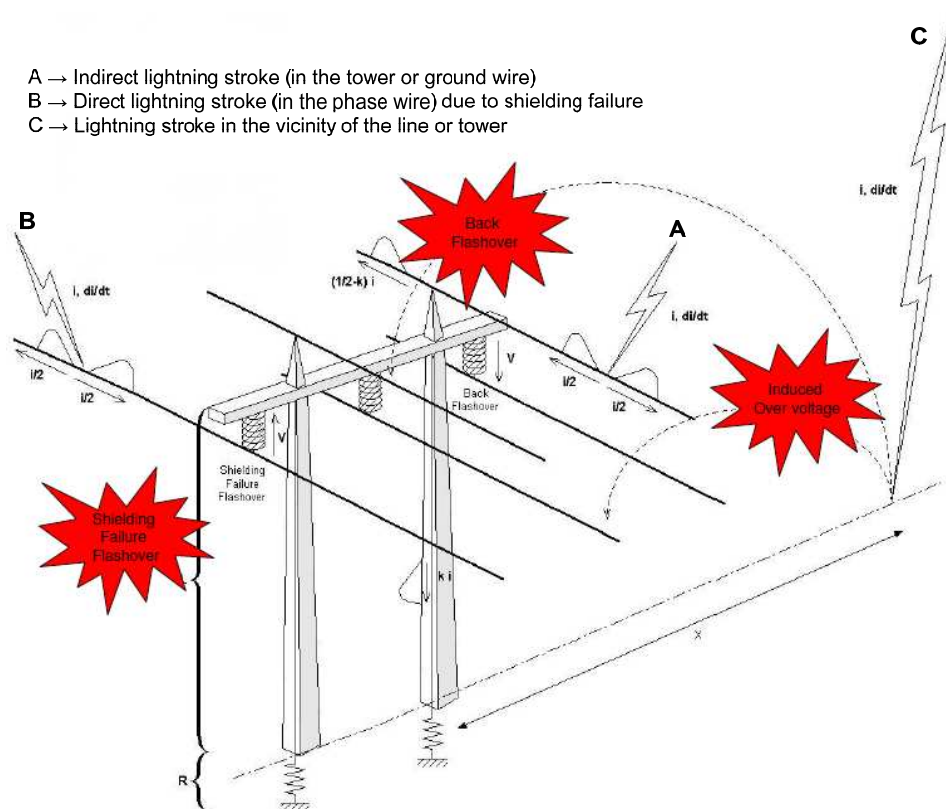


Figure 2.2: Causes of lightning impulse.

### 2.3. Streamer Mechanism Breakdown Initiated

An arc in the form of flashover or sparkover is the final product of a streamer mechanism between two electrodes (cathode and anode). All streamer mechanism processes take place through a sharp and narrow breakdown channel in situation where the dielectric pressure times the distance gap of the electrode are more than 5 atm.mm [2]. Once the breakdown has been initiated, the arc cannot be extinguished unless the voltage source is eliminated.

In gaseous dielectrics, an electron can easily be found because gas molecules can be ionized either by light, radio-active or cosmic radiation. Without the electric field (E) condition, electrons will eventually recombine with positive ions. On the contrary, when an electric field is applied, electrons will accelerate in the direction of the field with kinetic energy:

$$W = e \times E \times \lambda = e \times \frac{E}{p} \quad (2.2)$$

Where  $\lambda$  is the free path of electrons which is inversely proportional to the pressure P. During acceleration, depending on the gas pressure, electrons will be likely to collide with gas molecules. Collisions between electrons and gas molecules will release energy kinetic W. Based on the released kinetic energy, three reactions may occur:

- a. Elastic collision, the electron loses part of its energy to a heavy molecule.
- b. Inelastic collision, this reaction excites an atom in the gas molecule to a higher energy level.
- c. With a higher energy level the collision liberates an electron from the gas atom; as a result the positive atom  $A^+$  and two electrons are formed. This process is called ionization. Afterwards, if a positive atom is hit by an electron it falls back into its basic state by radiating photon.



Where h is the Planck's constant and  $\nu$  is the frequency of radiation.

Ionization is the most important stage for starting breakdown in gases. Furthermore, to give a better understanding of the ionization process, an ionization coefficient  $\alpha$  is introduced which is equal to the average number of ionizations per cm in the field direction. It is also equal to the number of new electrons.

The repeated ionization of gas molecules causes multiplication of a number of electrons which at distance x from a cathode in the homogeneous electric field is:

$$N_x = N_0 \exp(\alpha x) \quad (2.5)$$

Where  $N_0$  is the original number of electrons leaving the cathode. From the above equation, it can be concluded that the number of electrons will increase exponentially in the direction of the

anode.  $N_0$  electrons will further generate more electrons, creating an electron avalanche. In each ionization process, the electron leaves the positive gas ion behind because the ion moves 100 times slower than the electron. Ions move in the order of 1 to 100 mm/ $\mu$ s, while electrons move at 100 to 1000 mm/ $\mu$ s. Consequently, the positive ions are still at the position where they were formed when the electrons have moved further. Thus, a positive space charge is formed and around 75% of the number of ions are concentrated in the tip of the avalanche. Avalanches themselves do not cause breakdown, they only cause current leakage.

The positive space charge formed in the avalanche starts to affect the electric field causing the breakdown after the ions surpass a critical number. The critical number is about  $10^8$  ions. In an anode initiated streamer when the avalanche which contains about  $10^8$  ions has reached the anode, all electrons will be removed and the positive charge remains. About 75% of the ions in the tip of the avalanche which has a diameter roughly 30  $\mu$ m will enhance the electric field strength to about 1kV/mm. In a strong electric field, the ionization grows and the creation of photons will increase accordingly. With the high density of gas molecules, photons have even higher probability to hit the atom. This condition leads to violent ionization. As a result, new avalanches are created in the direction of the former space charge. The tip of the new avalanche melts with the previous one forming a filament which is known as streamer. When the streamer reaches the cathode, an extremely high field strength occurs due the accumulation of all field enhancement. This situation causes cold emission and the  $\gamma$ -process creates a secondary multitude number of electrons.  $\gamma$ -process is a process in which the positive ions left in the avalanche after ionizations collide with the cathode and release  $\gamma$  number of electrons. Furthermore, electrons will move in the filament in the anode direction and will neutralize the positive streamer. The streamer becomes conductive plasma; complete breakdown of the gap is obtained.

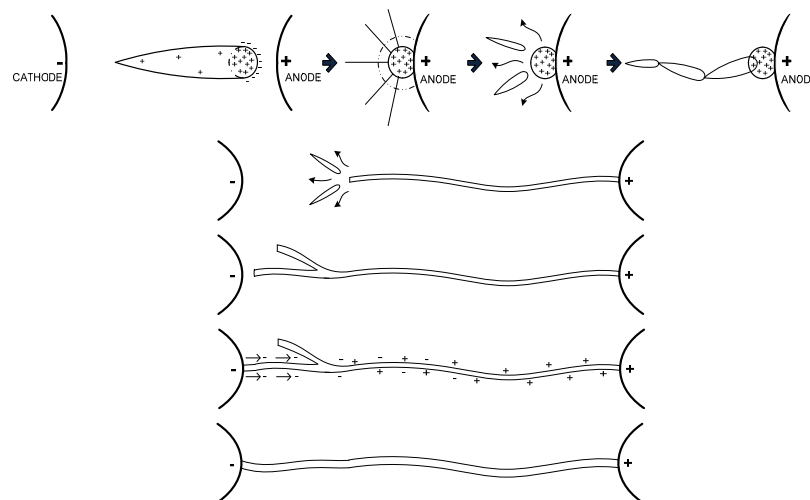


Figure 2.3: Streamer mechanism, anode initiated streamer [2].

In conditions where the electrode is stressed due to heavy overvoltage,  $\alpha$  becomes larger and the critical number of ions will be obtained before the space charge reaches the anode. The electric field is then affected, both before and after the avalanche. A fast formation of the space charge then takes place on both sides of the avalanche and breakdown follows. This phenomenon is known as the mid-gap streamer.

In order to give a better explanation of the voltage and current characteristics in the entire streamer mechanism process, the graph below is introduced:

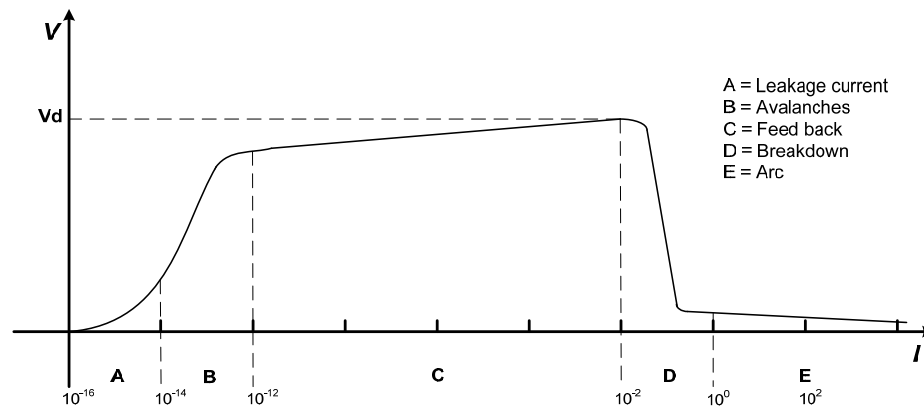


Figure 2.4: The V-I characteristic of a breakdown voltage [2].

When filamentary conductive plasma is formed, the voltage over the channel falls drastically and the circuit impedance determines current  $I$ . As long as the current is in the order of some amperes, the breakdown channel emits a strong ultraviolet light. Intensive elastic collisions heat the gas in the channel. This stage is called the spark stage. If the current is further increased, the radiated light turns white, the voltage drops to a low value and an arc is formed. A new ionization process occurs at this stage where the gas temperature increases to 5000 to 20000°C, and the velocity of the gas molecule is so large that it makes each molecule collision results in ionization. The conductivity of the plasma, the current and the gas temperature is further increased. Such an arc is difficult to extinguish. All these stages take place in a very short space of time which is 1 to 100 ns.

#### 2.4. An Unconstrained Long Fault Arc in Air

As stated in Chapter I, the dynamic interaction between a fault arc and a power system network is important for the correct operation of Single Pole Auto Reclosure (SPAR) and distance relay protection. In order to simulate SPAR and distance protection operation transient condition caused by arcing faults, a realistic fault arc model is needed. So far, several studies have shown different models of arcing faults in which mainly the theory of switching arc is elaborated. Although the fault and switching arc are not exactly similar, especially when switching the arc

length is limited in the arc chamber (constrained arc) while the fault arc is in the open air (unconstrained arc) and the switching arc is triggered by contact electrodes separation whereas the fault arc is triggered by lightning impulse overvoltage, the fault arc can be assumed to behave similarly to the switching arc. Hence, only thermal behavior of the arc is taken into account as a consideration, whilst the dielectric behavior of the arc and surrounding media is neglected because of the indefinite conditions around the arc column.

#### 2.4.1. Black Box Model

The switching arc model is recognized in three groups depending on their purpose; the black box model, the physical model and the parameter model which is derived from two previous models. The black box switching arc model is a useful mathematic model for simulating interaction between arcs and electrical circuits in transient studies. In this model, the relation between arc conductance and measurable parameters (arc voltage and current) is derived into simple mathematical equations which include arc behavior as the consideration. The well known black box models for circuit breaker transient studies are the Cassie and Mayr model. In the black box general form model, the dynamic behavior of an arc can be described according to arc conductance as a function of the power balance between electric input power and heat dissipation and time [12]:

$$g = F(P_{in}, P_{out}, t) = \frac{i_{arc}}{u_{arc}} = \frac{1}{R} \quad (2.6)$$

where  $g$  = instantaneous arc conductance  
 $P_{in}$  = power input to the plasma channel  
 $P_{out}$  = power transported, power input minus heat dissipation  
 $t$  = time  
 $i_{arc}$  = instantaneous arc current  
 $u_{arc}$  = instantaneous arc voltage  
 $R$  = instantaneous arc channel resistance

As described in the above equation momentary arc conductance varies if the power input and output are not in equilibrium. Momentary arc conductance can be expressed as a function of energy stored in the plasma channel:

$$g = F(Q) = F\left[\int_0^t (P_{in} - P_{out}) dt\right] \quad (2.7)$$

Finally, the general arc equation of the black box model is presented in the form of the change of the arc conductance:

$$\frac{1}{g} \frac{dg}{dt} = \frac{d[\ln(g)]}{dt} = \frac{F'(Q)}{F(Q)} (P_{in} - P_{out}) \quad (2.8)$$

Several assumptions have to be made in order solve above general arc equation. The Cassie model assumes that an arc channel has a constant temperature which is independent of the arc current as the diameter cylindrical shape of the arc channel varies. As electric energy to the channel increases, so the cross section area of the arc channel will also increase. The Cassie assumption is also adopted in the fault arc model used in this thesis [9].

#### 2.4.2. Fault Arc Model

In comparison with the switching arc which is a constrained arc, the length variation of the arcing fault is an important factor that determines the behavior of a long arc in air. The arc elongation is caused by several factors; the electro-dynamical force resulting from the supply current; the convection of the plasma and the surrounding air; the wind as an atmospheric effect; the vertical or horizontal position of the insulator.

Regarding the open-close operations of circuit breakers during single phase-to-ground faults in transmission lines, the dynamic fault arc can be distinguished as primary arc and secondary arcs. A primary arc is limited from the beginning of the arcing fault until the circuit breaker pole of the faulted phase opens to localize the fault. In the course of the fault duration, the heavy short circuit current flows through the primary arc, and makes the diameter of the arc column relatively large. A voluminous hot gas cloud will be formed around the arc channel which results in low dielectric strength. When the arc tries to bend or elongate due to the several factors mentioned above, dielectric breakdown will appear in the surrounding gas cloud that keeps the arc length virtually stable.

The secondary arc will be recognized after the fault has been localized with the open pole of circuit breaker by means of system protection. In this arc period, relatively small amount of current flow through the arc as a result of the inductive and capacitive coupling with the sound phases. Because of the low current magnitude, the cross section area of the channel will become smaller and the incidence of dielectric breakdown will be less. The arc then turns easy to elongate. The length of the secondary arc reaches up to ten times its original length before eventually becoming extinguished.

The extended theory of the switching arc can be applied to the model unconstraint fault arc in air, as shown in [9]. Both, the primary and secondary arcs are modeled on the basis of differential equations of arc conductance:



$$\frac{dg}{dt} = \frac{1}{\tau}(G - g) \quad (2.9)$$

with  $G$  = stationary arc conductance  
 $g$  = time varying arc conductance  
 $\tau$  = time parameter (time constant) of the arc

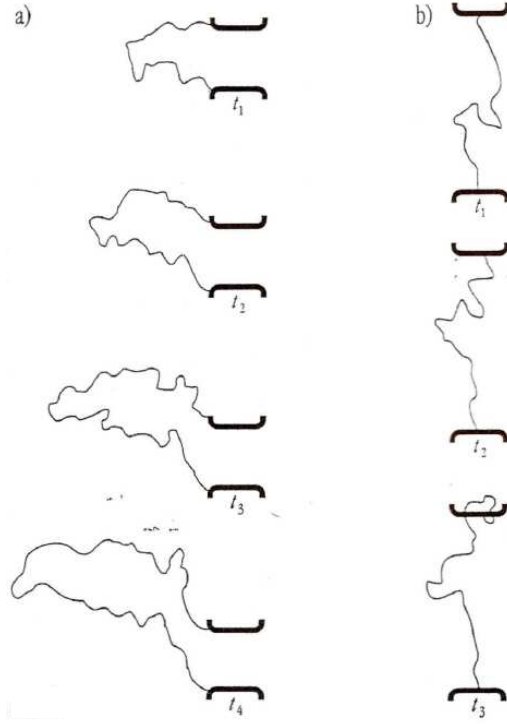


Figure 2.5: Variation of the secondary arc length as function of time for different string insulators [9];

a) 110 kV

b) 380 kV

Equation (2.8) is derived from the view point of control system theory based on energy balance in the arc channel. Stationary arc conductance itself can be physically explained as arc conductance when the arc current is maintained at the same value for sufficiently long enough periods under constant external situations. Thus, the stationary arc conductance  $G$  is given by:

$$G(i) = \frac{i_{arc}}{u_{st}} \quad (2.10)$$

$$u_{st}(i, l) = (u_0 + r_0 |i_{arc}|) \cdot I_{arc}(t) \quad (2.11)$$

$$G(i, l) = \frac{i_{arc}}{(u_0 + r_0 |i_{arc}|) \cdot I_{arc}(t)} \quad (2.12)$$

$$u_0 = \frac{u}{l_0} \quad (2.13)$$

$$r_0 = \frac{r}{l_0} \quad (2.14)$$

where  $u_{st}$  = stationary arc voltage (arc voltage gradient)

$u$  = total characteristic arc voltage in V

$r$  = total characteristic arc resistance in  $m\Omega$

$u_0$  = characteristic arc voltage per arc length in V/cm

$r_0$  = characteristic arc resistance per arc length in  $m\Omega/cm$

$l_{arc}$  = instantaneous arc length in cm

$l_0$  = initial length of the arc column (primary arc length) in cm

In a primary arc model, the arc length  $l_{arc}$  and the time parameter  $\tau$  are relatively constant. The arc length in this situation is represented by the gap length of the arcing horn ( $l_0$ ). While in a secondary arc current, the arc length and the time parameter will be changed in time as expressed in equation:

$$l_{arc} = (v_l \cdot t + 1) \cdot l_0 \quad (2.15)$$

$$\tau = \tau_0 - v_\tau (l_{arc} - l_0) \quad (2.16)$$

where  $v_l$  = speed of arc elongation in cm/ms

$\tau_0$  = initial time constant in ms

$v_\tau$  = speed of the time constant decrease in ms/cm

Based on previous expressions, the arc length will increase linearly when the secondary arc period begins. By contrast, the time constant is inversely proportional to the arc length.

The increasing arc length will be followed by the arc voltage and arc resistance incremental, and finally short circuit current will interrupted during steady arc extinction. The extinction of the arc is determined according to time derivative of instantaneous arc resistance  $dr/dt$  provided  $g$  is less than a predefined  $g_{min}$  per arc length. This considers only the thermal extinction of the arc. Subsequent dielectric reignitions possibilities in air are not taken into account because almost indefinite conditions in and around the arc following the extinction. Following extinction limits are determined empirically in [6]:

$$\frac{g_{min}}{l_{arc}} = 0.25 \mu mho / cm \quad (2.17)$$

$$\frac{\max\left\{\frac{dr}{dt}\right\}}{l_{arc}} = 64 k\Omega / (s.cm) \quad (2.18)$$

### III. DISTANCE PROTECTION AND DISCRETE FOURIER SERIES (DFS)

#### 3.1. Distance Protection

The problem of combining fast faults clearances with selective separation of the faulted area is a major point for the protection of power system. To meet these requirements, highspeed protection system for transmission that are suitable for use with the automatic reclosure of circuit breakers are under continuous development and are very widely applied. The distance protection relaying is the most commonly used protection in transmission and sub transmission line. The main reasons are:

- In basic operation, it is independent from communication link between the line ends, because it only needs input from local voltage and current provided by line or bus voltage transformer (VT) and line current transformer (CT). Here “local” refers to signal measured at relay location.
- The distance protection is a non-unit protection. In contrast to the differential protection for transformers or transmission lines which only covers a limited area, distance protection is not only applied as the main protection (zone 1), but it also serves as remote back up protection in the form of zone 2 up to zone 5 protection. It can easily adapt to create a unit protection scheme when applied with a signaling channel.

Regarding the overcurrent protection, phase and neutral overcurrent relays cannot differentiate the position of the fault point (dummy protection) and they are influenced by the source impedance variation (number of generating power plants supply to the system). Distance protection can discriminate if the fault point is in the forward or backward direction, and it is almost independent from the source impedance variation. It is similar with directional relays, but operation principle is different. Distance protection can effectively measure the terminal impedance between the relay location and the fault point which is resulted from the division between the input local voltage and current. If the measured impedance is lower than the setting impedance, an internal fault will be detected and a trip command will be issued to the circuit breaker. A distance protection is designed to operate only for fault incidents between the relay location and selected reach capability (balance point or tripping threshold) and remains stable for faults outside its operating region or zone. Besides that, it contains phase-to-phase and phase-to-earth elements that will respond to phase-to-phase or phase-to-ground faults in its operating area. For metallic fault with nearly zero resistance, the measured impedance is proportional to the

distance from the protection location to the fault point. That is why this kind of protection is called distance protection or under impedance protection, with code Z< (IEC) or 21 (ANSI).

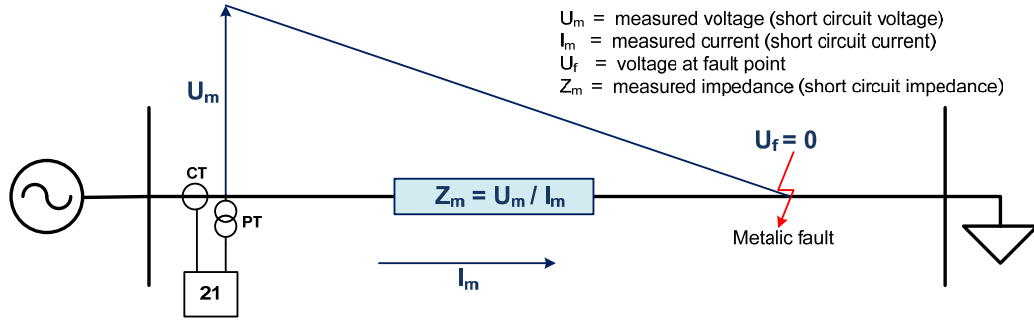


Figure 3.1: Distance protection, principle of operation

### 3.1.1. Distance Protection Setting

Nowadays, numerical distance relay protection provides up to 5 zones protection that can be set individually; forward, reverse or non-directional in direction. Each zone works independently on the basis of the input setting. The three important relay settings consist of time step (t), impedance (Z) range and resistive (R) range setting. Time stepped distance scheme ensures adequate discrimination for faults that may occur in different line section. Time setting for zone 1 is instantaneous. In the next zone, the grading time is usually 0.3 – 0.4 s, depending on the time coordination with distance relay in front or local and remote-back up protection, and also circuit breaker operating time consideration.

The impedance range setting is determined by the protected line reference. Typical impedance setting for 4 zones distance protection is:

$$\text{Zone1} = \text{from } 0.8 \text{ to } 0.9 \times Z_{\text{protected-line}} \Omega \quad (3.1)$$

$$\text{Zone2}(\text{minimum-setting}) = 1.2 \times Z_{\text{protected-line}} \Omega \quad (3.2)$$

$$\text{Zone2}(\text{maximum-setting}) = Z_{\text{protected-line}} + (0.5 \times Z_{\text{adjacent-line}}) \Omega \quad (3.3)$$

$$\text{Zone3} = 1.2 \times (Z_{\text{protected-line}} + Z_{\text{adjacent-line}}) \quad (3.4)$$

$$\text{Zone4reverse} = 0.25 \times Z_{\text{protected-line}} \Omega \quad (3.5)$$

Zone 1 safety margin of 10 – 20% ensures that there is no risk that zone 1 protection overreached the protected line due to errors caused by current and voltage transformers, inaccuracies in line impedance data and errors of relay setting and measurement. In order to decide which factors will be used for zone 1 setting, the following consideration is usually applied:

- 80% : for electro-mechanical distance protection
- 85% : for static and numerical distance protection, or for electro-mechanical distance protection when the line data is determined by measurement

- 90% : for static and numerical distance protection when the line data is determined by measurement

To assure full coverage of the line with those permissible errors, the range setting of zone 2 should be at minimum 120% of the protected line impedance or maximum additional 50% of the adjacent line from the protected line. In case where the adjacent line is a short line (zone 2 minimum is bigger than zone 2 maximum), the zone 2 maximum setting will be used. In the zone 3 setting, the consideration is that the setting should reach 2 substations in front of the relay. In this zone, an infeed factor caused by the contribution of short circuit current from other lines plays an important role. Zone 4 reverse is applicable for back-up protection in case of faults in the bus bar. The entire angle setting for each zone has a maximum value of line angle data. It depends on the distance protection characteristic and resistive range value.

Fault arcs in power systems have a resistive characteristic. They can have low resistance (metal bolted faults), or high resistance (faults caused by tree branches). When the protected line is not affected by the high resistive faults, line in cases when there are no trees around, the resistive range is established by fault arc resistance for phase-to-phase element setting and additional average tower footing resistance for phase-to-earth element setting. The non-linear fault arc resistance can be calculated empirically using Warrington formula:

$$R_A = \frac{28710}{I^{1.4}} \cdot L \quad (3.6)$$

where  $R_A$  = arc resistance in ohm  
 $L$  = length of arc in meter  
 $I$  = arc current in ampere

The calculation of arc resistance in (3.6) is enhanced in [12] to get better accuracy in the wide area of fault arc current by using equation:

$$R_A = \frac{2\sqrt{2}}{\pi} \cdot \frac{E_A L}{I} \quad (3.7)$$

where  $E_A$  = arc voltage gradient in V/m

$E_A$  is expressed in two ways, firstly by using a value between 1200 - 1500 V/m and secondly by using the formula:

$$E_A = 950 + \frac{5000}{I} \text{ V/m} \quad (3.8)$$

When high resistance fault is expected, two constraints are imposed upon the setting; it must be larger than the high resistance fault arc, but it must be lower than the measured apparent resistance due to heaviest load on the line (heaviest load resistance).

The guideline setting interpreted above is generally essential for single line circuit; in other cases like with parallel lines, multi-ended lines or series compensated lines, other considerations must be taken into account. That is why the protection in power systems does not only need a sense of “science” but also a sense of “art” to achieve best overall protection performance.

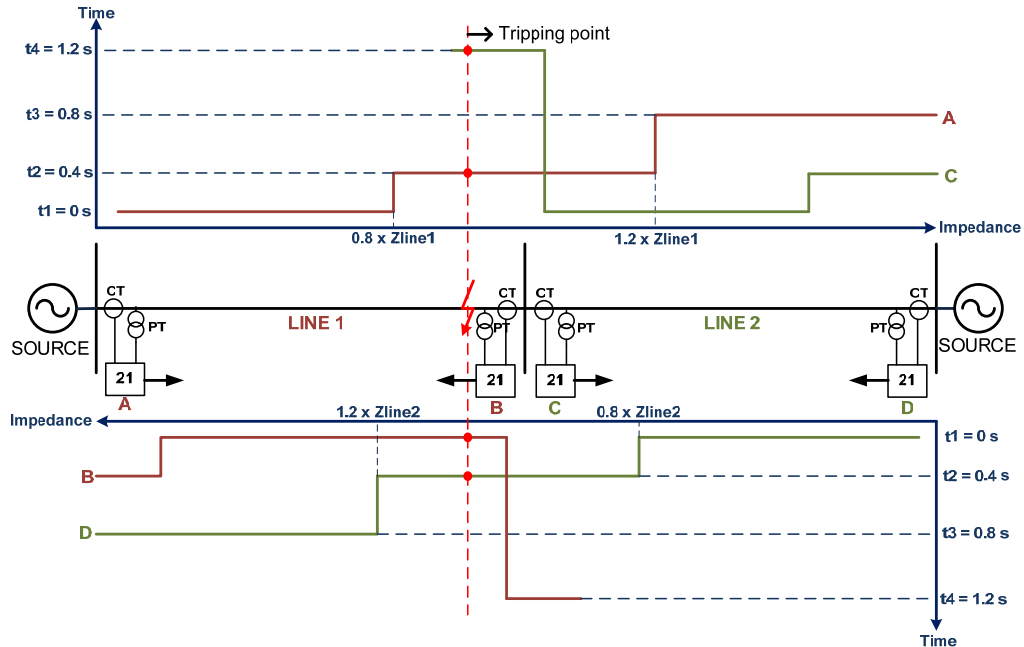


Figure 3.2: Setting example, single circuit double ended source

Figure 3.2 shows that relay A protects line 1 and line 2. It serves as the main protection in line 1 and it is set to operate instantaneously at first zone impedance setting range of  $80\% Z_{line1}$ . The zone 2 has longer operating time which is  $0.4\text{ s}$  and it reaches up to  $120\% Z_{line1}$ , whereas zone 3 reaches the next 2 substations with the time setting of  $0.8\text{ s}$ . Relay A and B are responsible for the main protection for line 1. At the fault point, relay A operates in zone 2 in  $0.4\text{ s}$ , while relay B trips instantaneously in zone 1. Relay D serves as back-up protection for relay B and it trips after  $0.4\text{ s}$ . The backward protection of relay C acts as a back-up protection for relay A and it will trip after  $1.2\text{ s}$ . This example is an example for basic scheme operation of distance protection. To increase the capability as a main protection, a signaling scheme is introduced, so both, relay A and relay B will operate instantaneously for the same fault point.

### 3.1.2. Impedance (R – X) Diagram

An impedance diagram is an important tool for evaluation of the behavior of distance protection. In this diagram, the protected line, the relay characteristic, the measured load impedance and the short circuit impedance as indicators of the relay performance in the system are represented in R-X diagram. By using complex R-X plane, it is easy to understand how the relay operates and the reaction of the relay with the presence of system faults can be analyzed.

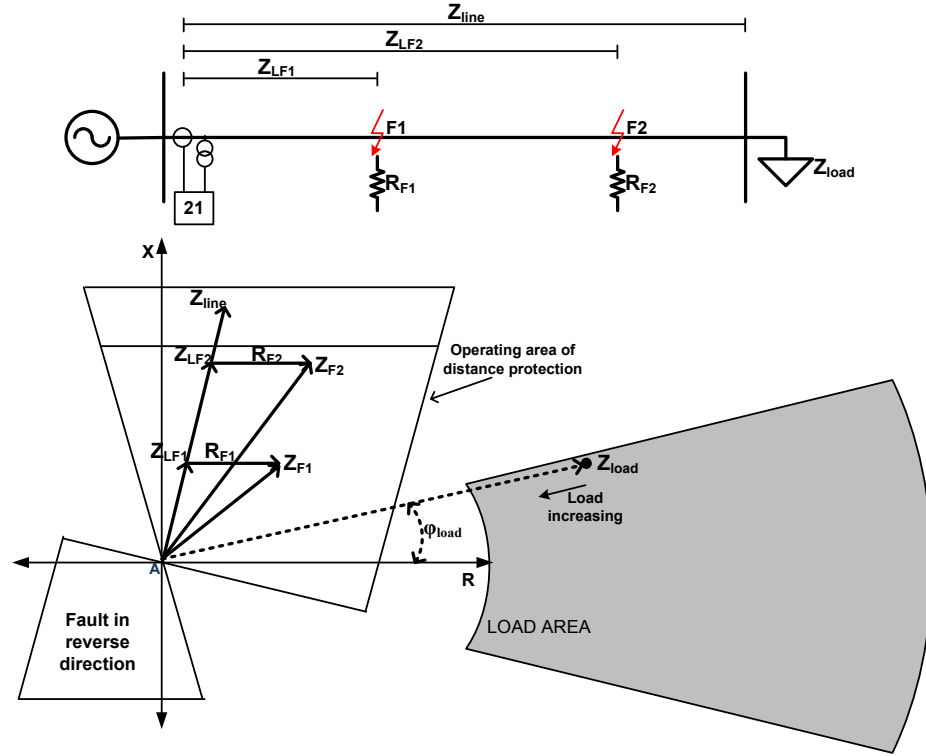


Figure 3.3: Load impedance, short circuit impedance and relay characteristic in R-X diagram with different fault locations [15].

Figure 3.3 shows three different situations: normal load, fault in F1 point and fault in F2 point. During normal load condition, the measured impedance corresponds to the load impedance which is inversely proportional to the load transfer ( $Z_{load} = U_{line}^2 / P_{load}$ ). As the load increases, the measured load impedance approaches the origin. The resistive range setting should be less than the maximum load impedance, as explained earlier, to avoid maloperation of the relay because of load encroachment. After fault inception, the measured impedance jumps to the short circuit impedance, which is usually smaller than the load impedance. Without the presence of fault resistance, the value corresponds to the line impedance between the relay and the fault location ( $Z_{LF1}$  and  $Z_{LF2}$ ). When fault resistance is present, additional resistive component ( $R_{F1}$  and  $R_{F2}$ ) is added to the line impedance. The measured fault impedance now becomes  $Z_{F1}$  and  $Z_{F2}$ . The operating area of the distance protection is defined by a fixed shape in R – X diagram. If fault occurs in backward direction of the relay, the measured impedance will appear in reverse direction of the operating area.

### 3.1.3. Distance Protection Characteristic

Most distance relay protection integrates distance elements into the basis of one or more of the following operating characteristic; susceptance, conductance, impedance, admittance or

mho, reactance and quadrilateral characteristic. These characteristics are recognized according to the shape of the operating zone plotted in impedance diagram, as can be seen in figure 3.4.

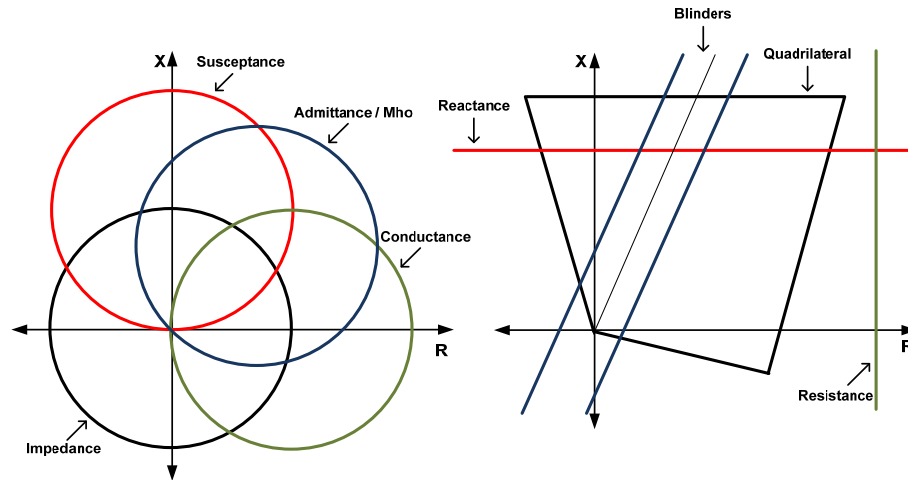


Figure 3.4: Basic distance protection characteristic

The impedance, reactance, resistance and blinders characteristic are inherently non directional and must be supervised by a directional element to avoid tripping for fault behind the relay. The reactance, resistance and blinders characteristic provide an exact limit of the relay range. They are incorporated together to form a quadrilateral characteristic which provides directionality, precise limit and wide resistive setting range.

The mho and quadrilateral characteristic are the most widely used characteristic in numerical distance protection. Distance relay manufacturers in UK and US use mho and quadrilateral characteristics in their products, for example Areva Micom P442 and GE Multilin URD60. While manufacturers in Asia and Europe mostly use only quadrilateral characteristic in distance relay, for example Toshiba GRZ100, Siemens 7SA511 and ABB REL511. Both characteristics have advantages and limitations. The quadrilateral characteristic has the advantage in wide area of resistive range, but relatively constant in reactance range, vice versa in the mho characteristic. The implementation of each characteristic depends on the necessity of the protected system, usually the mho characteristic is implemented in the phase-to-phase element and the quadrilateral characteristic is widely used in the phase-to-earth element.

#### 3.1.3.1. Mho Characteristic

The mho or admittance element is generally known as such because its characteristic is a straight line on an admittance diagram. When plotted on R – X diagram, mho characteristic is a circle with circumference passes through the origin, as illustrated in figure 3.5. Two main inputs are needed to design such characteristic; its diameter of the circle  $AQ$  and relay characteristic angle  $\phi$



which is the displacement angle of the diameter from the R axis. Both of them are influenced by the impedance range and resistive range setting. When the resistive range PQ is set to 0, the diameter comes into its minimum value which is equal to the impedance setting. In a similar situation, the relay characteristic angle becomes maximal and the same as line angle value. Meanwhile at higher resistive reach PQ', in the case of phase-to-earth element setting, the diameter of the circle grows larger and shifts to the R axis direction.

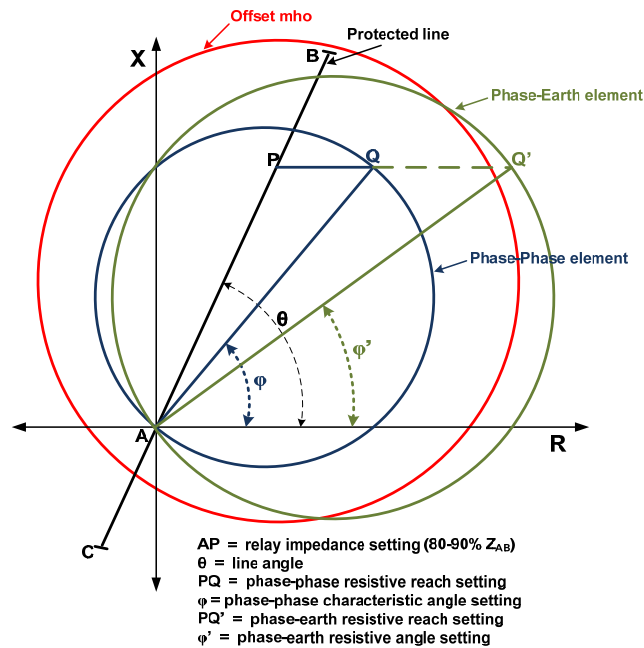


Figure 3.5: Mho characteristic in phase-to-phase and phase-to-earth element

Besides the resistive range limitation, other drawback of mho characteristic is under near bus bar fault location. At this situation mho characteristic may fail to operate when it is required to do so. In order to overcome this problem, offset mho characteristic is implemented as a fault detector or zone 3 element to complete zone 1 and zone 2 elements. With this complement, the relay can operate for close faults in both, forward and reverse direction.

### 3.1.3.2. Quadrilateral Characteristic

The polygonal quadrilateral characteristic is a flexible characteristic that allows wide range resistive range for better high resistive fault coverage. As described in figure 3.6, this characteristic is built by several setting elements that work independently. They consist of reactance range, resistive range, line angle, blinders angle for second and forth quadrant. The reactance range setting follows the protected line reactance, for example for zone 1 reactance range will be 80-90%  $X_{\text{protected line}}$ . The blinders angle is recommended at 25 to 15 degree for quadrant 2 and 15 degree for quadrant 4 [17]. The quadrilateral characteristic also experienced same problem with mho

characteristic when facing close bus bar faults in backward or forward condition. To anticipate this drawback non-directional quadrilateral with small reverse reactance range is implemented.

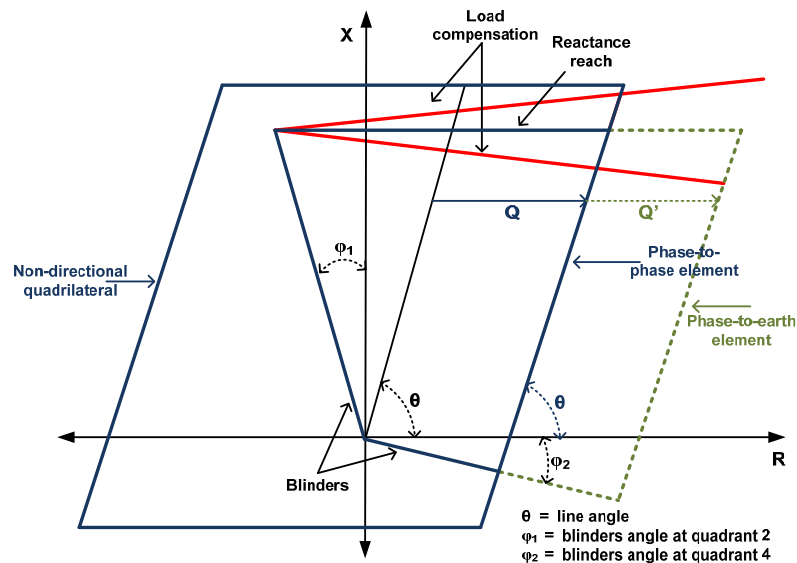


Figure 3.6: Quadrilateral characteristic in phase-to-phase and phase-to-earth element

Unlike the mho characteristic which has inconstant reactance range (following the curve of the circle), the quadrilateral characteristic possesses consistent reactance range. This condition may cause incorrect operation of the relay when load transfer between two systems at different voltage source angle appears prior to the fault. A load compensation is introduced to cope with this drawback which will tilt the reactance range up or down depending on the necessity. The load compensation is more important in phase-to-earth element where the resistive fault larger than in phase-to-phase element.

From now on, the discussion will be focused on the quadrilateral characteristic because all distance relays in 150 kV South Sumatera system use this kind of characteristic.

### 3.1.4. Impedance Measuring Principle

The short circuit fault calculation incorporates not only the positive sequence of the system but also negative (in case of phase-to-phase fault) and zero sequence (in case of phase-to-ground fault) factors. The purpose of this calculation is to find out current and voltage values in fault situation. In the distance protection operating principle, the rule is conversely. The terminal voltage and current of the fault condition are used as input for calculating the measured impedance. Then, the result is compared with the balanced point setting to decide whether the fault occurs inside or outside the operating area. The problem is that the measured loop impedance includes not only the positive sequence impedance but also the other components,

while the distance protection setting elements mostly use positive sequence component. This problem usually appears in case of setting calculation, testing of distance relay and evaluating distance relay performance.

Two new terms are now introduced, an ohm-loop domain and an ohm-phase domain. In the ohm-loop domain, the measured impedance consists of positive, negative and zero sequence impedance which depends on the type of the fault. In the ohm-phase domain, it is identical with positive sequence impedance. Generally, all brands of numerical distance relay apply ohm-phase domain in their phase-to-phase element. Whereas in the phase-to-earth element not all relays employ the ohm-phase impedance for their setting, some of them use the ohm-loop domain. The relationship between the fault incidents measured impedance with the design quadrilateral characteristic in single radial circuit, both for phase-to-phase and phase-to-ground faults will be discussed further.

#### 3.1.4.1. Phase-to-Phase Fault

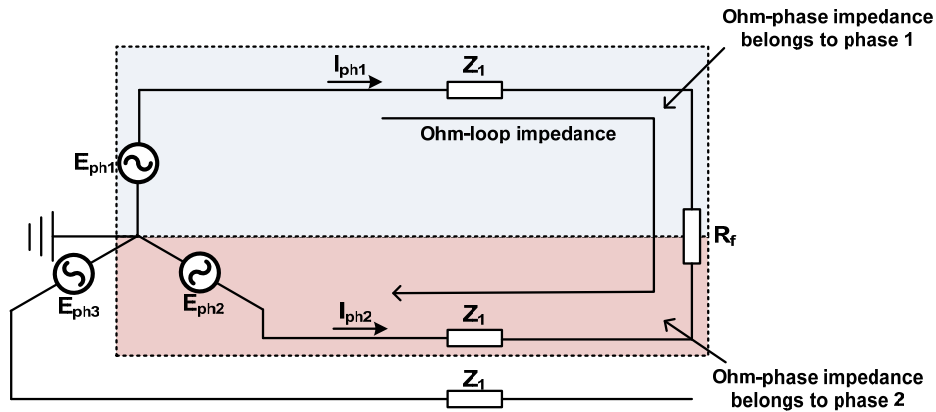


Figure 3.7: Phase-to-phase fault

Above figure illustrates double-phase fault in the power system, and the measured loop impedance in this situation is determined by:

$$Z_{ml} = Z_1 + Z_1 + R_f = \frac{E_{ph1} - E_{ph2}}{I_{ph1}} \quad (3.9)$$

where  $Z_{ml}$  = the measured ohm-loop impedance

$Z_1$  = the positive sequence impedance

$R_f$  = the fault resistance

$E_{ph}$  = the short circuit phase to earth voltage

$I_{ph}$  = the short circuit phase to earth current

In phase-to-phase fault, the measured impedance is a complex number determined according to:

$$Z_{ph-ph} = \frac{E_{ph-ph}}{I_{ph-ph}} = \frac{E_{ph1} - E_{ph2}}{I_{ph1} - I_{ph2}} \quad (3.10)$$

$$I_{ph1} = -I_{ph2} \quad (3.11)$$

Substituting equation (3.9) and (3.11) into equation (3.10) results in:

$$Z_{ph-ph} = \frac{2.Z_1 + R_f}{2} = Z_1 + \frac{R_f}{2} = Z_{mp} \quad (3.12)$$

Where  $Z_{mp}$  = the measured ohm-phase impedance

$Z_{mp}$  is the measured impedance in the reference of one of the faulted phase. Consequently, for double phase fault, the measured ohm-loop impedance is two times larger than the measured ohm-phase impedance or:

$$Z_{ml} = 2.Z_{mp} \quad (3.13)$$

If the input setting for zone 1 in the phase-to-phase element is  $Z_1 = R_1 + jX_1$  which is in the reference of the positive sequence impedance, then the design quadrilateral characteristic for both ohm-loop and ohm-phase domains are illustrated by:

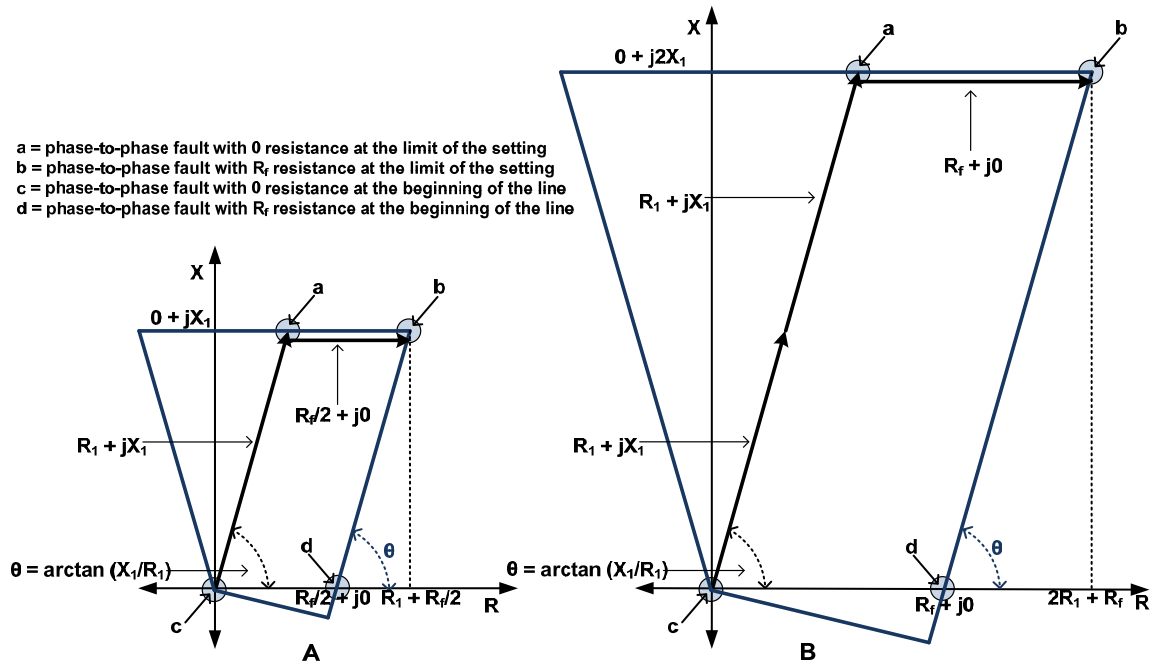


Figure 3.8: The design characteristic in ohm-phase (A) and ohm-loop (B) in phase-to-phase element

#### 3.1.4.2. Phase-to-Ground Fault

A phase-to-ground fault situation in solidly grounded network is illustrated in figure 3.9. For this fault, the measured ohm-loop impedance is calculated by:

$$Z_{ml} = Z_1 + R_f + Z_N = \frac{E_{ph1}}{I_{ph1}} \quad (3.14)$$

$$Z_N = \frac{Z_0 - Z_1}{3} \quad (3.15)$$

$$X_N = \frac{X_0 - X_1}{3} \quad (3.16)$$

$$R_N = \frac{R_0 - R_1}{3} \quad (3.17)$$

Where  $Z_N$  = the earth return impedance

$Z_0$  = the zero sequence impedance

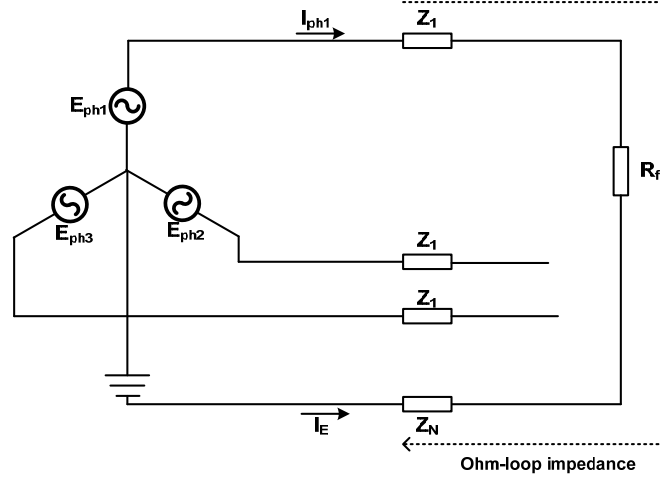


Figure 3.9: Phase-to-ground fault

Substituting equation (3.14) into (3.15) results in:

$$Z_{ml} = Z_1 + \frac{Z_0 - Z_1}{3} + R_f = \frac{2 \cdot Z_1 + Z_0}{3} + R_f = Z_1 \cdot \left( 1 + \frac{Z_0 - Z_1}{3 \cdot Z_1} \right) + R_f \quad (3.18)$$

$$K_N = \frac{Z_0 - Z_1}{3 \cdot Z_1} = \frac{Z_N}{Z_1} \quad (3.19)$$

$$Z_{ml} = Z_1 \cdot \left( 1 + \frac{Z_N}{Z_1} \right) + R_f = Z_1 \cdot (1 + K_N) + R_f \quad (3.20)$$

$$X_{ml} = X_1 \cdot \left( 1 + \frac{X_N}{X_1} \right) \quad (3.21)$$

$$R_{ml} = R_1 \cdot \left( 1 + \frac{R_N}{R_1} \right) + R_f \quad (3.22)$$

Where  $K_N$  = zero sequence compensation factor

For phase-to-ground faults the measured impedance is a complex number calculated according to equation:

$$Z_{ph-e} = \frac{E_{ph1}}{I_{ph1} - K_N \cdot I_E} \quad (3.23)$$

$$I_{ph1} = -I_E \quad (3.24)$$

$$E_{ph1} = I_{ph1} \cdot Z_1 + I_E \cdot Z_N + I_{ph1} \cdot R_f \quad (3.25)$$

Substituting formula (3.19), (3.24) and (3.25) into (3.23) results in:

$$Z_{ph-e} = \frac{I_{ph1} \cdot (Z_1 + Z_N + R_f)}{I_{ph1} \cdot (1 + K_N)} = \frac{Z_1 + Z_N + R_f}{1 + K_N} = \frac{Z_1 \cdot \left(1 + \frac{Z_N}{Z_1}\right) + R_f}{1 + \frac{Z_N}{Z_1}} = Z_1 + \frac{R_f}{1 + K_N} = Z_{mp} \quad (3.26)$$

In order to make the analysis easier the equation (3.26) is divided into resistive and reactive component:

$$X_{ph-e} = X_1 = X_{mp} \quad (3.27)$$

$$R_{ph-e} = R_1 + \frac{R_f}{1 + \frac{R_N}{R_1}} = R_{mp} \quad (3.28)$$

From equation (3.20), (3.21), (3.22), (3.26), (3.27) and (3.28), it can be concluded that the phase-to-ground fault ohm-loop impedance is  $(1 + K_N)$  times larger than the ohm-phase impedance.

$$Z_{ml} = (1 + K_N) \cdot Z_{mp} \quad (3.29)$$

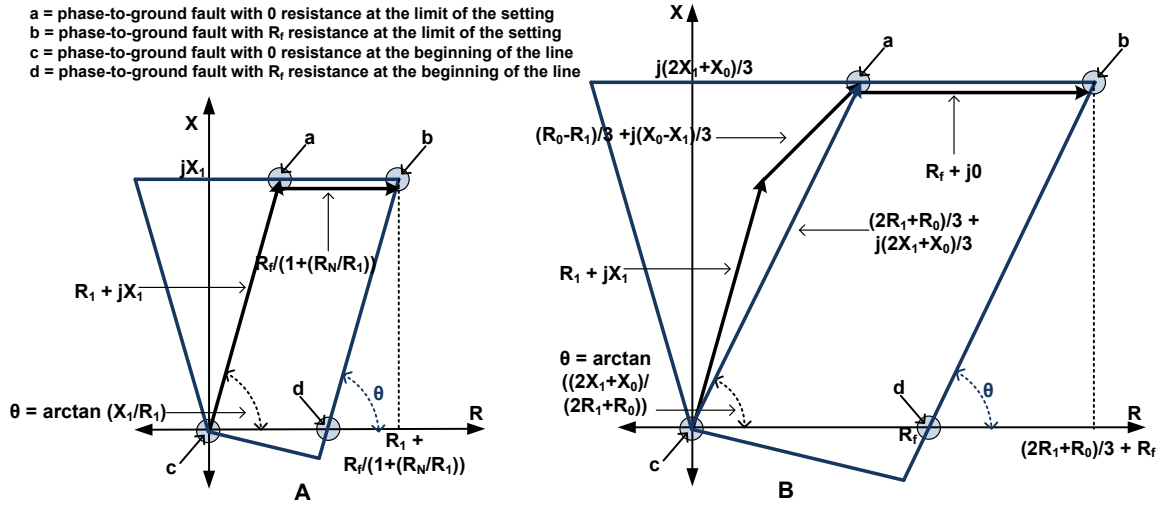


Figure 3.10: The design characteristic in ohm-phase (A) and ohm-loop (B) in phase-to-earth element

Some manufacturers use zero sequence compensation factor in the term of complex number  $K_N$ , like in Toshiba GRZ100 and ABB REL511 distance relay, whilst the others use resistive and reactive component  $R_N/R_1$  and  $X_N/X_1$ , for example in Siemens 7SA511 distance relay.

If the input setting for zone 1 in phase-to-phase element is  $Z_1 = R_1 + jX_1$ , which is in the reference of positive sequence impedance, and zero sequence impedance of the line is defined as

$Z_0 = R_0 + jX_0$ , then the design quadrilateral characteristic both, for ohm-loop and ohm-phase domains for phase-to-ground faults are illustrated by figure 3.10.

### 3.1.5. Distance Protection Application Problems

So far the analysis of distance protection is related to single radial circuit. In other cases implementation of the distance protection needs some setting adjustment due to configuration of the protected line. Adaptation of the setting with different kind of protected lines is important to avoid miss operation of distance relay. Some common cases implementing distance protection in different line configuration will be discussed further.

#### 3.1.5.1. Double Infeed Line (from Both Sides) without Load Transfer

In this configuration, a transmission line connects two systems A and B, as illustrated in figure 3.11. Initially it is assumed that sources A and B are in-phase or no load transfer through the line. When the fault occurs with constant fault resistance  $R_F$ , the short circuit current will flow from both sides. The short circuit current flowing from the opposite end ( $I_{SB}$ ) through the fault resistance takes part in an additional voltage drop.

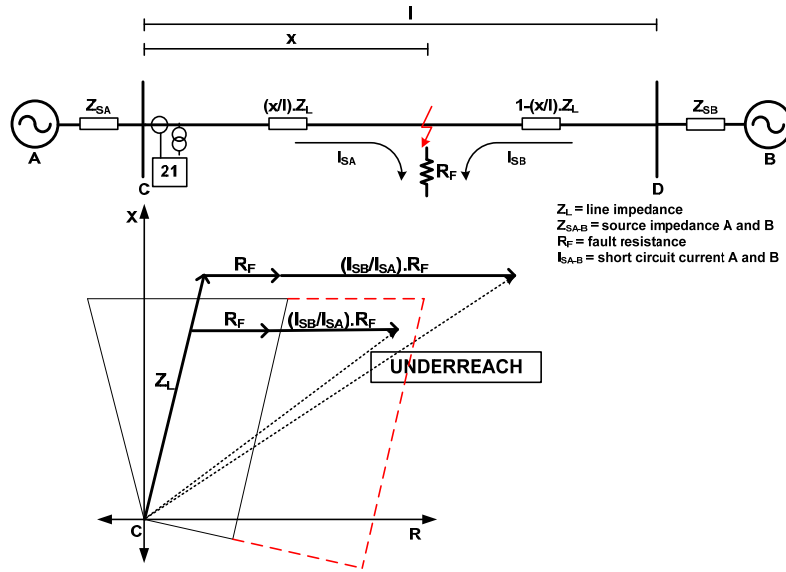


Figure 3.11: Influence of both sides infeed (without load transfer)

The measured fault resistance in terminal C is equal to:

$$U_C = I_{SA} \cdot Z_L + (I_{SA} + I_{SB}) \cdot R_F = I_{SA} \cdot (Z_L + R_F) + I_{SB} \cdot R_F \quad (3.30)$$

$$Z_C = \frac{U_C}{I_{SA}} = Z_L + R_F + \frac{I_{SB}}{I_{SA}} \cdot R_F = Z_L + R_F \cdot \left( 1 + \frac{I_{SB}}{I_{SA}} \right) \quad (3.31)$$

Equation (3.31) shows increase in the fault resistance by a factor  $1 + (I_{SB}/I_{SA})$ . Because of the additional short circuit current from the opposite source, the distance relay in point C sees larger fault resistance than it is supposed to be. At the time when the fault location is closer to the relay

point, the incremental fault resistance is lower because short circuit current  $I_{SB}$  decreases. This effect is particularly evident on long lines with strong opposite infeed ( $Z_{SB} \ll Z_{SA}$ ). The total measured impedance seen by the distance relay is in underreach position. It means that the fault incident is located inside the protection area ( $X_{\text{fault}} < X_{\text{setting}}$ ) but the measured impedance is outside the setting characteristic ( $R_{\text{fault}} > R_{\text{setting}}$ ). To avoid this situation, wider resistive range is implemented. Besides that, the signaling scheme can also be used as a solution.

The fault resistance in impedance diagram (figure 3.11) is the real fault resistance, if it will be transferred to distance protection element, the rule as explain in 3.1.4 about ohm-phase and ohm-loop domains must be taken into account. For example in phase-to-ground fault  $R_F$  is divided by factor  $(1+(R_N/R_L))$  for ohm-phase value.

### 3.1.5.2. Double Infeed Line (from Both Sides) with Load Transfer

Unlike the previous section, now real power transfer exists from system A to system B through long transmission line. The power transfer requires phase shift between two system voltages as described in:

$$P = \frac{U_C \cdot U_D}{X_L} \cdot \sin \delta_L \quad (3.32)$$

where  $P$  = real power transfer

$U_{C-D}$  = terminal C and D voltage

$X_L$  = reactance of transmission line

$\delta_L$  = phase shift between voltage C and D

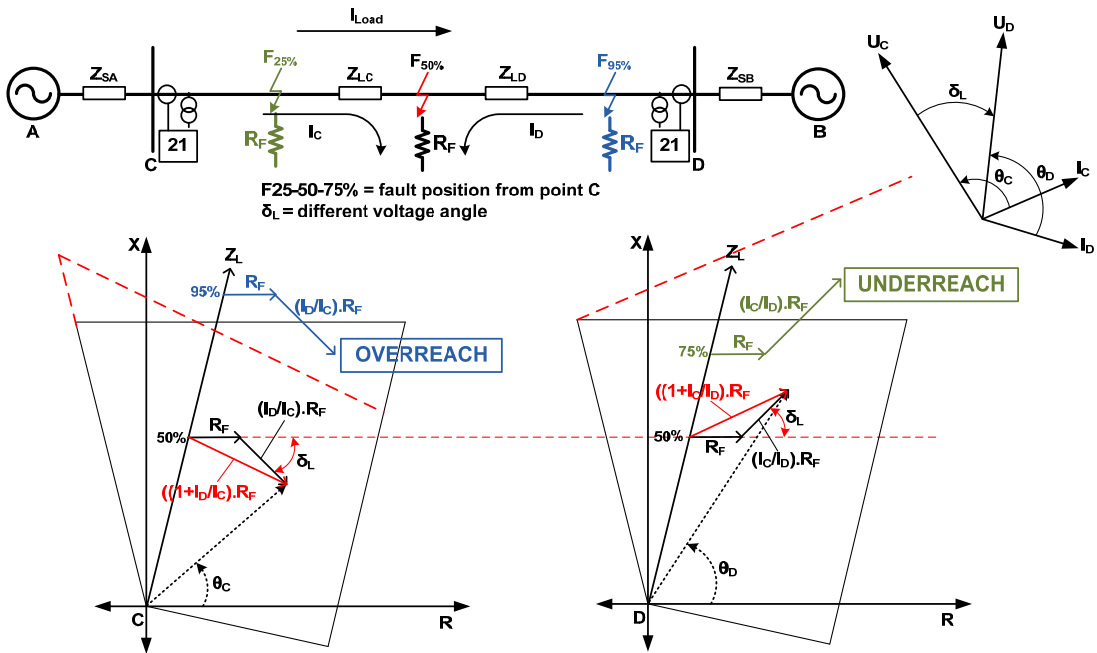


Figure 3.12: Influence of both sides infeed (with load transfer)



The equivalent circuit for this system condition is illustrated in figure 3.12. At short circuit fault incident, the feeding voltages have different angle. The voltage at sending end  $U_C$  leads the voltage at receiving end  $U_D$  by transmission line angle  $\delta_L$ , therefore the short circuit current from both sides is phase shifted by this angle. Consequently with constant fault resistance, the vector of additional measured resistance  $(I_D/I_C).R_F$  is tilted down at terminal C and tends to overreach the protection area of the relay for a fault located outside its setting, for example at  $F_{95\%}$ . Conversely, at receiving end, the vector  $(I_C/I_D).R_F$  is tilted up and tends to underreach outside the protection area, for fault example at  $F_{75\%}$ . To avoid this situation, a load compensation is applied to the distance relay at both sides. So, for an overreach condition, the fault is still in external operating area while in other side it embraces the underreaching impedance.

### 3.1.5.3. Intermediate Infeed

The source B and C connected to terminal (bus) E contribute to supplementary short circuit current fault incident in line 2. This additional short circuit current is seen by distance relay in terminal D as extra voltage drop and gives increasing measured impedance.

$$U_D = Z_{L1} \cdot I_A + Z_{L2} \cdot (I_A + I_B + I_C) \quad (3.33)$$

$$Z_D = \frac{U_D}{I_A} = Z_{L1} + Z_{L2} + \left( \frac{I_B + I_C}{I_A} \right) \cdot Z_{L2} \quad (3.34)$$

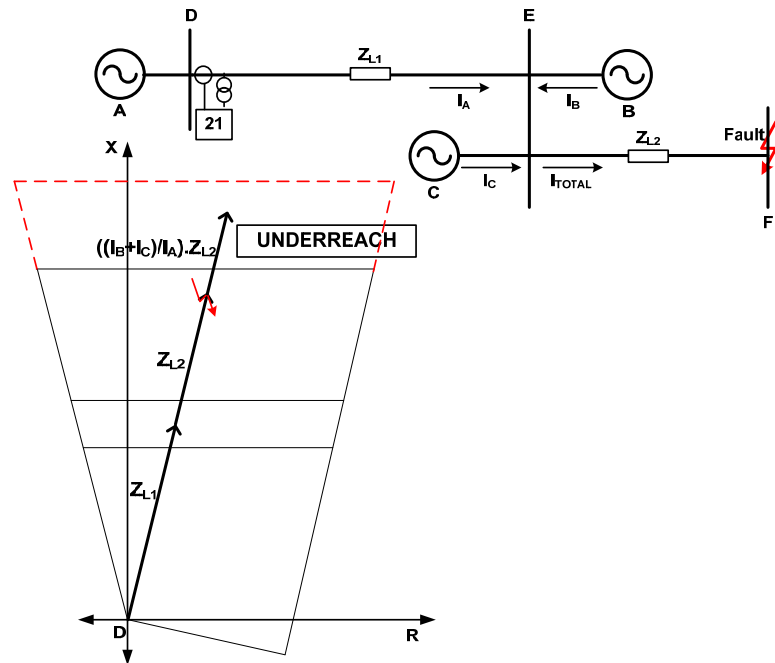


Figure 3.13: Intermediate Infeed

The additional short circuit current will influence the measured impedance by the distance relay in all fault point position in line 2. As a consequence the measured impedance in zone 2 and zone 3

seems larger than it should be by factor  $(I_B + I_C)/I_A$  and causes underreach condition. This case is especially important for back-up zone 3 setting where there is a possibility of blank zone 3 back up protection area. Therefore the recommended setting calculation for zone 3 impedance range in this case is taken into account by the infeed factor as in the equation below:

$$Zone3 = 1.2 \times \left( Z_{L1} + \frac{I_{Total}}{I_A} \cdot Z_{L2} \right) \Omega \quad (3.35)$$

#### 3.1.5.4. Parallel Lines

For parallel line configuration, a mutual inductive coupling of the current between each line exists. This effect can be neglected in the positive and negative sequence system either during load or for all short circuits without earth condition in the case of transposed line arrangement. In this case, the line may be considered as independent. On the other hand, earth faults are not affected with such arrangement, the zero sequence current of one line induces a voltage in the other line and vice versa. This situation is described in equation:

$$U_{01} = I_{01} \cdot Z_{01L} + I_{02} \cdot Z_{0M} \quad (3.36)$$

$$U_{02} = I_{02} \cdot Z_{02L} + I_{01} \cdot Z_{0M} \quad (3.37)$$

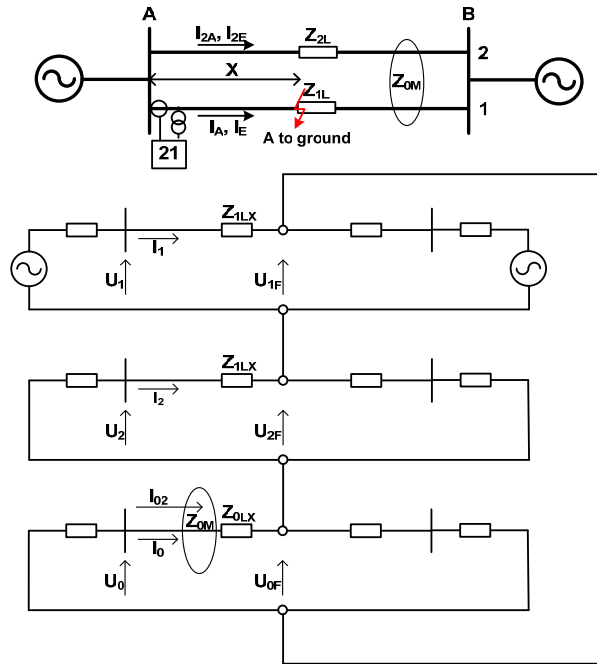


Figure 3.14: Parallel line with zero sequence mutual impedance

As illustrated in figure 3.14, the earth current of the healthy parallel line induces a voltage in the fault loop of the measured line and changes the measured short circuit voltage at the relay location, which results in error measurement.

The following equations can be derived from the symmetrical component equivalent circuit in figure 3.14 when single phase-to-ground fault occurs in line 1 in position X from bus A:

$$U_1 = Z_{1LX} \cdot I_1 + U_{1F} \quad (3.38)$$

$$U_2 = Z_{2LX} \cdot I_2 + U_{2F} \quad (3.39)$$

$$U_0 = Z_{0LX} \cdot I_0 + Z_{0M} \cdot I_{02} + U_{0F} \quad (3.40)$$

The summation of three above equations with following relationship is applied:

$$U_A = U_1 + U_2 + U_0 \quad (3.41)$$

$$0 = U_{1F} + U_{2F} + U_{0F} \quad (3.42)$$

$$I_E = 3 \cdot I_0 \quad (3.43)$$

$$I_A = I_1 + I_2 + I_0 \quad (3.44)$$

Then the result is:

$$U_A = Z_{1LX} \cdot (I_1 + I_2 + I_3) + I_0 \cdot (Z_{0LX} - Z_{1LX}) + Z_{0M} \cdot I_{20} \quad (3.45)$$

$$U_A = I_A \cdot Z_{1LX} + I_E \cdot \left( \frac{Z_{0LX} - Z_{1LX}}{3} \right) + I_{2E} \cdot \frac{Z_{0M}}{3} \quad (3.46)$$

By using equation (3.15) and by presupposing that  $Z_{1LX} = Z_{1L}$ ,  $Z_{0LX} = Z_{0L}$ , the short circuit voltage at relay location is determined by:

$$U_A = Z_{1L} \cdot \left( I_A + \frac{Z_{NL}}{Z_{1L}} \cdot I_E + \frac{Z_{0M}}{3 \cdot Z_{1L}} \cdot I_{2E} \right) \quad (3.47)$$

The measured impedance now can be calculated by using equation (3.23), (3.24) and (3.19):

$$Z_A = \frac{Z_{1L} \cdot \left( I_A + \frac{Z_{NL}}{Z_{1L}} \cdot I_E + \frac{Z_{0M}}{3 \cdot Z_{1L}} \cdot I_{2E} \right)}{I_A + K_N \cdot I_E} \quad (3.48)$$

$$Z_A = Z_{1L} \cdot \left( 1 + \frac{\frac{Z_{0M}}{3 \cdot Z_{1L}} \cdot I_{2E}}{I_A + K_N \cdot I_E} \right) \quad (3.49)$$

$$ME = \frac{\frac{Z_{0M}}{3 \cdot Z_{1L}} \cdot I_{2E}}{I_A + K_N \cdot I_E} \quad (3.50)$$

ME is the measuring error impedance. It can be seen that the measuring error is dependent on the polarity and magnitude ratio of the earth current in both lines. The influence of earth current to error impedance measurement is generally followed by rules:

- the measuring error is positive or impedance measurement is too large and results in zone underreach, when the earth current in both lines flow in the same direction,

- the measuring error is negative and leads to zone overreach when the earth currents flow in opposite direction.

The parallel line compensation is introduced to elude overreaching and underreaching condition caused by measuring error impedance. From equation (3.48), it is apparent that the fault impedance is measured correctly when there is additional mutual zero compensation factor ( $K_M$ ) times the sound earth current from side line ( $I_{2E}$ ) in the denominator, as described in equation:

$$Z_{ph-e} = \frac{U_{ph-e}}{I_{ph1} + K_N \cdot I_E + K_M \cdot I_{2E}} \quad (3.51)$$

$$K_M = \frac{Z_{OM}}{3 \cdot Z_{1L}} \quad (3.52)$$

By using above equation, the measuring result is  $Z_{1L}$  and the influence of the parallel line has been cancelled.

#### 3.1.5.5. Tower Footing Resistance

When the fault occurs in the form of sparkover or flashover in an isolator, the short circuit current flows from the phase conductor through the arc across the isolator and into the steel armoring of the tower and then further to earth. By this situation, at the fault location the arc resistance and the tower footing resistance are connected in series. With the presence of overhead ground wires (earth wires), the current passes through several parallel tower footing resistances to earth that will substantially reduced the resultant phase earth resistance. This situation is illustrated in figure 3.15. From this, then the effective tower footing impedance is derived:

$$Z_{EF} = \frac{R_{TF} \cdot \frac{1}{2} \cdot Z_{LW}}{R_{TF} + \frac{1}{2} \cdot Z_{LW}} \quad (3.53)$$

$$Z_{LW} = \frac{1}{2} \cdot Z_{EW} \cdot I_{AS} + \sqrt{\frac{(Z_{EW} \cdot I_{AS})^2}{4} + R_{TF} \cdot Z_{EW} \cdot I_{AS}} \quad (3.54)$$

$$Z_{EW} = R_{EW} + jX_{EW} \quad (3.55)$$

Where  $Z_{EF}$  = effective tower footing impedance

$R_{TF}$  = average tower footing resistance

$Z_{LW}$  = impedance of one ladder network (earth wire and tower footing resistance connected series-shunt)

$R_{EW}$  = earth wire resistance in ohm/km

$X_{EW}$  = earth wire reactance in ohm/km

$l_{AS}$  = average span between towers in km

If the  $Z_{LW}$  is assumed small in comparison with the tower footing resistance, the resulting earth fault impedance can be approximated with the following equation:

$$Z_{EF} = \frac{1}{2} \cdot \sqrt{R_{TF} \cdot Z_{EW} \cdot l_{AS}} \quad (3.56)$$

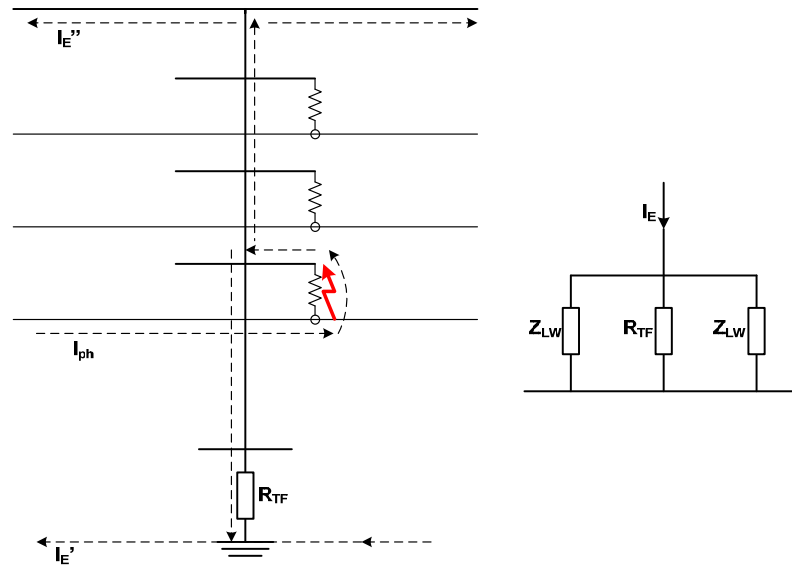


Figure 3.15: Fault resistance resultant on overhead lines [14]

### 3.1.6. Distance Protection Signaling Scheme

Basically the distance protection is a non-unit protection that provides back up protection for the adjacent line. The distance protection as non-unit protection also means that there is possibility for some part of the protected line where the main protection does not response the fault instantaneously. For example about 10-20% of the protected line length works at zone 2 delay time, as shown in figure 3.2. This situation cannot be tolerated in some applications for two main reasons: longer fault clearing time on the line for zone 2 may cause the system to become unstable, non simultaneous opening of the circuit breaker at both ends causes unsuccessful high speed auto reclosing operation.

In order to cover delay time area, a distance protection signaling scheme is applied. By using this scheme, the distance protection will serve as instantaneous main protection in all area of the protected line plus back up protection to adjacent line. In addition, the signaling scheme also uses as solution for underreach and overreach problems which are introduced in previous section. The purpose of the signaling or communication scheme is to transmit system condition information from one end of the protected line to the other including requests to initiate or prevent tripping of the remote circuit breaker. For complete operation, the signaling scheme requires supporting equipment that consists of:

- A Communication media which is used for transmit signal information. Generally this media comprises: pilot wires for distances of 25 km, Power Line Carrier (PLC) channels for distance up to 400 km, directional radio for approximately 50 km (longer distance via relay stations) and fiber optic cable up to 150 km for direct link communication otherwise repeater amplifiers is needed.
- Additional 2 input and 1 output contacts are incorporated in the distance relay for exchanging information between communication media and the relay. Two input contacts are employed as input for channel in service and carrier receive signal. Channel in service signal represents healthy condition of communication media. Carrier receive signal is the signal that has been sent from opposite end line through the media and received by the relay. The output signal is used for carrier send signal which is sent from the signaling scheme in the relay to another relay at the remote end through the media.

Each distance relay manufacturer gives specific names to their signaling scheme, but fundamentally they consist of four kinds of scheme: a transfer tripping scheme, a blocking scheme, a zone 1 extension scheme and a weak infeed scheme.

#### 3.1.6.1. Permissive Underreach Transfer Trip (PUTT)

PUTT is one of permissive tripping scheme variant. In this case besides the underreaching distance zone (usually the first zone) trips the local circuit breaker instantly it simultaneously sends a signal to the remote end. At remote end, if the fault senses in zone 2 area in the perspective of the relay and receives underreaching signal, then the relay will trip instantaneously. In this way, delay tripping time zone 2 is reduced so the circuit breaker at both sides will trip and reclose approximately at the same time.

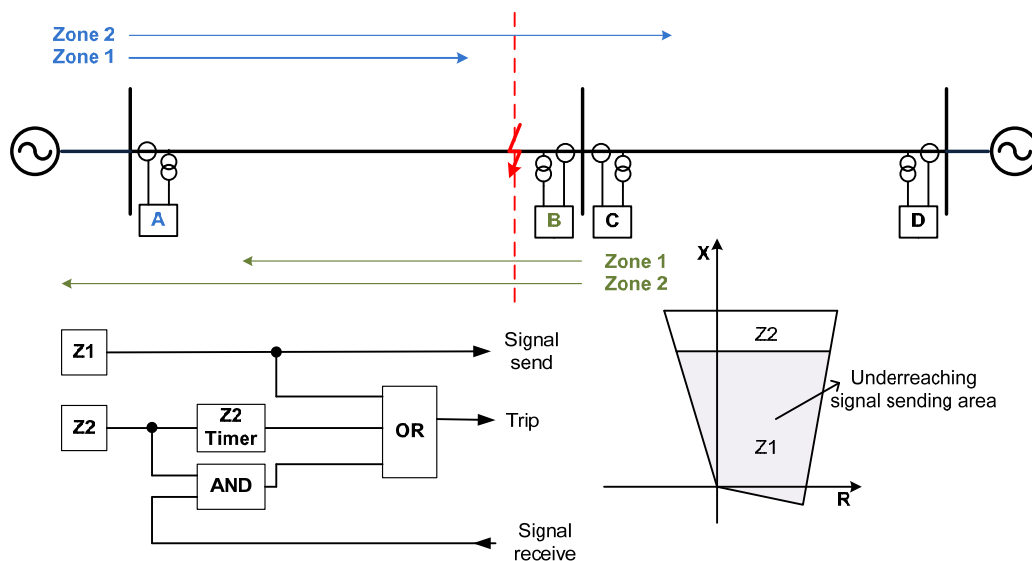


Figure 3.16: Permissive Underreach Transfer Trip

This kind of permissive tripping scheme is usually implemented in long transmission line. From the number of communication channel point of view, PUTT is more profitable because it only needs one communication channel for effective operation. As illustrated in figure 3.16, at fault inception involving zone 1 and zone 2 at each side (distance relay A and B), only distance relay that feels zone 1 fault area (distance relay B) will send the signal.

### 3.1.6.2. Permissive Overreach Transfer Trip (POTT)

In POTT scheme, at the moment the distance relay senses fault in the overreaching zone 2 area, it will instantaneously send signal to the relay in remote end. It must keep in mind that zone 1 protection area is part of zone 2 area, therefore zone 1 is also part of overreaching distance zone. At the time when the remote end relay senses the fault in delay time zone 2 area and receives signal from other side, the relay will give order to the circuit breaker to switch off instantaneously.

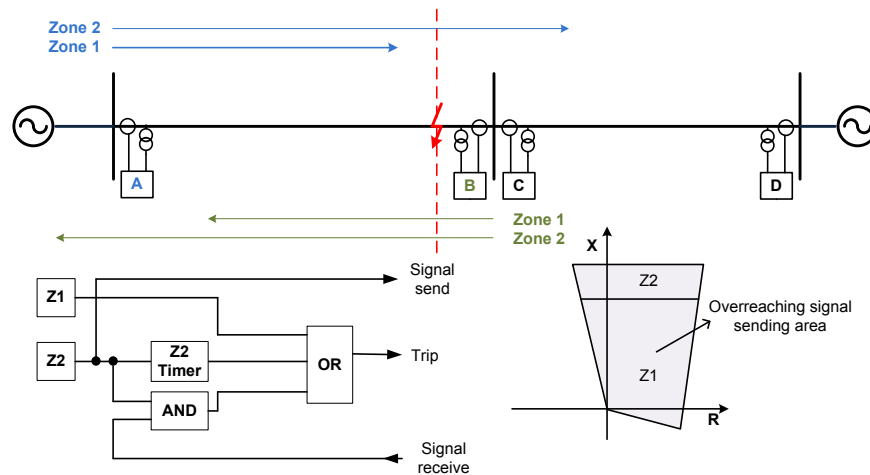


Figure 3.17: Permissive Overreach Transfer Trip

Since the signaling channel is keyed by overreaching zone 2 element then at the same time distance relay on each side will send signal simultaneously. Therefore two communication channels are needed in this method, one frequency for each direction of signaling. POTT method is usually used for the short line feeders, especially when the overhead line or cable is so short that the underreaching zone can no longer be used because the smallest setting is not sufficient.

### 3.1.6.3. Blocking Overreaching Scheme

In contrast with the permissive trip which accelerates tripping of the delay zone area, blocking scheme occupies signal for prevent tripping. The blocking overreaching scheme uses reverse overreaching distance scheme, inverse logic for signal receive input and channel in service as additional inputs. The channel in service input supervises the blocking mode tripping circuit, so it will isolate trip circuit if the signaling channel fails. Signaling is initiated only for faults outside the

protected line and signaling transmission takes place over healthy line section. Instantaneous fault clearance occurs when no signal is received and the overreaching zone 2 distance element looks into the fault. The signaling channel is keyed by reverse looking distance element (in this case zone 3). Similar with PUTT, only one communication channel is needed in blocking scheme.

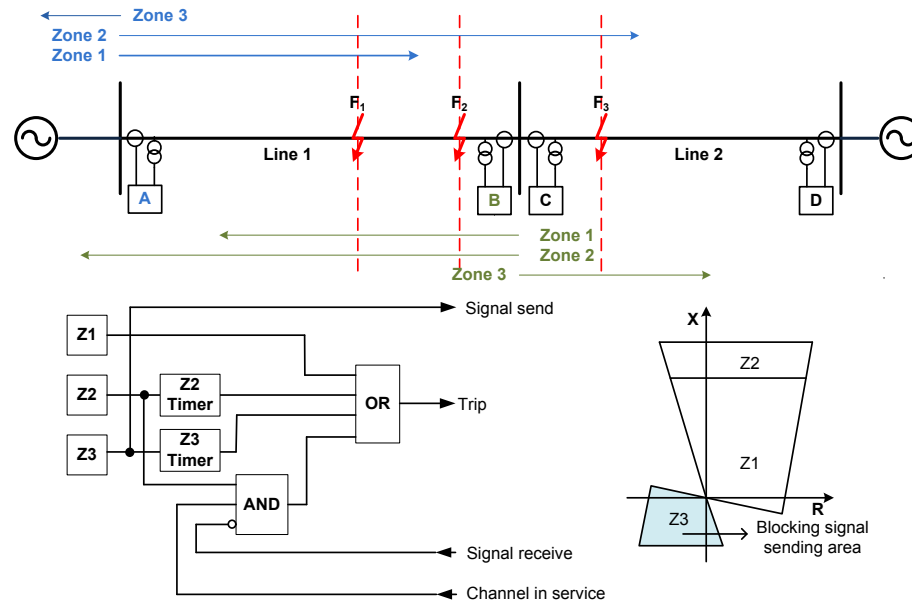


Figure 3.18: Blocking Overreaching Scheme

The logic scheme and several fault incidents are shown in figure 3.18. A fault at  $F_1$  is seen by relay A and B in zone 1 area, as a result the fault is cleared instantaneously at both ends. No transmission signal occurs at this situation because zone 3 element is looking away from the protected section. Fault 2 ( $F_2$ ) is seen by zone 2 element at end A and by zone 1 element at end B. Again no signal transmission takes place. Therefore as a result of signal receive inversion, relay A works instantaneously. A fault at  $F_3$  is detected by the reverse looking zone 3 element of relay B, and the forward looking zone 2 element of relay A. The zone 1 element of relay C would normally clear the fault. Preventing the zone 2 element of relay A from tripping, the reverse looking element of relay B sends a blocking signal to relay A. If the relay C fails to clear the fault instantaneously, the trip signal will be given by relay B after zone 3 delay time. It is important to set impedance range of zone 3 element of relay B greater than zone 2 element of relay A to avoid zone 2 element instant tripping initiation when the reverse looking zone 3 fails to see an external fault.

#### 3.1.6.4. Zone 1 Extension Scheme

The purpose of this scheme is to extend instantaneous zone 1 protected coverage area with its auto reclose facility where no communication channels available. Therefore, a channel in service inversion input becomes part of this method. The zone 1 extension maximum impedance range setting is equal to zone 2 impedance range but usually it sets lower than that. The



disadvantage of the zone 1 extension scheme is: the external faults within the zone 1 extension impedance range setting result instant tripping of the circuit breaker external to the faulted section; for example, the external fault  $F_2$  in the distance relay A point of view as shown in figure 3.19. In this case the impedance range must be set carefully.

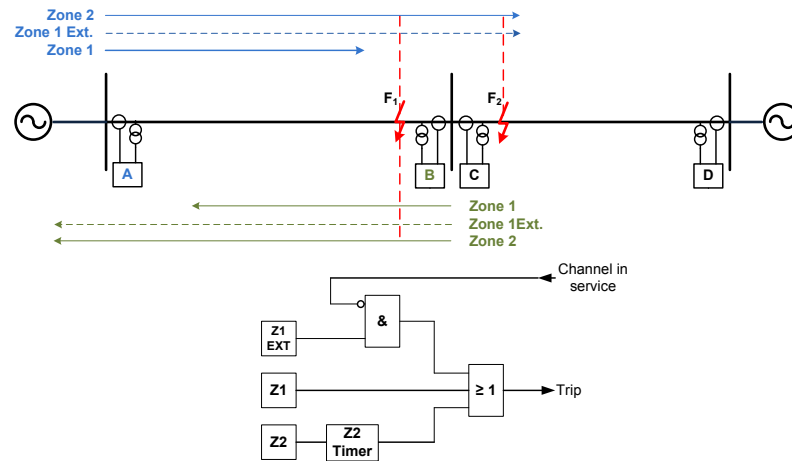


Figure 3.19: Zone 1 Extension Scheme

### 3.1.6.5. Weak Infeed Scheme

Simple single line circuit with weak infeed condition is illustrated in figure 3.20. In that figure, the distance relay B experiences weak infeed condition because there is no source behind its bus that will trigger the relay at fault situation. Bus B only experiences voltage drop at fault condition without current flow to the fault point. At this condition, the distance relay B will not detect the fault. To overcome this condition, weak infeed scheme is implemented that enable a signal to be sent from the distance relay A and under voltage conditions in bus B.

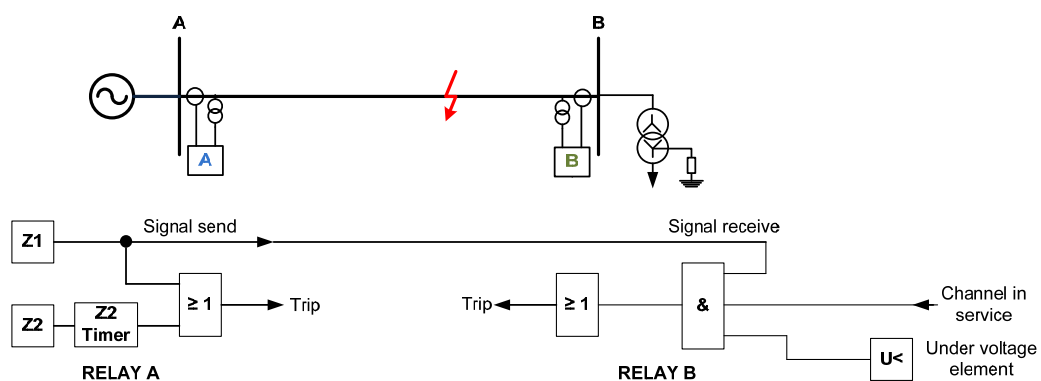


Figure 3.20: Weak Infeed Scheme

## 3.2. Recursive Discrete Fourier Series (DFS)

There are several algorithms that usually apply to do impedance calculation in the numerical distance relay. The algorithms use either single fundamental frequency model, such as

Fourier and curve fitting (least square) techniques, or non-single frequency model as shown in the R – L differential equation below:

$$u(t) = R.i(t) + L \cdot \frac{di(t)}{dt} \quad (3.57)$$

In the R – L differential equation, the instantaneous voltage and current is used for the direct calculation of R and X by using differential equation. In other method, sampled currents and voltages are initially transformed into phasor quantities (real and imaginary components) by means of orthogonal filters and then the short circuit impedance R and X are calculated. DC component and harmonics are already filtered out. Therefore only fundamental frequency ( $f_0$ ) is taken into account. Equations with vector quantities in the frequency domain which correspond with equation (3.57) are:

$$U = R.I + jX.I \quad (3.58)$$

$$X = \omega_0.L = 2\pi.f_0.L \quad (3.59)$$

Equation (3.58) in the term of real and imaginary components:

$$U_{re} + jU_{imj} = (R + jX) \cdot (I_{re} + jI_{imj}) \quad (3.60)$$

$$U_{re} = R.I_{re} - X.I_{imj} \quad (3.61)$$

$$U_{imj} = X.I_{imj} + R.I_{imj} \quad (3.62)$$

By substituting equation (3.61) and (3.62), two equations are available for R and X calculation:

$$X = \frac{U_{imj}.I_{re} - U_{re}.I_{imj}}{I_{re}^2 + I_{imj}^2} \quad (3.63)$$

$$R = \frac{U_{re}.I_{re} + U_{imj}.I_{imj}}{I_{re}^2 + I_{imj}^2} \quad (3.64)$$

Later on in this thesis, the recursive Discrete Fourier Series (DFS) filter is used for the determination of the voltage and current phasors to do impedance calculation.

### 3.2.1. The Fourier Series

A Fourier series of discrete harmonics are normally used to represent any periodic function  $f(t)$ . It can be represented in a trigonometric and a complex form. In trigonometric form, a non-sinusoidal waveform  $f(t)$  repeating with an angular fundamental frequency  $\omega_0$  can be expressed as:

$$f(t) = \frac{a_0}{2} + \sum_{n=1}^{\infty} a_n \cdot \cos(n \cdot \omega_0 \cdot t) + \sum_{n=1}^{\infty} b_n \cdot \sin(n \cdot \omega_0 \cdot t) \quad (3.65)$$

$$a_0 = \frac{2}{T} \cdot \int_{t_1}^{t_1+T} f(t) dt \quad (3.66)$$

$$a_n = \frac{2}{T} \cdot \int_{t_1}^{t_1+T} f(t) \cdot \cos(n \cdot \omega_0 \cdot t) dt \quad (3.67)$$

$$b_n = \frac{2}{T} \cdot \int_{t_1}^{t_1+T} f(t) \cdot \sin(n \cdot \omega_0 \cdot t) dt \quad (3.68)$$

Where T is the period of fundamental component;  $n \cdot \omega_0$  the n-th harmonic angular frequency and  $t_1$  is an arbitrary time.

By combining corresponding sine and cosine terms of the same frequency, equation (3.65) can be written as:

$$f(t) = \sum_{n=0}^{\infty} A_n \cdot \cos(n \cdot \omega_0 \cdot t + \theta_n) \quad (3.69)$$

$$A_0 = \frac{a_0}{2}, \theta_0 = 0 \quad (3.70)$$

$$A_n = \sqrt{a_n^2 + b_n^2}, \theta_n = \tan^{-1} \frac{b_n}{a_n} (n=1, 2, 3, \dots) \quad (3.71)$$

In some applications, it is more convenient to use the complex phasor form of Fourier series as shown in equation:

$$f(t) = \sum_{n=-\infty}^{\infty} F_n \cdot e^{jn\omega_0 t} \quad (3.72)$$

$$F_n = (a_n + jb_n) \text{ for } n < 0 \quad (3.73)$$

$$F_n = (a_n - jb_n) \text{ for } n > 0 \quad (3.74)$$

$$F_n = \frac{a_0}{2} \text{ for } n = 0 \quad (3.75)$$

By substituting equation (3.66) – (3.68) into (3.69), a new equation in  $F_n$  is obtained:

$$F_n = \frac{1}{T} \cdot \int_{t_1}^{t_1+T} f(t) \cdot e^{-jn\omega_0 t} dt, n = \pm 1, \pm 2 \dots \pm \infty \quad (3.76)$$

$$F_n = \frac{1}{T} \cdot \int_{t_1}^{t_1+T} f(t) dt, n = 0 \quad (3.77)$$

Summarizing above explanation, it is apparent that any periodic function  $f(t)$  can be represented in one of the two ways: a time domain representation, where the time history is described by using the equation which defines the function  $f(t)$ ; a frequency domain representation, where the waveform is described by the magnitude and the phase of a number of sinusoidal components of frequency  $n \cdot \omega_0$  ( $n = 1, 2, \dots$ ) that makes up the signal.

### 3.2.2. The Full and Half Cycle Window Fourier Algorithms

The basic approach of these algorithms is to extract the fundamental component ( $n = 1$ ) of a waveform by correlating one cycle of the faulted waveform with store reference sine and cosine waves. In full-cycle algorithm, if  $U_x$  and  $U_y$  are the real and imaginary components of the phasor

that represents the fundamental component of the faulted waveform  $u(t)$ , then according to equation (3.67)  $U_x$  can be expressed as:

$$U_x = a_1 = \frac{2}{T} \int_{t_0}^{t_0+T} f(t) \cdot \cos(\omega_0 t) dt \quad (3.78)$$

Let  $N$  be the number of samples per cycle of the fundamental component,  $\Delta t$  the sampling time interval,  $t_k = k \cdot \Delta t$  the time of the  $k$ -th sample and  $T = N \cdot \Delta t$  the period of the fundamental component. The integral form that appears in equation (3.78) can then be evaluated into:

$$U_x \approx \frac{2}{N \cdot \Delta t} [u(t_0) \cdot \cos \omega_0 t_0 + u(t_1) \cdot \cos \omega_0 t_1 + \dots u(t_k) \cdot \cos \omega_0 t_k + \dots u(t_N) \cdot \cos \omega_0 t_N] \cdot \Delta t$$

$$U_x = \frac{2}{N} \cdot \sum_{k=0}^N u_k \cdot \cos\left(\frac{2\pi k}{N}\right) \quad (3.79)$$

Similarly, it is possible to approximate imaginary part  $U_y$  in the term of discrete waveform samples as follows:

$$U_y = \frac{2}{N} \cdot \sum_{k=0}^N u_k \cdot \sin\left(\frac{2\pi k}{N}\right) \quad (3.80)$$

Equation (3.79) and (3.80) can also be used to calculate the real and imaginary parts  $I_x$  and  $I_y$  of the fundamental current component from faulted current waveform samples  $i(t)$ .

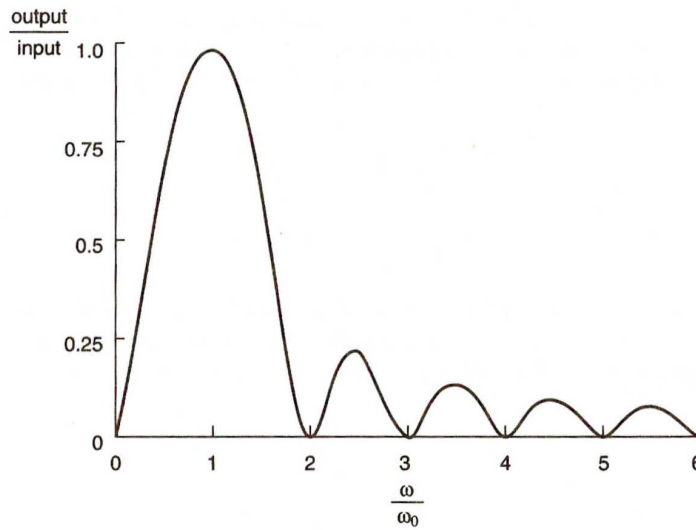


Figure 3.21: The full – cycle window frequency response [10]

Figure 3.21 illustrates the magnitude of the periodic function in the frequency domain ( $n = 1, 2, 3, 4, 5, 6$ ) when the full-cycle window algorithm is implemented. It can be seen that DC ( $n = 0$ ) and harmonic ( $n > 1$ ) components are completely filtered out, so the result is completely immune to error due to discrete harmonic distortion of the signal measurement.

Unlike the full-cycle window where the algorithm uses full-cycle period  $T$ , the half-cycle window algorithm provides information which correspond to only half cycle. If  $U_{x1/2}$  and  $U_{y1/2}$  are

the real and imaginary parts of the phasor that represents the fundamental component derived from a half-cycle window, then equation (3.63) and (3.64) become:

$$U_{x1/2} = a_1 = \frac{2}{T/2} \cdot \int_{t_0}^{t_0+T/2} f(t) \cdot \cos(\omega_0 \cdot t) dt \quad (3.81)$$

$$U_{y1/2} = a_1 = \frac{2}{T/2} \cdot \int_{t_0}^{t_0+T/2} f(t) \cdot \sin(\omega_0 \cdot t) dt \quad (3.82)$$

Following the same procedure as explained before, it is possible to express  $U_{x1/2}$  and  $U_{y1/2}$  in terms of waveform samples  $k$  such that:

$$U_{x1/2} = \frac{4}{N} \cdot \sum_{k=0}^{N/2} u_k \cdot \cos\left(\frac{2\pi k}{N}\right) \quad (3.83)$$

$$U_{y1/2} = \frac{4}{N} \cdot \sum_{k=0}^{N/2} u_k \cdot \sin\left(\frac{2\pi k}{N}\right) \quad (3.84)$$

By comparing equation (3.79) and (3.80) with equation (3.83) and (3.84), it can be seen that the half-cycle window algorithm uses only half number of samples of those used in the full-cycle window. Although calculation of half-cycle window is faster but it has disadvantage of introducing error, specifically due to the presence of even harmonic as shown in figure 3.22.

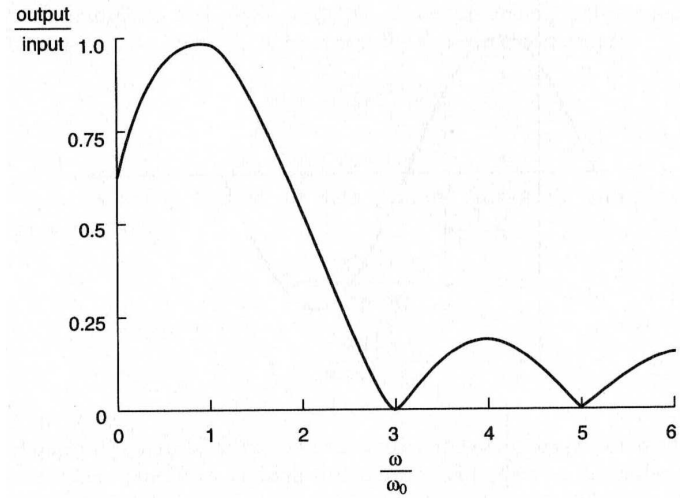


Figure 3.22: The half-cycle window frequency response [10]

### 3.2.3. The Recursive Form

Sampling data in the half and full-cycle window Fourier algorithms is limited only in one or half time period. If the periodic function that needs to be sampled is more than one period, then the recursive form of half or full – cycle window Fourier is applied.

Equation (3.79) and (3.80) for full-cycle window can be expressed in complex exponential form:

$$U = \frac{2}{N} \cdot \sum_{k=0}^N u_k \cdot e^{-jk\theta} \quad (3.85)$$

where  $\theta = \omega_0 \cdot \Delta t$

The computed angle at sample  $\phi_k$  express as:

$$\phi_k = \tan^{-1} \left( \frac{U_{yk}}{U_{xk}} \right) = \tan^{-1} \left( \frac{U_y}{U_x} \right) - k \cdot \theta \quad (3.86)$$

Equation (3.86) means that the computed angle is decreased by the angle  $\theta$  at each sample point. In the recursive form application, it is necessary to correct the rotation. For example, the complex form for the computation involving samples ending at L is examined without the factor  $2/N$ .

$$U_L = \sum_{k=L-N+1}^L u_k \cdot e^{-j(k+L-L)\theta} \quad (3.87)$$

To keep the result of the computation stationary, equation (3.87) is rotated by angle  $(N-L)\theta$ :

$$U_{Lrot} = U_L \cdot e^{j(N-L)\theta} = \sum_{k=L-N+1}^L u_k \cdot e^{-jk\theta} \quad (3.88)$$

$$U_{(L-1)rot} = \sum_{k=L-N}^{L-1} u_k \cdot e^{-jk\theta} \quad (3.89)$$

$U_{(L-1)rot}$  is sampled before  $U_{Lrot}$  therefore:

$$\begin{aligned} U_{Lrot} &= U_{(L-1)rot} + \left[ u_L \cdot e^{-jL\theta} - u_{(L-N)} \cdot e^{-j(L-N)\theta} \right] \\ U_{Lrot} &= U_{(L-1)rot} + \left[ u_L - u_{(L-N)} \cdot e^{-jN\theta} \right] \cdot e^{-jL\theta} \end{aligned} \quad (3.90)$$

Equation (3.90) is the recursive form equation in the complex form. For the full-cycle window  $N\theta = 2\pi$ , and the recursive form of the full-cycle algorithm in real and imaginary part becomes:

$$U_{xnew} = U_{xold} + (u_{new} - u_{old}) \cdot \cos(L\theta) \quad (3.91)$$

$$U_{ynew} = U_{yold} + (u_{new} - u_{old}) \cdot \sin(L\theta) \quad (3.92)$$

In full-cycle algorithm, when  $u_{new} = u_{old}$  then the value of  $U_{xynew}$  and  $U_{xyold}$  is same.

For the half-cycle window  $N\theta = \pi$ , and the recursive form of the half-cycle algorithm in real and imaginary part becomes:

$$U_{xnew} = U_{xold} + (u_{new} + u_{old}) \cdot \cos(L\theta) \quad (3.93)$$

$$U_{ynew} = U_{yold} + (u_{new} + u_{old}) \cdot \sin(L\theta) \quad (3.94)$$

## IV. FAULT ARC AND IMPEDANCE EXTRACTION MODEL AND SIMULATION

### 4.1. The Fault Arc Modeling

The fault arc model used in this thesis is based on the arc model developed by Kizilcay and Pniok in [6] and [9]. As explained previously in Chapter 2, equations for the primary arc model are:

$$\frac{dg}{dt} = \frac{1}{\tau_0} (G - g) \quad (4.1)$$

$$G = \frac{i_{arc}}{(u_0 + r_0 |i_{arc}|) \cdot I_0} \quad (4.2)$$

The time constant and the arc length are relatively constant in this stage ( $\tau_0$  and  $I_0$ ). In the sparkover condition,  $I_0$  is a gap between arcing horns in the string insulator which is equipped by a pair of arcing horn. In the flashover condition it represents the surface string insulator creepage distance without arc fitting. After the faulted pole of the circuit breaker is opened by the protection device, the secondary arc stage begins which is modeled according to:

$$\frac{dg}{dt} = \frac{1}{\tau} (G - g) \quad (4.3)$$

$$G = \frac{i_{arc}}{(u_0 + r_0 |i_{arc}|) \cdot I_{arc}} \quad (4.4)$$

$$I_{arc} = (v_f \cdot t + 1) \cdot I_0 \quad (4.5)$$

$$\tau = \tau_0 - v_\tau \cdot (I_{arc} - I_0) \quad (4.6)$$

At this stage the arc current and the arc column diameter become lower than their condition in the previous stage. The arc length starts to increase as a result of lower dielectric breakdown and at the same time the arc time constant is decreased. Gradual rise of the arc length creates a steady arc extinction state where the arc conductance ( $g$ ) is reduced until nearly zero mho. The arc extinction final limit is determined empirically and only considered the thermal extinction without taken into account the possibility of subsequent dielectric reignition in air:

$$\frac{g_{min}}{I_{arc}} = 0.25 \mu mho / cm \quad (4.7)$$

$$\frac{\max\{\frac{dr}{dt}\}}{I_{arc}} = 64 k\Omega / (s.cm) \quad (4.8)$$

According to the primary arc, the secondary arc and the arc extinction limit formulas above the complete fault arc is modeled by using MODELS language in ATPDraw-EMTP as illustrated in

figure 4.1. From the figure, it can be seen that apart from constant arc parameter input value ( $u_0$ ,  $r_0$ ,  $l_0$ ,  $v_l$  and  $v_\tau$ ), the arc model also utilizes inputs directly from an electrical circuit which consist of the circuit breaker status and the fault arc current. The main output of the model is arc resistance value that feeds into a time varying non-linear resistance (type 91) in the electrical circuit. Other output is open command which is issued to open a switch (type 13) in series with the resistance after all the extinction limits are fulfilled, and to stop the fault arc calculation [11]. In this way, interaction between dynamic fault arc and power system networks is built.

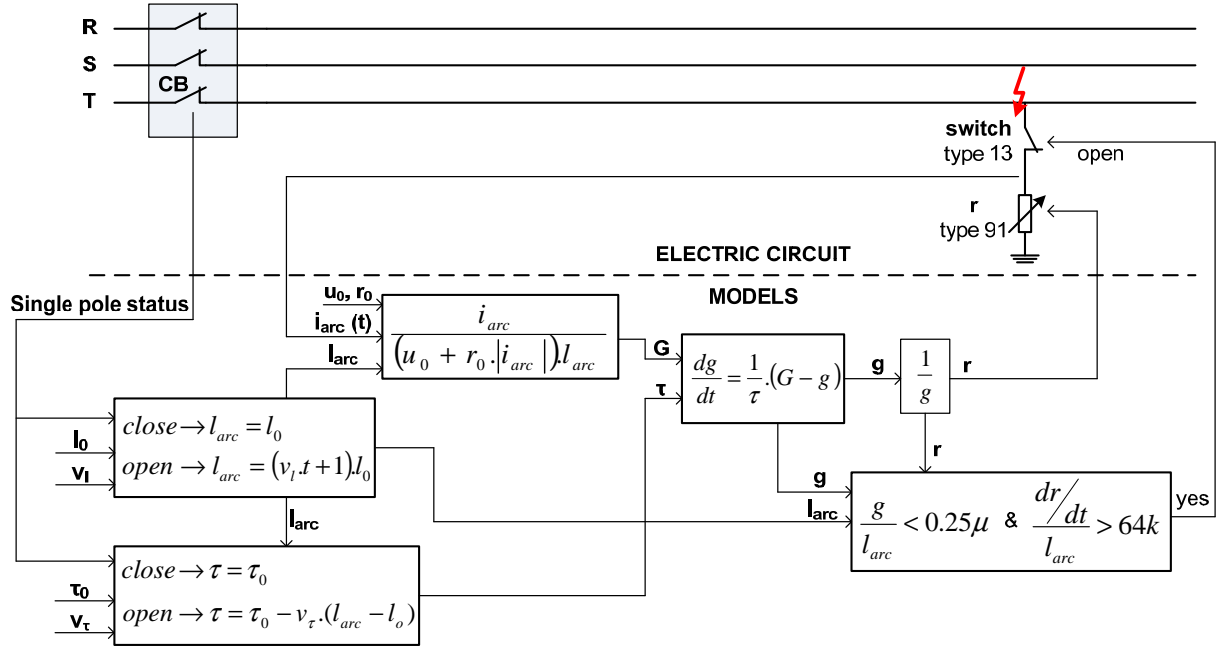


Figure 4.1: Fault arc block diagram representation

#### 4.2. The Impedance Extraction Modeling

The impedance value measured by the distance relays is at fundamental frequency. Although the input current and voltage consist of harmonics, they are filtered in such a way so the final output takes into account impedance at fundamental frequency. Since an impedance extraction will also be used for distance relay performance evaluation, it is important to get impedance value in the fundamental frequency. The algorithm used for impedance derivation is the recursive full-cycle Discrete Fourier Series (DFS) which is also widely used in the distance protection. The current and voltage samples are transformed into phasor quantities by the recursive full-cycle DFS filter according to:

$$U_{real} = \frac{2}{N} \cdot \sum_{k=0}^{N-1} u_k \cdot \cos\left(\frac{2\pi k}{N}\right) \quad (4.9)$$

$$U_{inj} = \frac{2}{N} \cdot \sum_{k=0}^N u_k \cdot \sin\left(\frac{2\pi k}{N}\right) \quad (4.10)$$



$$U_{real} = \frac{2}{N} \cdot \sum_{k=N}^{\infty} (u_{k(new)} - u_{k(old)}) \cdot \cos\left(\frac{2\pi k}{N}\right) \quad (4.11)$$

$$U_{imj} = \frac{2}{N} \cdot \sum_{k=N}^{\infty} (u_{k(new)} - u_{k(old)}) \cdot \sin\left(\frac{2\pi k}{N}\right) \quad (4.12)$$

Outputs from equation (4.9) up to (4.12) are used for the calculation of the short circuit impedance R and X:

$$X = \frac{U_{imj} \cdot I_{real} - U_{real} \cdot I_{imj}}{I_{real}^2 + I_{imj}^2} \quad (4.13)$$

$$R = \frac{U_{real} \cdot I_{real} + U_{imj} \cdot I_{imj}}{I_{real}^2 + I_{imj}^2} \quad (4.14)$$

On the basis of equation (4.9) to (4.14) the impedance is extracted by using MODELS in every time step as shown in figure 4.2. The current and voltage which contain harmonics are taken from the electric network and employed as input for the model. For the first N calculation, equation (4.9) and (4.10) are used to calculate  $U_{real}$  and  $U_{imj}$ . As for the next N calculation, recursive form is implemented through equation (4.11) and (4.12). In this way, the fundamental impedance value is calculated for each time step. Then, the computed X and R are used for the arc and the distance protection analysis.

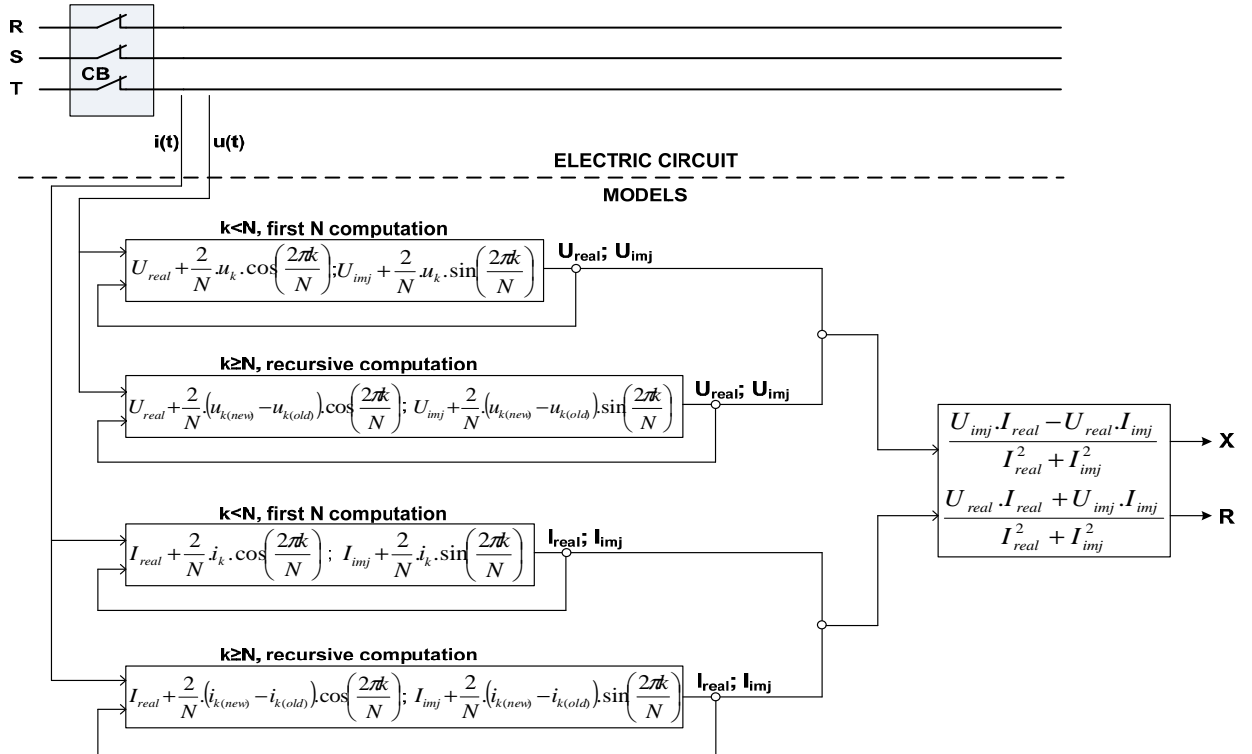


Figure 4.2: Impedance extraction block diagram representation

In case of phase-to-phase or phase-to-ground fault impedance extraction, input  $i(t)$  and  $u(t)$  are replaced by the faulted phase current and voltage. According to equation (3.10) in Chapter 3, for phase-to-phase fault, the impedance will be calculated by:

$$Z_{ph-ph} = \frac{E_{ph1} - E_{ph2}}{I_{ph1} - I_{ph2}} \quad (4.15)$$

For example, in phase A-B fault, input  $i(t)$  and  $u(t)$  will be replaced by:

$$u(t) = u_A(t) - u_B(t) \quad (4.16)$$

$$i(t) = i_A(t) - i_B(t) \quad (4.17)$$

In case of phase-to-ground fault, equation (3.19) and (3.23) in Chapter 3 are applied:

$$Z_{ph-e} = \frac{E_{ph1}}{I_{ph1} + K_N \cdot I_E} \quad (4.18)$$

$$K_N = \frac{Z_0 - Z_1}{3 \cdot Z_1} = \frac{Z_N}{Z_1} \quad (4.19)$$

For a phase A-to-ground fault, input  $i(t)$  and  $u(t)$  will be calculated according to:

$$u(t) = u_A(t) \quad (4.20)$$

$$i(t) = i_E(t) + K_N \cdot i_E(t) \quad (4.21)$$

$$i_E(t) = i_A(t) + i_B(t) + i_C(t) \quad (4.22)$$

#### 4.3. Simulation of The 20 kV Synthetic Test Circuit and Fault Arc Analysis

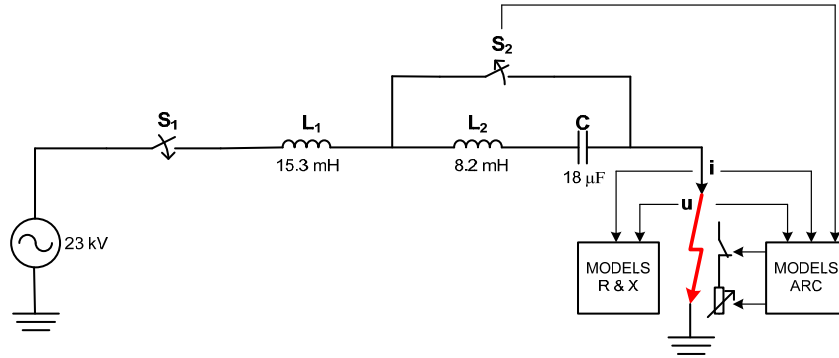


Figure 4.3: 20 kV synthetic test circuit for 380 kV insulator testing

An example which utilizes 20 kV test circuit with 380 kV string insulator arrangements was introduced in [9]. In order to verify the fault arc model that is computed by MODELS in ATPDraw with the real one, the same 20 kV test circuit as shown in figure 4.3 is rebuilt and simulated. Switch  $S_1$  is in 'normally open' position and it will be closed to initiate the primary arc stage until the arc is eventually extinguished. Switch  $S_2$  is in 'normally close' position and it will be opened to start the secondary arc state. It will be closed again right after achieving arc extinction limit.  $S_2$  represents Single Pole Auto Reclosure (SPAR) of the circuit breaker.  $L_1$  serves as source short circuit impedance.  $L_2$  and  $C$  serve as mutually coupling between the faulted phase and the sound phases.

In order to see whether the model is in agreement with the real situation or not, the actual measurements of the synthetic test (the arc current and arc voltage) are compared by the simulation result. The arc parameters data for 380 kV string insulator arrangements are:  $u_0 = 9.65$  V/cm,  $r_0 = 1.62$  m $\Omega$ /cm,  $l_0 = 350$  cm,  $\tau_0 = 1$  ms,  $v_t = 0.285$   $\mu$ s/cm and  $v_l = 45$  cm/ms. The simulation time step is 50  $\mu$ s.

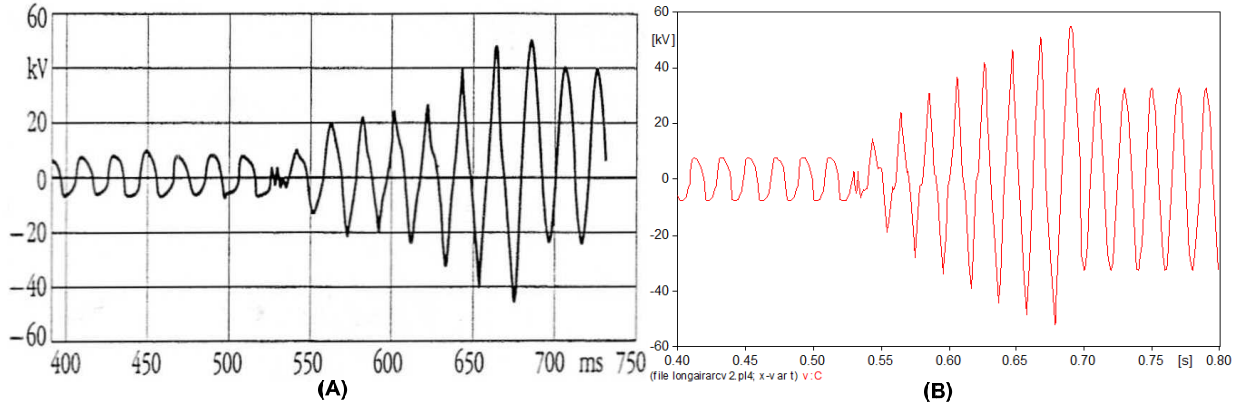


Figure 4.4: Comparison between measured arc voltage [9] (A) and arc voltage simulation result (B)

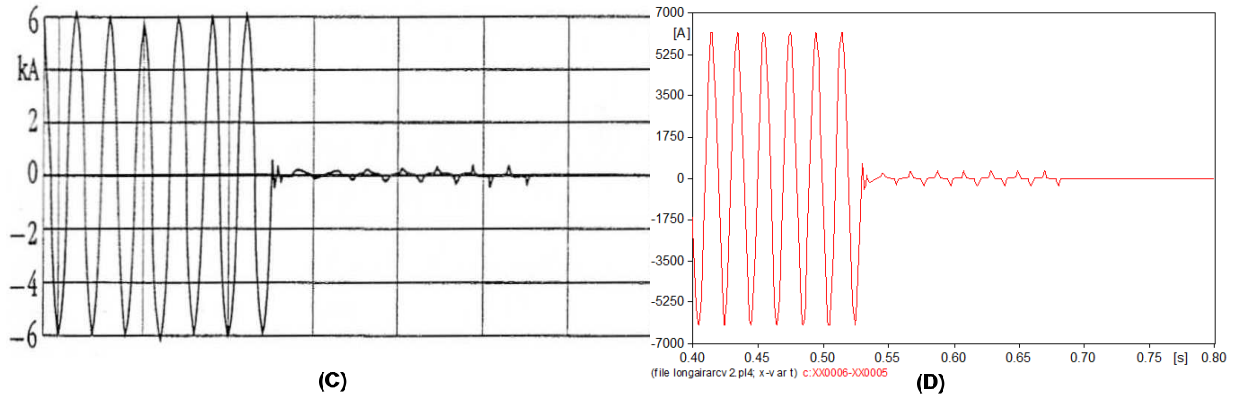


Figure 4.5: Comparison between measured arc current [9] (A) and arc current simulation result (B)

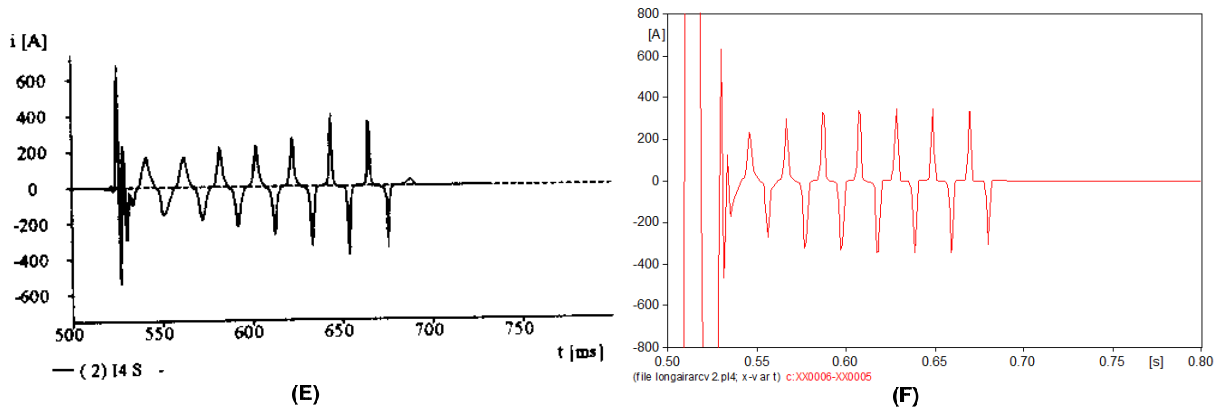


Figure 4.6: Comparison between measured secondary arc current [9] (A) and secondary arc current simulation result (B)

The comparison between the current and voltage arc measurement records with the simulation outputs are displayed in figure 4.4 to 4.6. It can be seen that both the magnitude and the shape of current and voltage wave as well as the arc duration are closely similar to each other.

In other words, the fault arc model established in the simulation can be adopted to represent the fault arc for distance protection performance analysis. The challenging part is to determine the primary arc parameters ( $u_0$ ,  $r_0$  and  $\tau_0$ ) for different voltage level and the secondary arc parameters behavior ( $v_l$  and  $v_t$ ). The determination of these parameters will be discussed further in the next sub section.

Figure 4.7 and 4.8 show all important results of the simulation. In figure 4.7, the arc voltage and current behavior for different arc stage is illustrated. The primary arc voltage is lower than the normal voltage; it represents short circuit voltage. The primary arc duration in this case is 0.524 s. As soon as the secondary arc state begins, the arc voltage gradually increases as a response to the reduced arc current and the secondary arc parameter influence. The arc voltage will reach the recovery voltage value after the arc is extinguished, in about 0.16 ms. By contrast, the arc current magnitude has a high value in the primary arc state due to lower arc resistance. In the secondary state, the current is much lower than the previous stage due to high arc resistance and mutual coupling L1 and C.

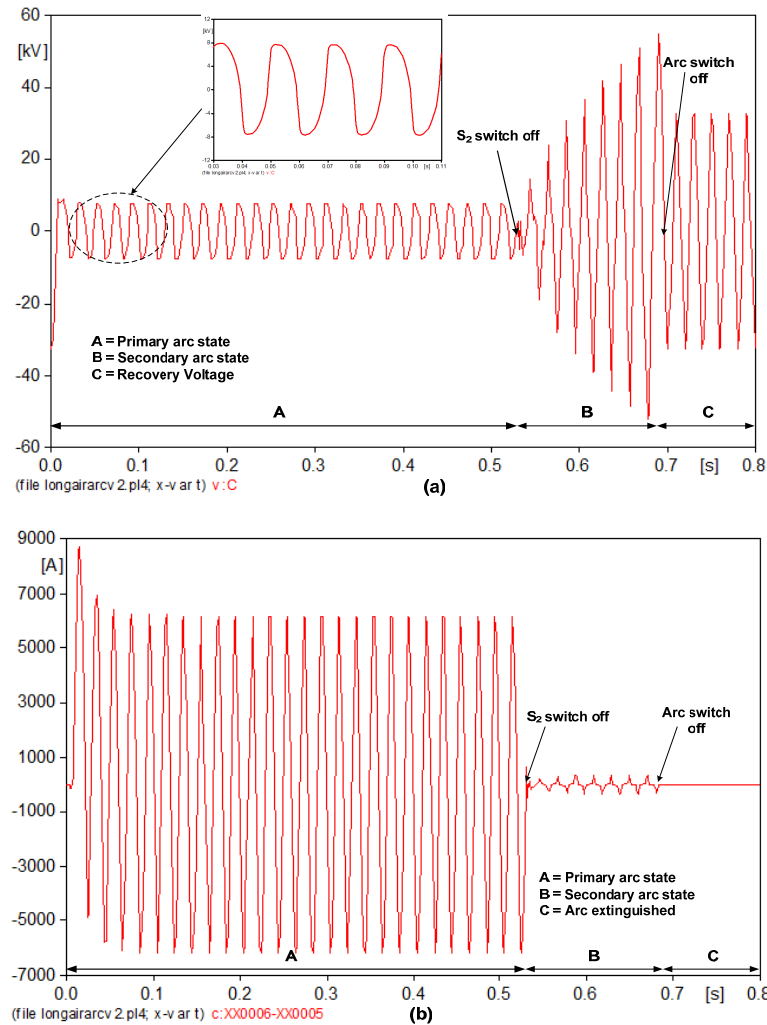


Figure 4.7: The simulation arc voltage (a) and current (b)

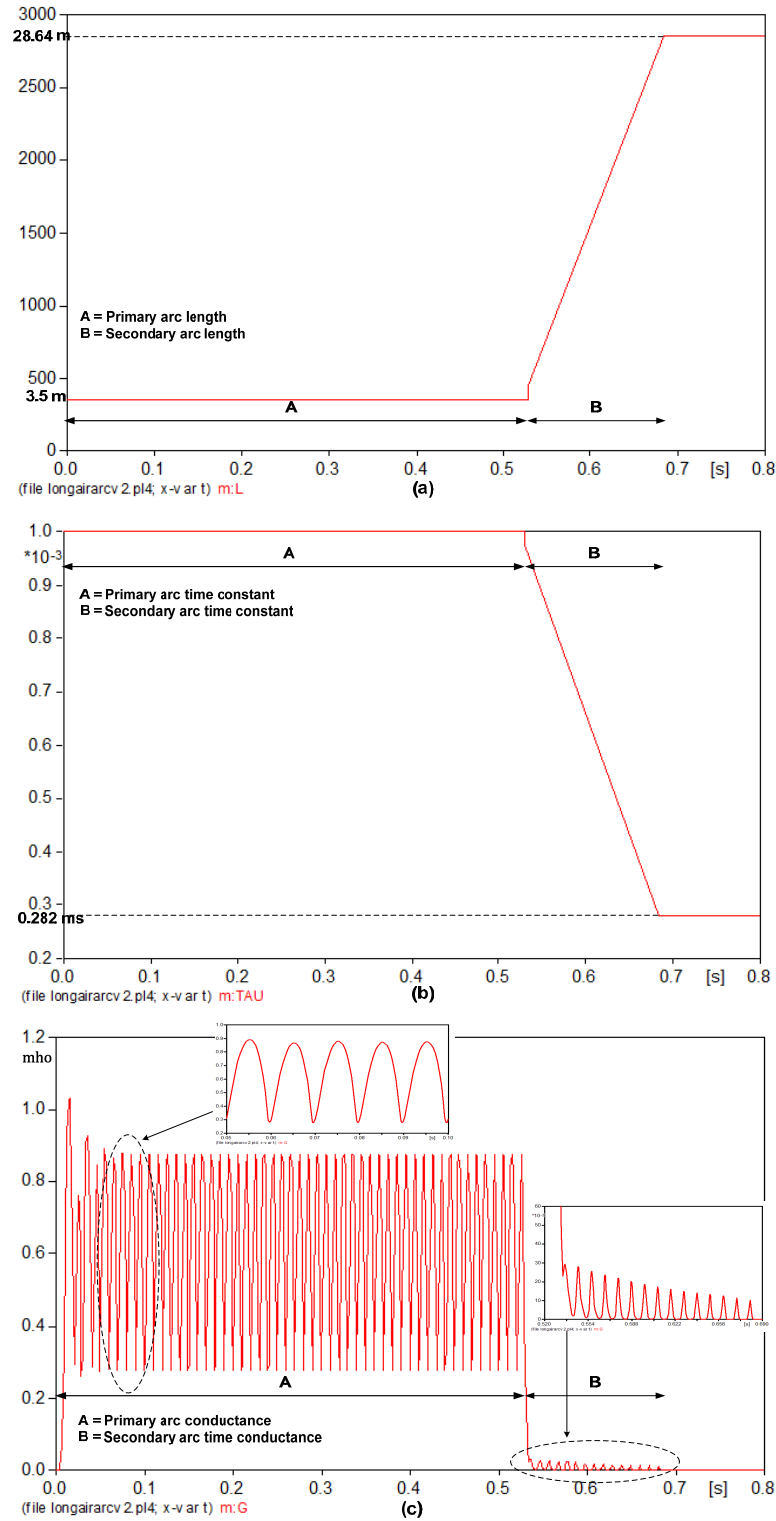


Figure 4.8: The simulation arc length (a), arc time constant (b) and arc conductance (c)

During the arc duration, the arc length elongates linearly approximately 8 times its original length, from 3.5 m to 28.64 m (figure 4.8). Conversely, the time constant in the secondary stage decreases linearly to 0.282 ms. The arc length, arc time constant and arc duration are highly dependent on selected time parameter,  $v_i$  and  $v_r$ , and the extinction limit value. These values are derived empirically in [6] to fit with the measurement condition which is based on steady arc

extinction phenomena. In practice, the air movement, wind velocity, convection of the plasma and electro-dynamical force highly affect the secondary arc. These random phenomenas are difficult to be defined and to be implemented in digital simulation. However, existing time parameters and extinction limit method are sufficient to determine maximum dead time setting and to realize the SPAR studies. In the last graph at figure 4.8, the characteristic of the fault arc is represented by a time varying conductance. The arc conductance is a source of high order harmonics which distort the arc voltage into a near square wave (fig 4.7).

Another important fact from the arc studies is arc volt-ampere characteristic as shown in figure 4.9 and 4.10. In this characteristic, the relation between arc voltage and current are shown in a hysteresis loop. The hysteresis loop of the arc occurs in the first and third quadrant of the plane, and indicates the predominantly resistive nature of the arc. In general for primary and secondary arcs, when the current increases, the arc voltage also increases proportionally with the current. Until a certain value (about 30 % of the current peak in primary arc in this case), the arc voltage becomes constant although the current rises continuously. With the decrease of the current, the arc voltage decreases approximately linear to the current, viewing constant arc resistance characteristic. Two different voltage behaviors during increase and decrease current occur. The more the current increases, the arc temperature becomes higher due to the accumulated arc energy, and also as a result of increasing arc conductivity [4]. During the primary arc stage, the characteristic approximately follows the same path. Unlike previous stage, the situation is different for the secondary arc stage. The characteristic has different value in each cycle of secondary arc because at this stage the arc elongates and the arc resistance becomes inconsistent.

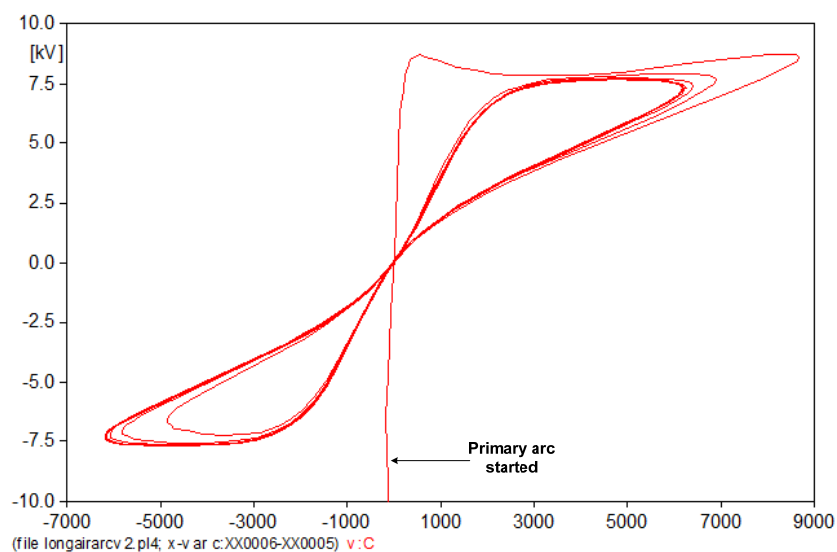


Figure 4.9: Primary arc volt-ampere characteristic

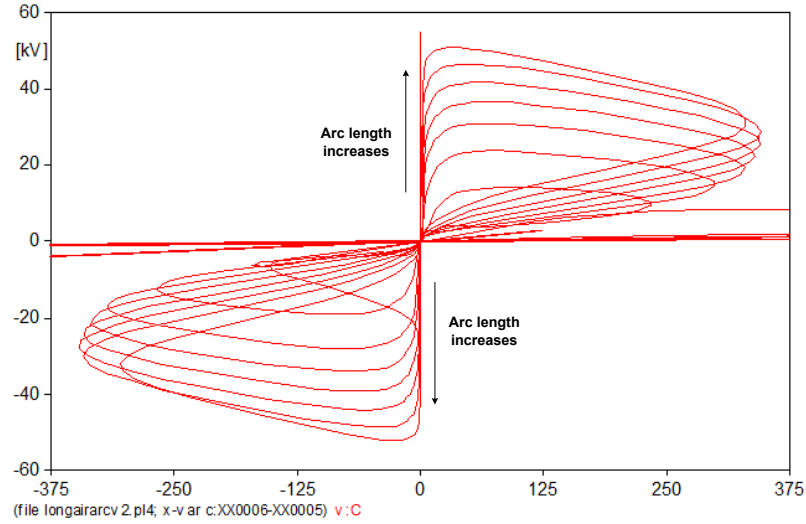


Figure 4.10: Secondary arc volt-ampere characteristic

As mention before, the non-linear arc with dominant resistive characteristic in nature is the source of harmonics which takes effect in the arc voltage and the current shape. If the arc voltage and current are put at the same graph, it is obvious that the arc current slightly lags the arc voltage as shown in figure 4.11. To strengthen this hypothesis, the impedance extraction model developed in section 4.2 is applied to reveal the fundamental frequency (50 Hz) impedance characteristic of the short circuit arc. With time step ( $\Delta t$ ) 50  $\mu$ s and fundamental period ( $T_0$ ) 20 ms, 400 number of samples per cycle (N) is yield. The curves of R and X as a result of impedance extraction are viewed in figure 4.11 and 4.12. The first N after recursive DFS computation initiation is the transition interval; therefore it does not represent the real fundamental impedance. It can be seen that the fault arc has not only resistive identity but also inductive behavior, which can be assigned to the non-linear characteristic of the arc. The primary arc impedance in this case is constant with  $R = 1.36 \Omega$  and  $X = 0.24 \Omega$ . While the secondary arc impedance increases and depends on the arc time constant and arc elongation.

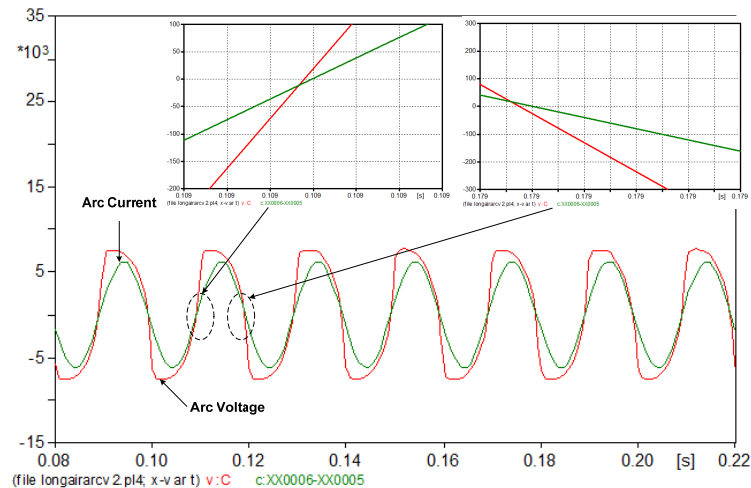


Figure 4.11: The arc current lags the arc voltage

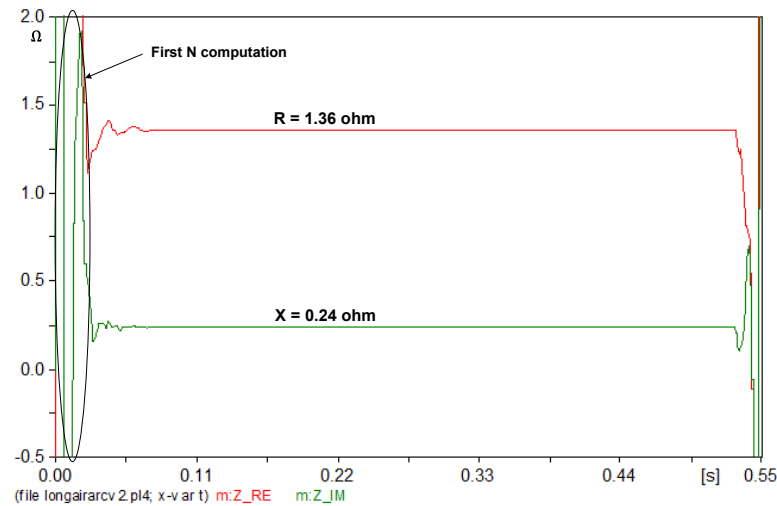


Figure 4.12: Fundamental frequency primary arc impedance

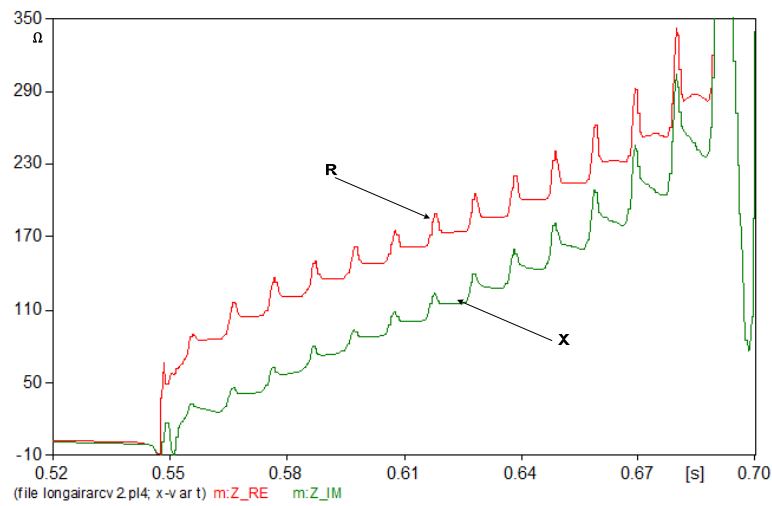


Figure 4.13: Fundamental frequency secondary arc impedance

#### 4.4. The Arc Parameters in 150 kV System

The purpose of this section is to find out the arc parameters  $u_0$ ,  $r_0$ ,  $\tau_0$  and  $v_i$  in 150 kV system by reconstructing several single phase-to-ground arcing faults condition in South Sumatra 150 kV system using ATPDraw software. After the faults condition are simulated, the terminal voltage and current simulation results are compared with the measurements taken from distance protection disturbance recorders. And by adjusting the arc parameters value the simulation is repeated until the simulation results fit with the measurements. Two main points should be considered when fitting arcing fault in South Sumatra overhead transmission lines:

- Initial length of the arc column  $l_0$ . There are two types of string insulator in South Sumatra 150 kV system that determine  $l_0$ . Firstly, the string insulator which is equipped with arcing horn or arc fitting, in this type  $l_0 = 120$  cm. Hereinafter this type is called as type A. Secondly, the string insulator without the arc fitting. In this case  $l_0$  is assumed 150 % the length of string insulator (143 cm),  $l_0 = 215$  cm and this type is further called as type B. The assumption of  $l_0$  in this type



is based on the fact that the primary arc current flows in the concave surface of string insulator having a tendency to breakdown and create shorter path bypassing the concave area. These two types will be analyzed separately in different cases in this section.

- b. Effective tower footing impedance  $Z_{EF}$ . There are three parameters that determine  $Z_{EF}$  as explained in 3.1.5.5.; the earth wires impedance  $Z_{EW}$ , average span between towers  $l_{AS}$  and tower footing resistance  $R_{TF}$ . In 150 kV South Sumatera system, all overhead lines use the same type of earth wire, GSW 55, which has value  $R_{EW} = 1.35 \Omega/\text{km}$  and  $X_{EW} = 0.77 \Omega/\text{km}$ . The average span between towers is 0.4 km. And the tower footing resistance is in the range of 2 - 20  $\Omega$ . The effective tower impedance ( $Z_{EF}$ ) value for  $R_{FT}$  5, 10 and 15  $\Omega$  describe in table below by calculation using equation (3.53) – (3.55) in Chapter 3:

Table 4.1. Effective tower impedance for different  $R_{FT}$  value

NO	$R_{FT}$ $\Omega$	$R_{EW}$ $\Omega/\text{km}$	$X_{EW}$ $\Omega/\text{km}$	$Z_{EW}$ $\Omega/\text{km}$	$l_{AS}$ km	$Z_{LW}$ $\Omega$	$Z_{EF}$ $\Omega$	$R_{EF}$ $\Omega$	$X_{EF}$ $\Omega$
1	5	1.35	0.77	1.55 $\angle$ 29.70	0.4	2.09 $\angle$ 17.40	0.87 $\angle$ 14.42	0.84	0.22
2	10	1.35	0.77	1.55 $\angle$ 29.70	0.4	2.81 $\angle$ 16.67	1.24 $\angle$ 14.63	1.20	0.31
3	15	1.35	0.77	1.55 $\angle$ 29.70	0.4	3.37 $\angle$ 16.34	1.52 $\angle$ 14.70	1.47	0.39

From the data in the table above, it is apparent that the tower footing resistances become low due to the presence of earth wires as a good conductor. It can be seen that the effective footing impedance contains inductive component besides the resistive part. In single phase-to-ground fault  $Z_{EF}$  will take part as constant impedance fault which can affect the impedance measurement by the distance relay, especially in the case of infeed from opposite side. According to this reason, it is necessary to put  $Z_{EF}$  in series with non – linear arc resistance in fault arc situation.

Previous power (primary) arc test research [8] presented the pattern of a primary arc parameter ( $u_0$ ,  $r_0$  and  $\tau_0$ ) in 20, 110 and 220 kV systems in relation to the length of the arc fitting and the short circuit current as shown in the next figure.

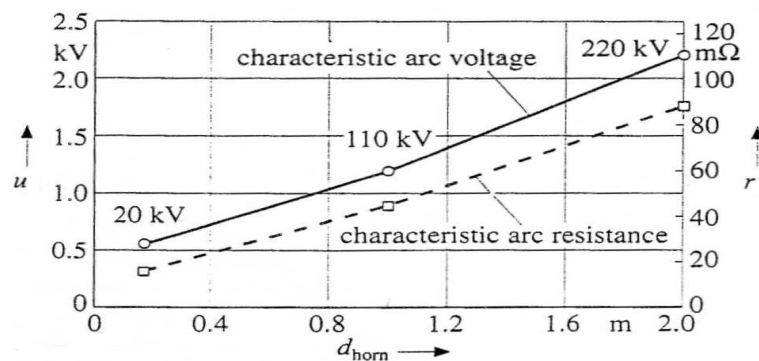


Figure 4.14:  $u$  and  $r$  versus the arcing horn gap  $l_0$  [8]

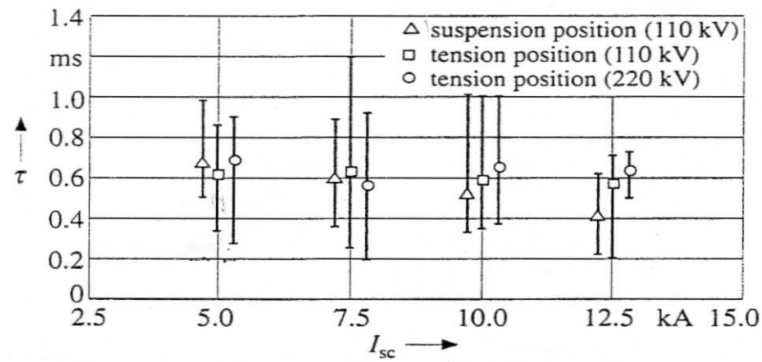


Figure 4.15:  $\tau_0$  versus different short circuit current [8]

Above figures are used as guidelines for adjusting primary arc parameters  $u_0$ ,  $r_0$  and  $\tau_0$ . In figure 4.14, the relationship between characteristic arc voltage and resistance with primary arc length in different voltage level obtained from power arc test are presented. Figure 4.15 describes the arc time constant range value in different string insulator position (suspension/vertical and tension/horizontal arrangements) in relation with the difference of the short circuit current.

In the arc simulation, here and next chapter, the speed of time constant decrease parameter ( $v_t$ ) is inversely proportional with the primary arc length ( $l_0$ ) [6] as shown in equation below:

$$v_t = 0.1 / l_0 \text{ ms/cm} \quad (4.23)$$

#### 4.4.1. Arcing Fault on 15 February 2007, Type A string Insulator

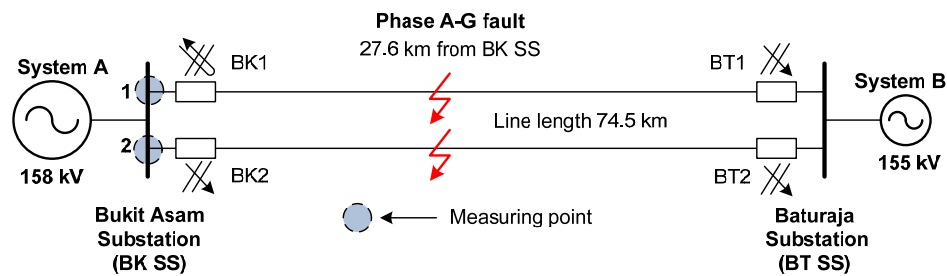


Figure 4.16: Fault situation on 15 February 2007, 23:00

Figure 4.16 illustrates two arcing faults (phase A to ground) in 150 kV line 1 and 2 between Bukit Asam and Baturaja Substation. In this line section, all string insulators are type A insulator with  $l_0 = 120$  cm. Based on fault recorders data, the fault location are 27.6 km from Bukit Asam substation. Other important data obtained from fault recorders in each line side are shown in table 4.2.

Table 4.2. Fault data 15 February 2007, 23:00

Fault Recorders Position		BK 1	BK 2	BT 1	BT 2
Fault Trigger assumed at (ms)		0			
Circuit Breaker (CB) sequence	Trip Pole A (ms)	57.4	59.9	81.7	101.7
	Trip Pole B (ms)	-	789.8	81.7	-
	Trip Pole C (ms)	-	797.3	81.7	-
	Close Pole A (ms)	784.5	797.3	-	-
	Close Pole B (ms)	-	-	-	-
	Close Pole C (ms)	-	-	-	-
	At the end of fault	Close 3 Pole	Close Pole A only	Open 3 Pole	Close pole B and C only
	Dead time SPAR setting (ms)	700	700	700	700
Voltage inception angle (°)		75.6	73.8	75.6	73.8
Pre-fault Load Transfer (MW)		75.4	75.2	-74.5	-74
Pre-fault Load Transfer (MVAR)		2.07	2.08	3.83	3.73
Pre-fault Voltage Phase A (kV)		90.8	91.5	89	89.2
Pre-fault Voltage Phase A-B (kV)		158	158	155	155
Pre-fault Current Phase A (A)		270	260	268	270
Pre-fault Voltage-Current angle (°)		3.1	3	184.4	184.5

According to above fault data, the arcing fault situations are rebuilt in ATPDraw-EMTP software. Total simulation fault duration is 1.155 s, with pre-fault duration 340 ms and the simulation time step ( $\Delta t$ ) 10  $\mu$ s. To represent each component of the network, model elements provided by ATPDraw software are used either for single element or for building a new component. Besides arc and impedance extraction model, the main elements used in this simulation are transmission line model, generator model, circuit breaker model and impedance model.

#### 4.4.1.1. The Transmission Line Model

Several line models are available in ATP Draw – EMTP software. They are lumped parameter models (RLC  $\pi$  and RL coupled), distributed parameter lines with constant parameters, lines with constant or frequency dependent parameters (PI, Bergeon, JMarti, Semlyen and Noda) which are calculated by means of the Line and Cable Constant (LCC) supporting routine of ATP - EMTP. PI section model is often used for short transmission line, where the travelling time is less than the simulation time step [13]. When the travelling time is larger than the simulation time step, frequency dependent model is utilized. Figure 4.17 illustrated flowchart for transmission line model selection.

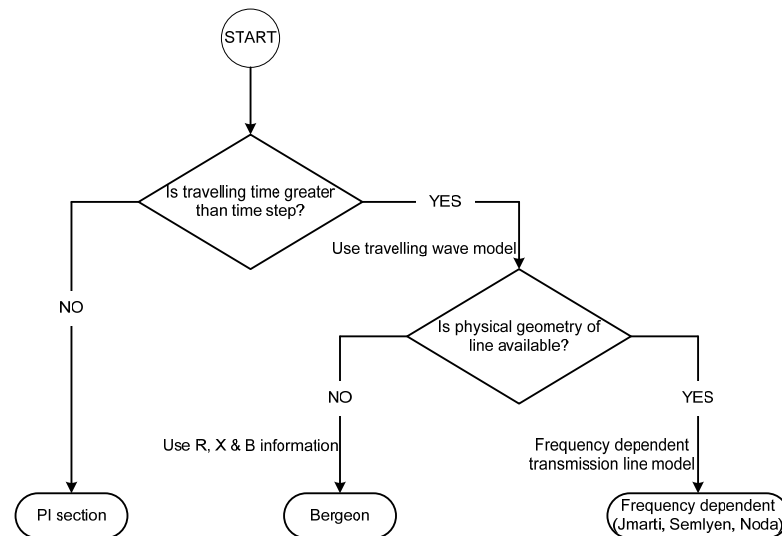


Figure 4.17: Flowchart for transmission line model selection [13]

According to the above decision tree, frequency dependent model is used for calculating overhead line parameters. The calculated line parameters are positive sequence impedance, zero sequence impedance, mutual coupling between phase in the same line and mutual coupling between lines. The overhead line Bukit Asam – Baturaja consists of unbundle phase wire conductor ACSR 240/40 mm<sup>2</sup> and ground wire GSW 55 mm<sup>2</sup>. The physical geometry of line (tower and wire) is shown in table 4.3 and figure 4.18. The comparison between JMarti and Semlyen calculation results, with the reference of PI model data by using verified option in LCC menu, show that JMarti model produces a better result in zero, positive and mutual sequence impedances.

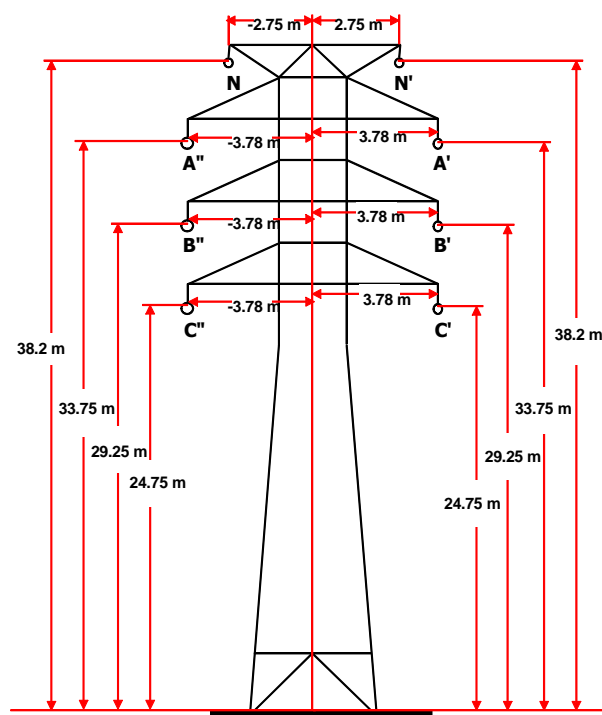


Table 4.3. Bukit Asam-Baturaja conductor & earth wire data

DATA PARAMETER		VALUE
ACSR 240/40 mm <sup>2</sup>	outer radius $r_{out}$ (mm)	9.481
	inner radius $r_{in}$ (mm)	3.545
	dc resistance at 30°C $r_{dc}$ (Ω)	0.1247
GSW 55 mm <sup>2</sup>	outer radius $r_{out}$ (mm)	4.183
	inner radius $r_{in}$ (mm)	0
	dc resistance $r_{dc}$ (Ω)	1.35
Earth resistivity (Ωm)		100




Figure 4.18: Bukit Asam-Baturaja tower construction data and LCC symbol

All above technical data employ as input for LCC JMarti model. In the simulation ATPDraw-EMTP software will calculate all necessary line parameters.

#### 4.4.1.2. The Generator Voltage Source Model

Element AC 3-ph type 14 uses as generator voltage source model for represent system A and B three phase voltage input. The data input for AC 3-ph type 14 in system A and B are shown in table below. Maximum amplitude phase voltage data are calculated by multiplication of phase to phase voltage with  $(2^{\frac{1}{2}} / 3^{\frac{1}{2}})$ .

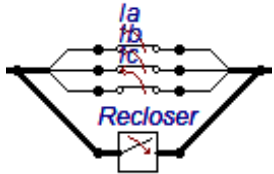
Table 4.4. AC 3-ph type 14 simulation data and symbol

DATA PARAMETER	SYSTEM A	SYSTEM B	SYMBOL
Max amplitude phase voltage (V)	129006.46	126556.97	
Frequency (Hz)	50	50	
Phase shift (°)	101.5	103	

#### 4.4.1.3. The Circuit Breaker Model

The circuit breaker model incorporates 4 elements connected in parallel for representing circuit breaker with single shot SPAR operation. Those elements consist of three time controlled switches and one 3-phase switch. Each time controlled switch symbolizes each pole of the circuit breaker and 3-phase switch expresses single shot SPAR operation. The circuit breaker simulation data is taken from fault data in table 4.2 with additional pre – fault time 340 ms as shown in table below.


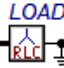

Table 4.5. Circuit breaker simulation data and symbol

CB POSITION		BK 1	BK 2	BT 1	BT 2	SYMBOL
Pole A	Closing time (s)	-1	-1	-1	-1	
	Opening time (s)	0.3974	0.3999	0.4217	0.4417	
Pole B	Closing time (s)	-1	-1	-1	-1	
	Opening time (s)	-	1.1298	0.4217	-	
Pole C	Closing time (s)	-1	-1	-1	-1	
	Opening time (s)	-	1.1373	0.4217	-	
SPAR	Closing time (s)	1.17	1.1373	-	-	
	Opening time (s)	-	-	-	-	

#### 4.4.1.4. The Impedance Model

There are 4 components in the simulation that are modeled by using impedance element (resistance or reactance) either in 3 phase or single phase. All those components with their setting input are described in table 4.6.

Table 4.6. The impedance model simulation data and symbol

IMPEDANCE MODEL		SYSTEM A	SYSTEM B	ATP DRAW MODEL & SYMBOL
3 phase short circuit impedance ( $Z_{sc}$ )	Pos. sequence $Z_1$ ( $\Omega$ )	$1.21 + j10.1$	$13.83 + j57.3$	Symmetric RL coupled line 
	Zero sequence $Z_0$ ( $\Omega$ )	$0.94 + j9.14$	$70.52 + j119.8$	
3 phase load model ( $\Omega$ )			115	RLC-Y-3 phase 
1 phase eff. footing tower impedance $Z_{ef}$ ( $\Omega$ )		$1.2 + j0.31$		RLC-1 phase 

System A is stronger than system B. By using Digsilent software, the 3-phase impedance sort circuit is calculated. Stronger system has lower  $Z_{sc}$  than weaker system. According to pre-fault data condition, the load flow prior to the fault is to Baturaja direction. Based on this data, the load model is placed in Baturaja substation. The average tower footing resistance is assumed  $10 \Omega$ , with respect to this value  $Z_{EF}$  is calculated and put in series with the fault arc.

#### 4.4.1.5. Simulation Results

With the recorded fault data reference in table 4.2, and by using all models component in previous explanation, arcing fault occurrence on 15 February 2007 at 23 hours is duplicated in ATP Draw as shown in figure 4.19. To fit with the terminal voltage and current measurements, the arc parameters are adjusted by applying graphs in figure 4.14 and 4.15 as guidelines.

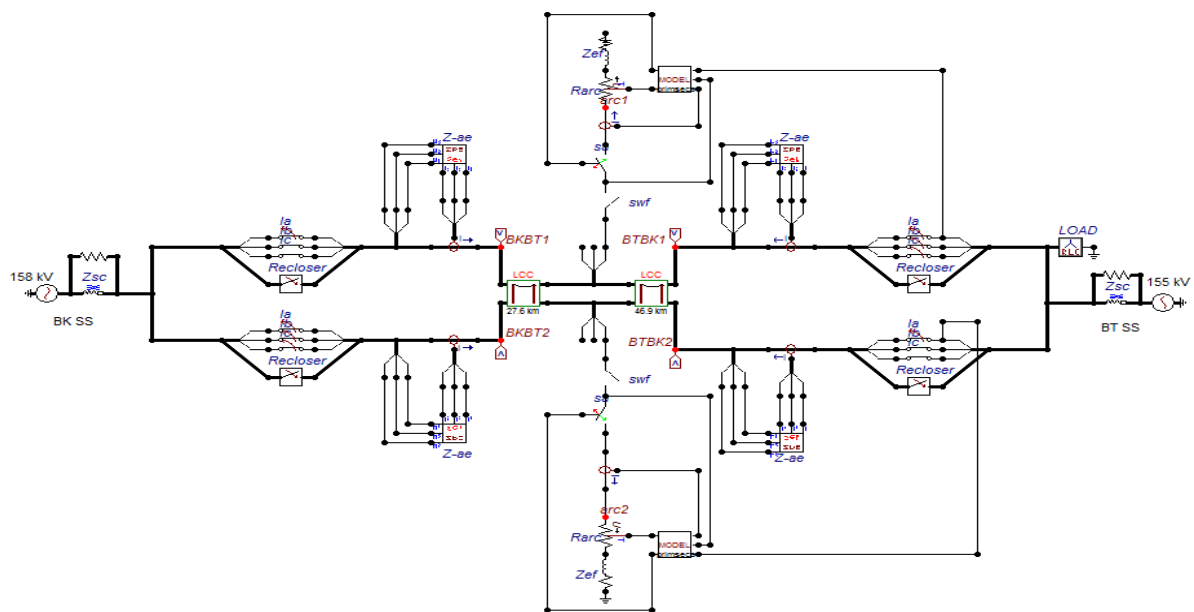


Figure 4.19: ATP Draw model of fault arc on 15 February 2007

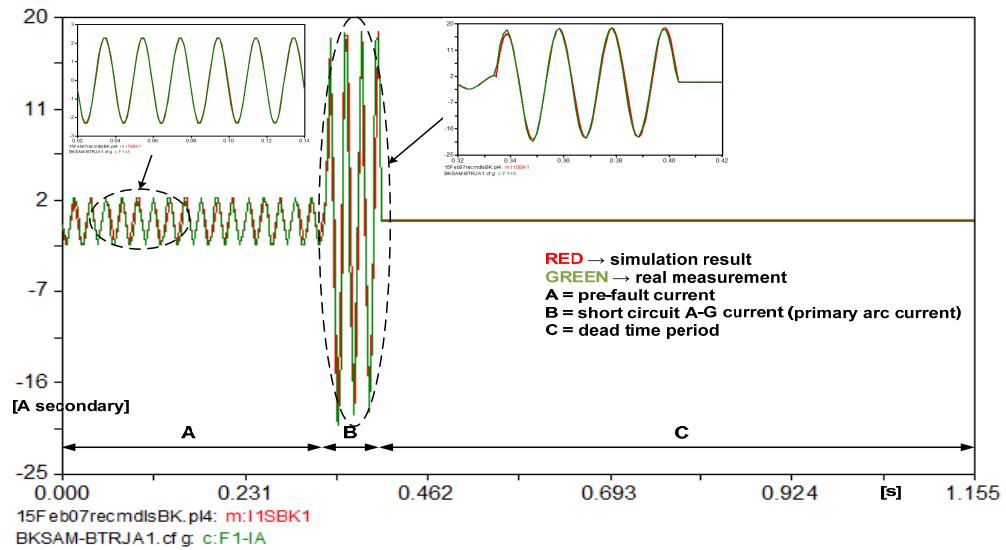


Figure 4.20: Terminal current comparison (phase A) at line 1 Bukit Asam substation

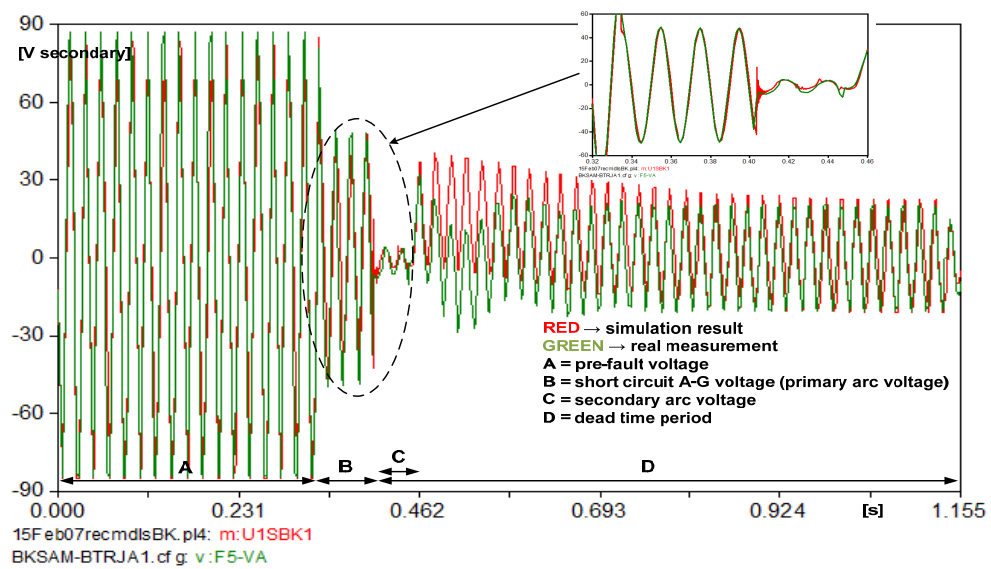


Figure 4.21: Terminal voltage comparison (phase A) at line 1 Bukit Asam substation

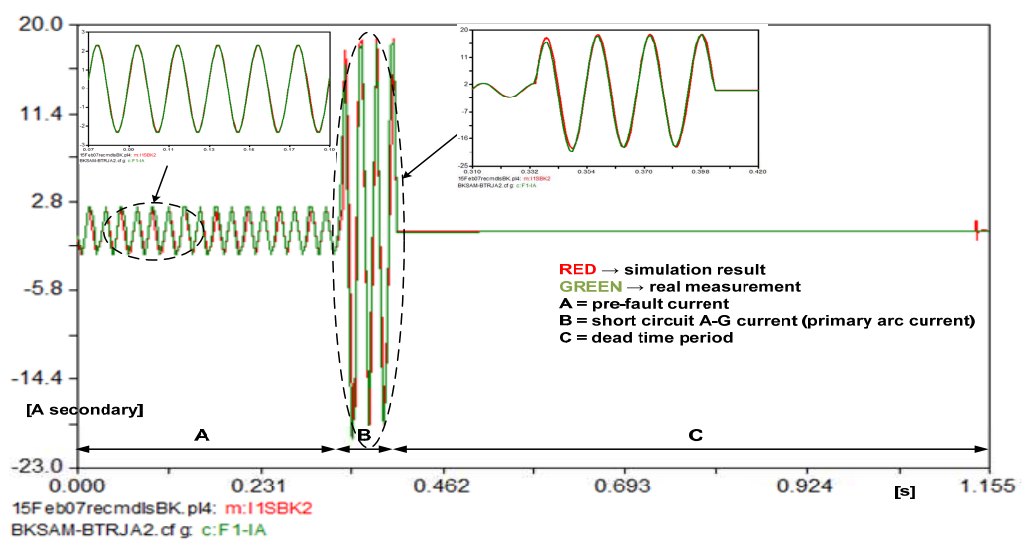


Figure 4.22: Terminal current comparison (phase A) at line 2 Bukit Asam substation

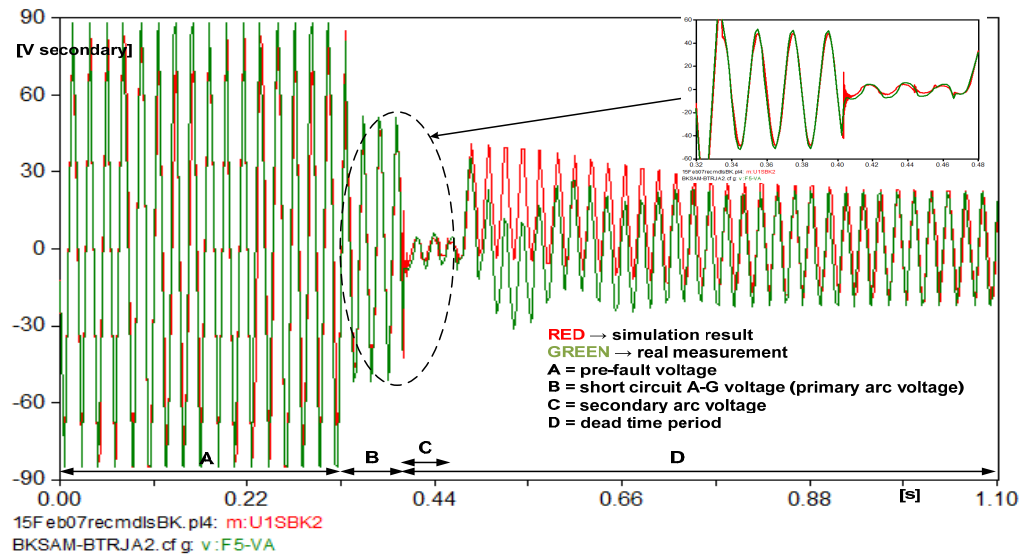


Figure 4.23: Terminal voltage comparison (phase A) at line 2 Bukit Asam Substation

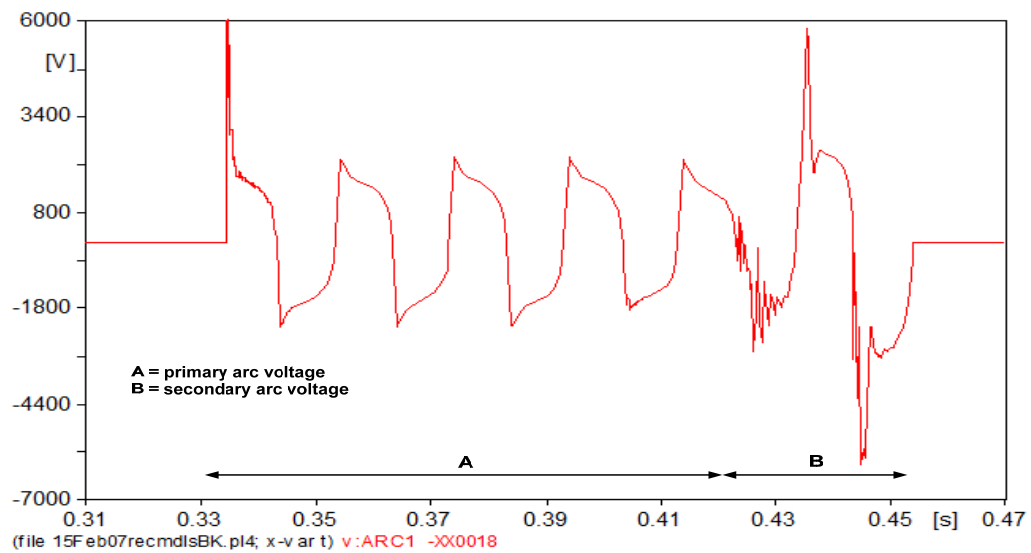


Figure 4.24: Line 1 arc voltage estimation, 15 February 2007

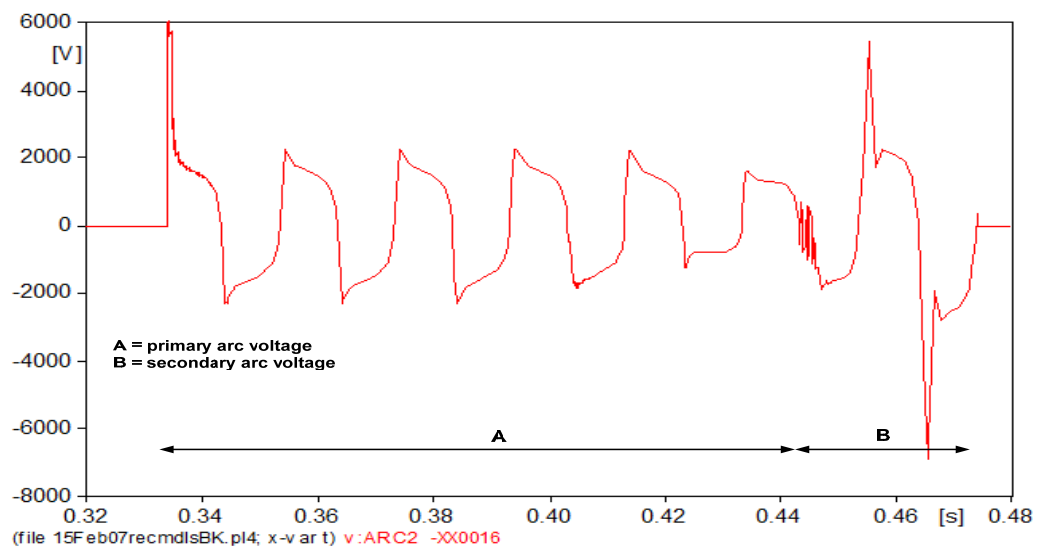


Figure 4.25: Line 2 arc voltage estimation, 15 February 2007



Table 4.7. Arc parameters final adjustment result, fault arc 15 February 2007

ARC PARAMETER	FAULT ARC A-G LINE 1	FAULT ARC A-G LINE 2
$l_0$ (cm)	120	120
$u$ (kV)	1.38	1.38
$r$ (m $\Omega$ )	53	53
$\tau_0$ (ms)	0.5	0.5
$v_l$ (cm/ms)	45	35
$v_t$ ( $\mu$ s/cm)	0.833	0.833
final arc length (cm)	294.4	333.7
primary arc duration (ms)	88.98	89.1
secondary arc duration (ms)	30.63	50.88

The final adjustment results are compared with the actual data measurement records at Bukit Asam Substation side in figure 4.20 – 4.23. Note that the current and voltage value are all in secondary side value with current transformer (CT) ratio 800/5 and voltage transformer (PT) ratio 150/0.1. The extinction limits in equation (4.7) and (4.8) are applied in the simulation fault arc model. The final arc parameters for fault arc in line 1 and line 2 including their duration and length are displayed in table 4.7. It can be concluded that graphs in figure 4.14 and 4.15 propose precise approximation arc parameters value ( $u_0$ ,  $r_0$  and  $\tau_0$ ) in 150 kV voltage level for type A string insulator with  $l_0 = 120$  cm.

In Chapter 5, the distance protection performance will be evaluated at fault arc incident with post processing plot file in ISA TDMS software. To know whether the impedance generates by post processing calculation in ISA TDMS software is same with the result of the impedance extraction model in MODELS or not, both impedance extraction methods from fault arc 15 February 2007 simulation are compared.

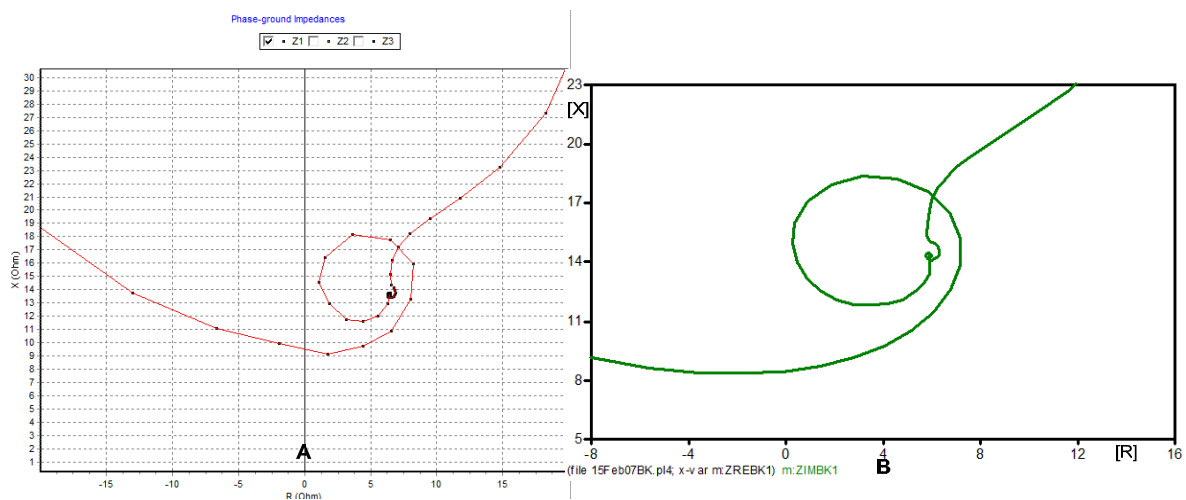


Figure 4.26: A. TDMS ISA impedance extraction, B. ATP Draw impedance extraction

Figure 4.26 describes that the result of post processing impedance extraction in ISA TDMS is similar with the impedance extraction method developed in MODELS. Both impedance extraction methods are reliable for terminal impedance analysis. The sampling rate – solution time step in graph A and B are 10 kHz – 100  $\mu$ s and 100 kHz – 10  $\mu$ s. In reality, the sampling rate of digital protection relay is much lower than this value.

#### 4.4.2. Arcing Fault on 3 March 2006, Type B String Insulator

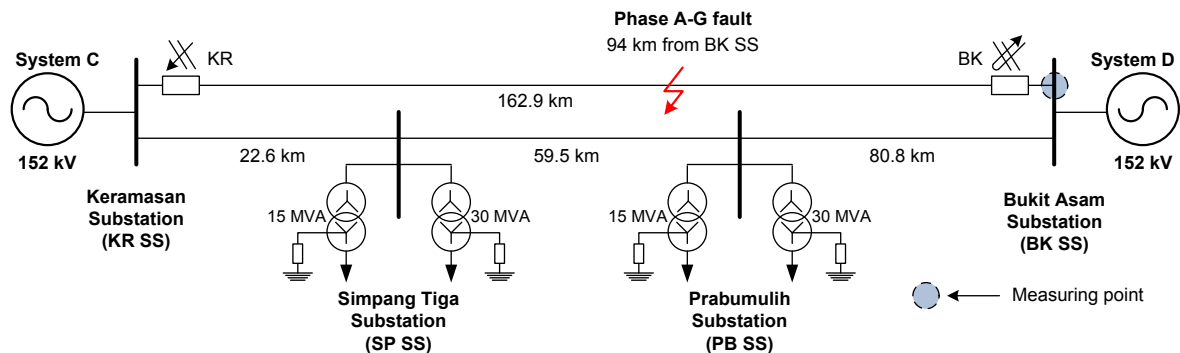


Figure 4.27: Fault situation on 3 March 2006, 04:30

Figure 4.27 illustrates arcing fault condition (phase A-to-ground) in line 150 kV express feeder Keramasan – Bukit Asam substation. In this line section, all string insulators are type B with  $l_0$  assumed 215 cm. Based on fault recorders data, the fault location is 90 km from Bukit Asam substation. At the pre-fault condition, the load flows from Keramasan to Bukit Asam substation. In the next line, the feeder passes through two other substations with two power transformers at each substation. Other important data obtained from fault recorders at Keramasan and Bukit Asam side are shown in table 4.8.

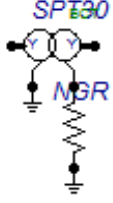
Table 4.8. Fault data 3 March 2006, 04:30

Fault Recorders Position		KR	BK
Fault Trigger assumed at (ms)		0	
Circuit Breaker (CB) sequence	Trip Pole A (ms)	72.5	62.5
	Trip Pole B (ms)	77.5	-
	Trip Pole C (ms)	80.0	-
	Close Pole A (ms)	-	766.6
	Close Pole B (ms)	-	-
	Close Pole C (ms)	-	-
	At the end of fault	Open 3 Pole	Close 3 Pole
	Dead time SPAR setting (ms)	700	700
Voltage inception angle (°)		109.7	109.7
Pre-fault Load Transfer (MW)		53.9	53.4
Pre-fault Load Transfer (MVAR)		21.1	11.5
Pre-fault Voltage Phase A (kV)		85.7	88.6
Pre-fault Voltage Phase A-B (kV)		152	152
Pre-fault Current Phase A (A)		210	200
Pre-fault Voltage-Current angle (°)		25.2	195.1

#### 4.4.2.1. Simulation Models

The model elements used to simulate fault arc on 3 March 2006 are the same as the previous fault analysis with additional power transformer model. The transformer is modeled by BCTRAN routine in ATPDraw. The data parameters for modeling 15 MVA and 30 MVA power transformers are displayed in table 4.9.

Table 4.9. The transformer model simulation data and symbol

DATA PARAMETER		15 MVA	30 MVA	ATP DRAW MODEL & SYMBOL
Voltage Rating		150/20 kV	150/20 kV	
Connection		YN-yn0	YN-yn0	
Open Circuit Test	Position	LV-LV	LV-LV	
	Voltage (%)	100	100	
	Current (%)	0.102	0.14	
	Losses (kW)	13	23.203	
Short Circuit Test	Position	HV-LV	HV-LV	
	Impedance (%)	12.5	12.99	
	Power (MVA)	15	30	
	Losses (kW)	108	104.045	

The short circuit impedances for system A and B behind each substation are more or less the same, for the system A:  $Z_{1sc} = 1.72 + j19.9$   $Z_{0sc} = 7.59 + j58.99$ ; and for the system B:  $Z_{1sc} = 1.65 + j14$   $Z_{0sc} = 10.4 + j45$ . Tower and wire geometry as data input for LCC JMarti model are illustrated and mentioned in the figure and the table below.

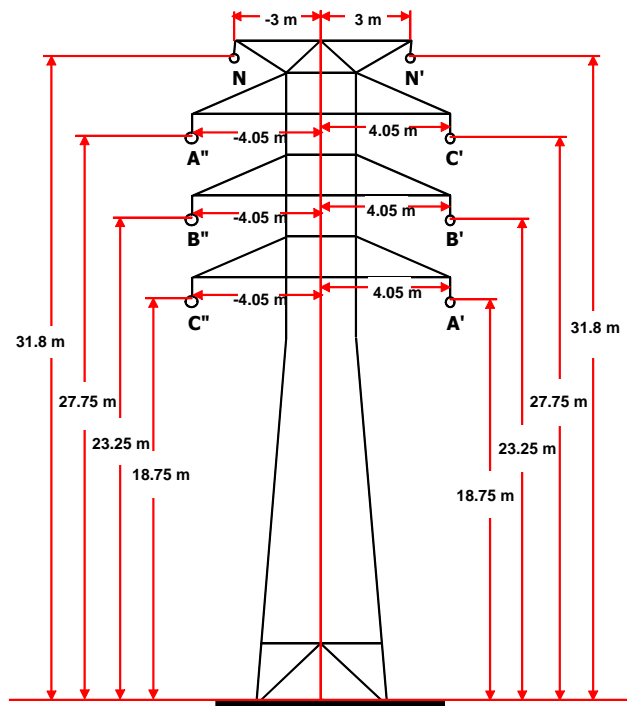


Figure 4.28: Keramasan – Bukit Asam tower construction data

Table 4.10. Keramasan – Bukit Asam conductor & earth wire data

DATA PARAMETER		VALUE
ACSR 280/35 mm <sup>2</sup>	outer radius $r_{out}$ (mm)	9.997
	inner radius $r_{in}$ (mm)	3.2939
	dc resistance at 30°C $r_{dc}$ ( $\Omega$ )	0.1068
GSW 55 mm <sup>2</sup>	outer radius $r_{out}$ (mm)	4.183
	inner radius $r_{in}$ (mm)	0
	dc resistance $r_{dc}$ ( $\Omega$ )	1.35
Earth resistivity ( $\Omega m$ )		30 & 100

#### 4.4.2.2. Simulation Results

According to fault data at table 4.8, the arcing fault situation is rebuilt in ATPDraw-EMTP software. Total simulation fault duration is 1.15 s, with pre-fault duration 335 ms and the solution time step  $\Delta t$  10  $\mu$ s. ATPDraw model of arcing fault on 3 March 2006 and its simulation results in comparison with the measurements are described in the figure below:

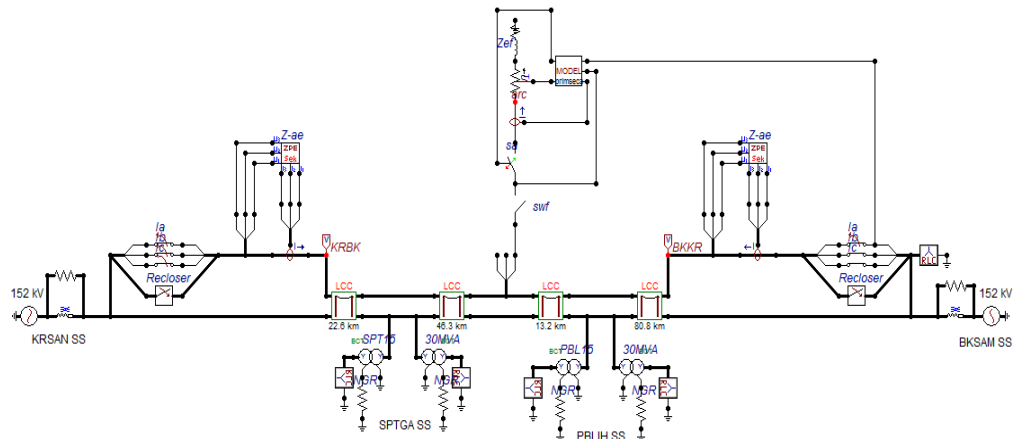


Figure 4.29.ATP Draw model of fault arc on 3 March 2007

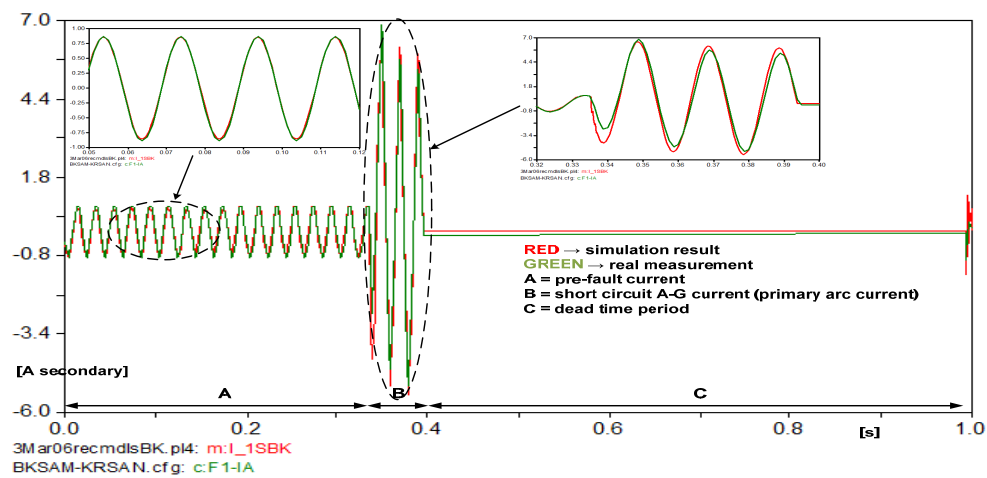


Figure 4.30: Terminal current comparison (phase A) at Bukit Asam substation

Table 4.11. Arc parameters final adjustment result, fault arc 3 March 2006

ARC PARAMETER	FAULT ARC A-G
$l_0$ (cm)	215
$u$ (kV)	0.9
$r$ (m $\Omega$ )	40
$\tau_0$ (ms)	0.9
$v_l$ (cm/ms)	22
$v_t$ ( $\mu$ s/cm)	0.466
final arc length (cm)	1407.5
primary arc duration (ms)	58.6
secondary arc duration (ms)	251.5

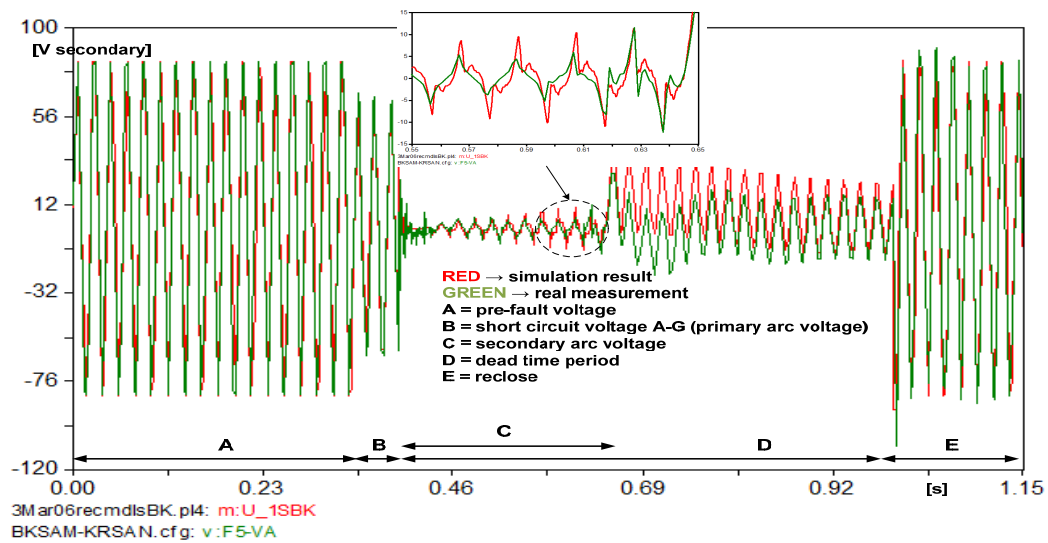


Figure 4.31: Terminal voltage comparison (phase A) at Bukit Asam substation

The terminal current and voltage after the arc parameter final adjustment are compared with the actual measurement data at Bukit Asam substation side in figure 4.30 – 4.31. Note that the current and voltage value are all in secondary side value with current transformer (CT) ratio 1600/5 and voltage transformer (PT) ratio 150/0.1. The final arc parameters of phase A-to-ground in express feeder Keramasan – Bukit Asam including the arc duration and length are displayed in table 4.11. In the case of type B string insulator, the graph in figure 4.14 cannot be used as reference for characteristic voltage and impedance ( $u$  and  $r$ ) arc parameter adjustment. At  $l_0 = 215$  cm in 150 kV voltage level,  $u$  and  $r$  tend to decrease more than previous case for type A string insulator with  $l_0 = 120$  cm.

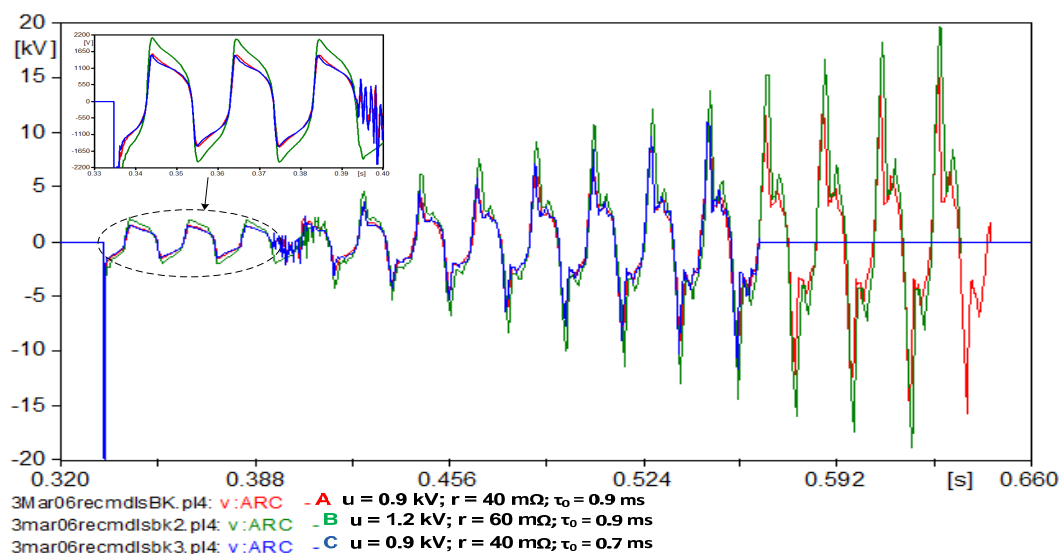


Figure 4.32: Arc voltage estimation with  $u$ ,  $r$  and  $\tau_0$  variation; 3 March 2006

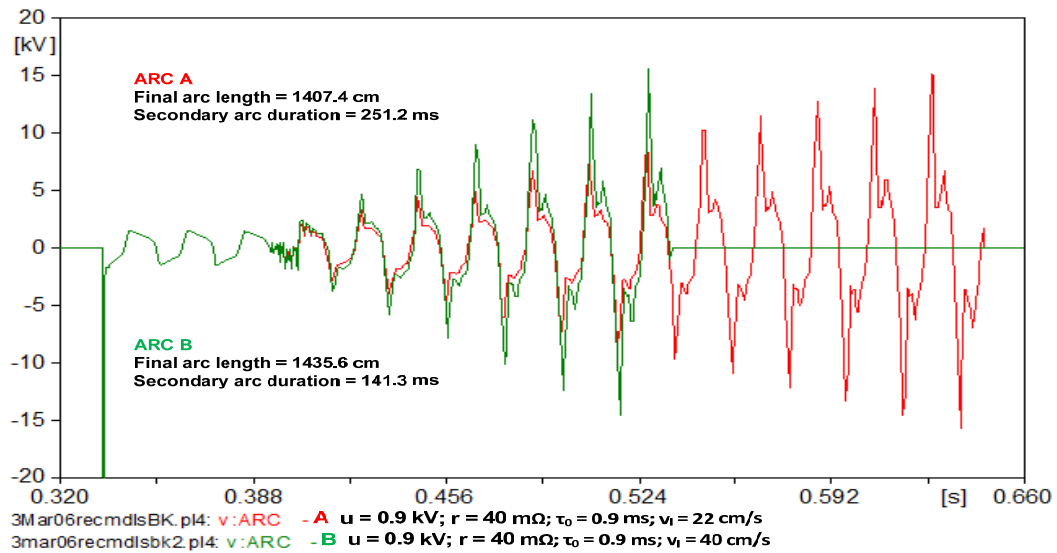


Figure 4.33: Arc voltage estimation with  $v_l$  variation; 3 March 2006

Figure 4.32 and 4.33 show the effect of  $u$ ,  $r$ ,  $\tau_0$  and  $v_l$  variation on the arc voltage estimation. Lower  $\tau_0$  parameter gives shorter secondary arc duration. Higher  $u$  and  $r$  parameter tend to increase the magnitude of primary and secondary arc voltage. In the other case, speed of arc elongation is increased to 40 cm/s. With the variation of  $v_l$ , the secondary arc voltage magnitude and the final arc length increase, whereas the secondary arc duration is shorter than in the case of lower  $v_l$ .

#### 4.5. Conclusion

1. The arc model developed by MODELS in ATPDraw-EMTP gives similar result with measurements. This model can be adopted as fault arc representation in further studies.
2. Although an arc has resistive characteristic in nature, impedance extraction at fundamental frequency reveals that the arc also has inductive behavior. It is also apparent that the primary arc stage has more or less constant impedance at its fundamental frequency.
3. Impedance extraction generated by post processing calculation in TDMS software gives similar result with impedance extraction model developed by using MODELS in ATP Draw. Both methods can be used for terminal impedance analysis of distance protection.
4. Correlation between  $I_0$  versus  $u$  and  $I_0$  versus  $r$  in different voltage level as shown in figure 4.14 is only valid for arc occurrence in string insulator which is equipped with arcing horn (type A); while for arc occurrence in string insulator without arcing horn those relationships cannot be used as reference.
5. The arc parameters in 150 kV voltage level based on two cases in South Sumatera system are:

Table 4.12. Arc parameters, fault arc 15 February 2007 and 3 March 2006

ARC PARAMETER	CASE 1 LINE 1	CASE 1 LINE 2	CASE 2
String insulator	Type A	Type A	Type B
$l_0$ (cm)	120	120	215
$u$ (kV)	1.38	1.38	0.9
$r$ (m $\Omega$ )	53	53	40
$\tau_0$ (ms)	0.5	0.5	0.9
$v_l$ (cm/ms)	45	35	22
$v_r$ (ms/cm)	0.833	0.833	0.466
final arc length (cm)	294.4	333.7	1407.5
primary arc duration (ms)	88.98	89.1	58.6
secondary arc duration (ms)	30.63	50.88	251.5

6. The dead time SPAR setting in South Sumatera system (700 ms) is more than enough to cover secondary arc duration based on several fault records data.
7. The relationship between arc parameters and the arc voltage describes as: the characteristic voltage and resistance ( $u$  and  $r$ ) are proportional to the primary and secondary arc voltage magnitude; the time constant ( $\tau_0$ ) parameter is proportional to the secondary arc duration; the speed of arc elongation ( $v_l$ ) is proportional to the secondary arc voltage magnitude but inversely proportional with the secondary arc duration.

## V. FAULT ARC SIMULATION CONDITION IN 150 KV SYSTEM AND DISTANCE PROTECTION PERFORMANCE EVALUATION

### 5.1. General

The purpose of this chapter is to simulate fault arc occurrences in South Sumatera 150 kV system based on the arc model and parameters obtained in Chapter 4, and to evaluate the performance of the existing distance protection setting to response to those faults. The fault arc condition will be simulated with ATPDraw-EMTP. The setting characteristic will be designed and evaluated by post processing impedance extraction in TDMS software based on terminal current and voltage of the fault arc simulation. Figure 5.1 illustrates South Sumatera 150 kV system with several phase-to-ground fault arc points that will be simulated alternately. String insulator type B (without arcing horn) is used in the line section Simpang Tiga to Bukit Asam substation. Outside this section, type A (with arcing horn) is implemented.

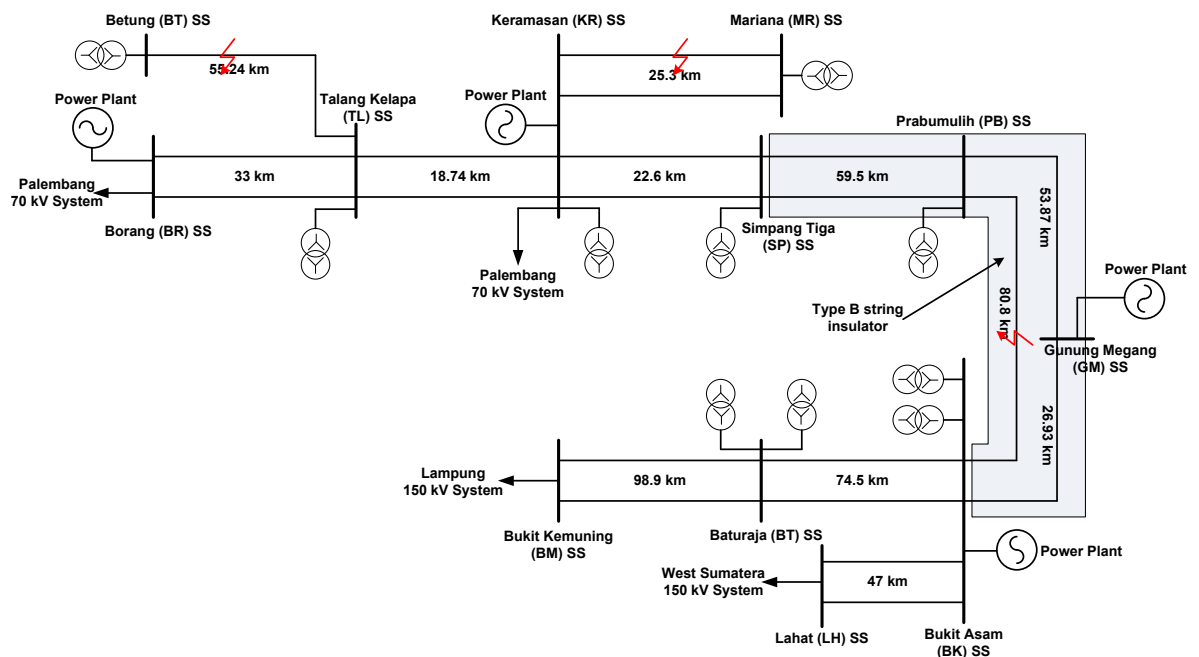


Figure 5.1. South Sumatera 150 kV system

During normal operating condition, South Sumatera system exports power to its surrounding systems from 4 main operating power plants. The data for load model is taken from a log-sheet of real operation condition on 23 January 2009 at 20.00. The total load and generation power in South Sumatera system at that time are 424.4 MW/128.1 MVAR and 532 MW/128.7 MVAR. The load data together with voltage data on each substation are used as a reference for



simulating pre-fault condition of the system. Number of active power plant unit data are employed for the calculation of the short circuit impedance of each power plant and other systems.

A fault clearing time is an important aspect for simulating a fault condition in the system. The Fault clearing time describes the total duration of a system protection, which consists of the relay protection, the signaling scheme and the circuit breaker, from the detection of the fault by relay protection until clearing the fault by opening of the circuit breaker. According to PLN standard, SPLN52 – 1, the maximum total fault clearing time in 150 kV system is 120 ms; with distribution of 40 ms for the relay pick-up and operating time, 20 ms for signaling time and 60 ms for opening time of the circuit breaker. In this chapter, because the main focus is only at zone 1 distance protection performance, the two others factor can be ignored. The total fault arc duration in the simulation will be 40 ms which also represent the primary arc duration.

Regarding the fault arc simulation and distance protection evaluation, besides maximum fault clearing time, other criteria that must be considered are:

a. Distance protection sampling rate.

The numerical distance protection investigated in this system has sampling rate ( $f_s$ ) 12048.2 Hz, or in sampling period ( $\Delta t$ ) 0.83 ms, or  $15^\circ$  electrical degrees. This relay protection will be operated in zone 1 setting if the measured impedance is continuously in the area of zone 1 setting for 13.3 ms or 16 times of sampling. Furthermore, to make the analysis easier, the post processing impedance extraction will be converted into sampling rate 12048 Hz and 16 times of sampling will be used as a reference for evaluating distance relay performance in zone 1.

b. Effective tower footing impedance  $Z_{ef}$ .

Because the average tower footing resistance in South Sumatera system is  $10 \Omega$ , as described in Chapter 4,  $Z_{ef} = 1.2 + j0.31 \Omega$  is connected in series with the fault arc model.

c. Design characteristic setting.

All distance relays in 150 kV South Sumatera system adopt quadrilateral characteristic for their setting. The design characteristic of investigated distance relay is plot in R – X plane by using design distance characteristic in TDMS software. With this software, the quadrilateral characteristic is designed in ohm-phase domain both phase-to-phase and phase-to-ground elements.

d. Positive and zero sequence impedance data.

PLN database line impedances data which are also based on calculation (not measurement) have different value in comparison to LCC JMarti routine calculation of ATPDraw-EMTP. Differences are especially in the zero sequence impedance which reaches up to 50 %. These differences influence zero sequence compensation factor ( $K_N$ ) value and the distance relay

performance analysis. Based on those considerations, the distance protection setting is recalculated by using LCC JMarti calculation impedances data.

e. Arc Parameters.

Table 5.1 shows the arc parameters which are used in the fault arc simulation.

*Table 5.1. The arc parameters for the fault arc simulation*

ARC PARAMETER	Type A String Insulator	Type B String Insulator
$l_0$ (cm)	120	215
$u$ (kV)	1.38	0.9
$r$ (m $\Omega$ )	53	40
$\tau_0$ (ms)	0.5	0.9
$v_l$ (cm/ms)	22	22
$v_t$ (ms/cm)	0.833	0.466

Speed of arc elongation ( $v_l$ ) is set to the same value 22 cm/s for both types of insulator, based on the lowest speed obtained in Chapter 4, in order to see the maximum secondary arc duration for dead time setting evaluation.

- f. The measured terminal current, voltage, impedance and setting impedance are all in the primary side value.
- g. Single Pole Auto Relosure (SPAR) is triggered only by zone 1 phase-to-ground element, and signaling scheme elements, other than those elements the distance relay will issue three pole tripping to the circuit breaker without reclose operation. Two and three poles auto reclosure is not activated.

There are three fault phase A-to-ground points that will be simulated and analyzed alternately in this chapter. Those fault points consist of radial single circuit, radial double circuit and non-radial double source double circuit.

## 5.2. Design Quadrilateral Characteristic in Ohm-phase Domain

As explained in Chapter 3, both phase-to-phase and phase-to-ground setting elements can be designed either in ohm-phase or ohm-loop domains. Distance relay manufacturers have specific design domain for their products. Table 5.2 shows distance relay types with their design domain.

*Table 5.2. Distance relay types and design domain*

SETTING ELEMENTS		ABB REL511	Siemens 7SA511	GE UR-D60	Toshiba GRZ100
Phase-to-phase	Zone 1	Ohm-phase	Ohm-phase	Ohm-phase	Ohm-phase
	Zone 2				
	Zone 3				
	Zone 4				
Phase to ground	Zone 1	Ohm-loop	Ohm-phase	Ohm-phase	Ohm-phase
	Zone 2				Ohm-phase
	Zone 3				Ohm-loop
	Zone 4				Ohm-loop

The design characteristic in TDMS software for distance performance evaluation uses ohm-phase domain in all setting element.

In this part, Keramasan – Mariana 4 zones setting example will be discussed and be implemented to the design characteristic element in TDMS software. The 25.3 km protected line Keramasan – Mariana section has positive and zero sequence impedance data as follows:  $Z_1 = 1.01 + j7.46 = 7.52 \angle 82.28^\circ \Omega$ ,  $Z_0 = 7.13 + j25.31 = 26.49 \angle 74.37^\circ \Omega$ . Because this section is a radial network and normally operated in double circuit line (as illustrated in figure 5.1), the adjacent protected line for zone 2 and 3 calculation is the parallel line itself which has the same positive and zero sequence impedance. The impedance range setting and zero sequence compensation factors ( $K_N$ ) for this line are:

$$\text{Zone1} = 80\% \cdot Z_{1\text{protected-line}} = 0.81 + j5.97\Omega \quad (5.1)$$

$$\text{Zone2}_{\text{minimum}} = 120\% \cdot Z_{1\text{protected-line}} = 1.21 + j8.95\Omega \quad (5.2)$$

$$\text{Zone2}_{\text{maximum}} = Z_{1\text{protected-line}} + 50\% \cdot Z_{1\text{adjacent-line}} = 1.52 + j11.18\Omega \quad (5.3)$$

$$\text{Zone3} = Z_{1\text{protected-line}} + Z_{1\text{adjacent-line}} = 2.02 + j14.91\Omega \quad (5.4)$$

$$\text{Zone4}_{\text{reverse}} = 25\% \cdot Z_{1\text{protected-line}} = 0.23 + j1.68\Omega \quad (5.5)$$

$$K_N = \frac{Z_0 - Z_1}{3 \cdot Z_1} = 0.845 \angle -11.02^\circ \quad (5.6)$$

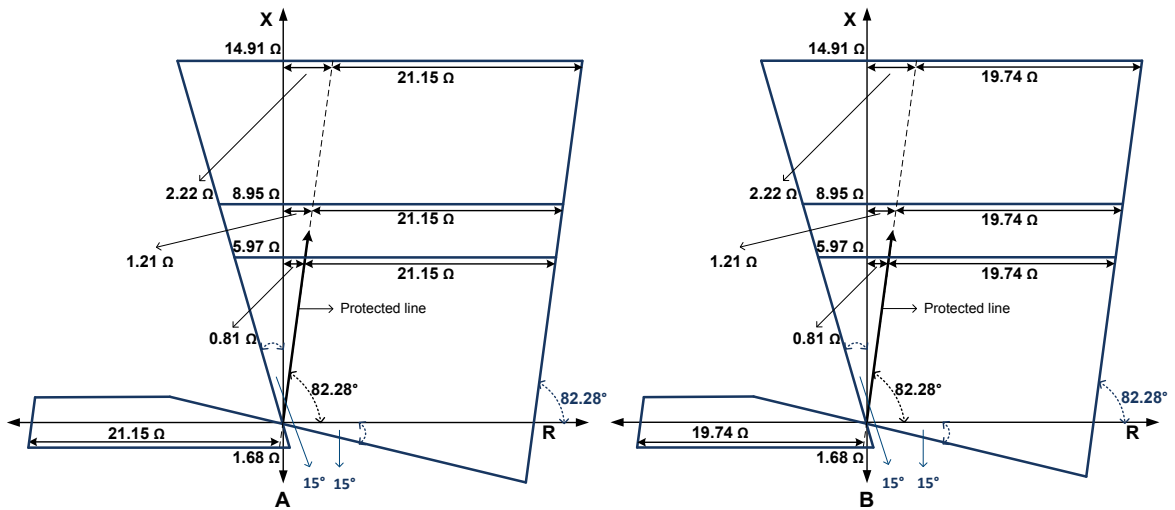


Figure 5.2. Phase-to-phase (A) and phase-to-ground (B) quadrilateral characteristic element in ohm-phase domain

From above calculation result, zone  $2_{\text{minimum}}$  is larger than zone  $2_{\text{maximum}}$ . In this situation, zone  $2_{\text{minimum}}$  employs as zone 2 setting. All zones occupy same resistive range in their setting which calculates base on the maximum load transfer and the transmission track area which is passed by transmission line considerations. For phase-to-ground and phase-to-phase elements the resistive

range setting is 59.6  $\Omega$  and 42.3  $\Omega$ . Both resistive range is in ohm-loop domain, to convert them into ohm-phase domain equation (3.13) and (3.28) in Chapter 3 are used.

$$R_{ph-e} = \frac{R}{1 + \left( \frac{R_0 - R_1}{3.R_1} \right)} = \frac{59.6}{1 + 2.02} = 19.74 \Omega \quad (5.7)$$

$$R_{ph-ph} = \frac{R}{2} = \frac{42.3}{2} = 21.15 \Omega \quad (5.8)$$

According to the above calculation, the design quadrilateral characteristic both, for phase-to-phase and phase-to-ground elements are illustrated in figure 5.2.

### 5.3. Radial Single Circuit Case (Talang Kelapa – Betung)

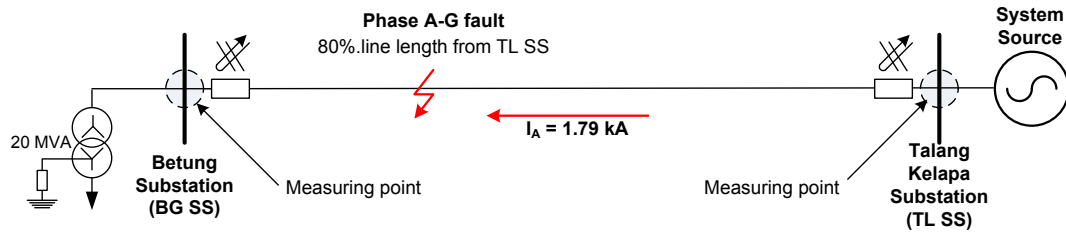


Figure 5.3. Radial single circuit case; Talang Kelapa – Betung.

In Betung – Talang Kelapa section, the infeed current occurs only in TL SS side because system source is connected to its bus, while in BG SS there is only load without source. This condition is perfect example to describe the fundamental impedance behavior in response to the arc (primary arc) fault phase A-to-ground and the effective tower footing impedance. The analysis of impedance and distance relay setting is focused in zone 1 protection area.

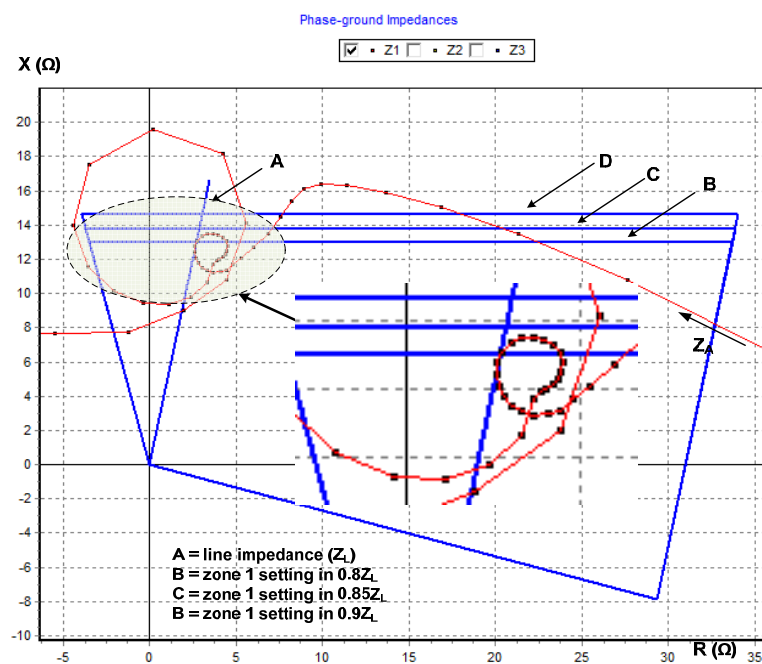


Figure 5.4. Fault impedance phase A ( $Z_A$ ) trajectory at TL side.

Figure 5.4 shows phase A fault impedance trajectory ( $Z_A$ ) and different zone 1 setting (80, 85 and 90 %  $Z_L$ ) in R – X plane at TL side when the fault occurs at 80% of the line length from TL SS (80%  $Z_L$ ). Each black dot in the  $Z_A$  path represents the sampling period 0.833 ms. In this fault condition, the  $Z_A$  trajectory comes into the line impedance  $Z_L$ , but it is slightly shifted to the right position of 80 %  $Z_L$  and a bit higher. This describes the effect of the primary arc impedance ( $Z_{ARC}$ ) and the effective tower footing impedance ( $Z_{EF}$ ). The total impedance  $Z_{ARC}$  and  $Z_{EF}$  as a result of impedance extraction in the fundamental frequency is more or less constant  $2.14 + j0.41 \Omega$ , as shown in figure 5.5. The secondary arc duration of this simulation is 0.031 s.

As stated earlier in this chapter, the distance relay will be operated if the impedance continuously inside the protection area at least 13.3 ms or 16 times sampling period. For zone 1 setting 80%. $Z_L$ , the  $Z_A$  trajectory is inside the protection area but not continuously 13.3 ms. In this situation, the distance relay does not operate supposedly, there is possibility it will operate after 40 ms. For zone 1 setting 85 and 90%. $Z_L$ , the  $Z_A$  trajectory is continuously inside the protection area for more than 13.3 ms. In this way, the distance relay will operate as expected in 13.3 ms, less than maximum permitted time 40 ms. Based on this case, it is recommended to increase zone 1 setting into 85 or 90%. Because of the current and voltage transformer error measurement as well as the impedance line error value consideration, 85%. $Z_L$  is a proper choice for zone 1 setting.

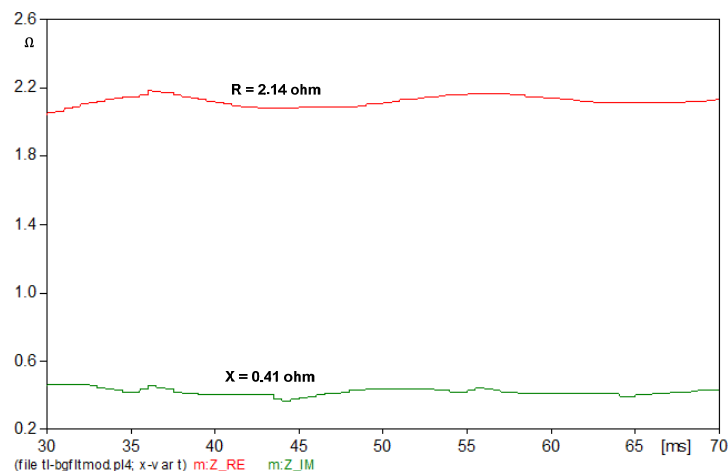


Figure 5.5. Total fault impedance ( $Z_{ARC}$  and  $Z_{EF}$ ) value

In BG SS side, the distance relay does not operate at all because there is no infeed source that will trigger the relay. The relay only feels phase A drop of voltage. The  $Z_A$  plotting and the distance relay setting are shown in figure 5.6. There, it is apparent that  $Z_A$  trajectory is far away at left position of the setting. To overcome this situation, the weak infeed signaling scheme is implemented. This scheme incorporates an undervoltage element and the signal receive element which is sent from the distance relay of zone 1 area in TL side, as explained before in Chapter 3 section 3.1.6.5. When the voltage is below the undervoltage setting and at the same time signal

from opposite distance relay is received, the trip command is issued to the circuit breaker and the SPAR operation is triggered.

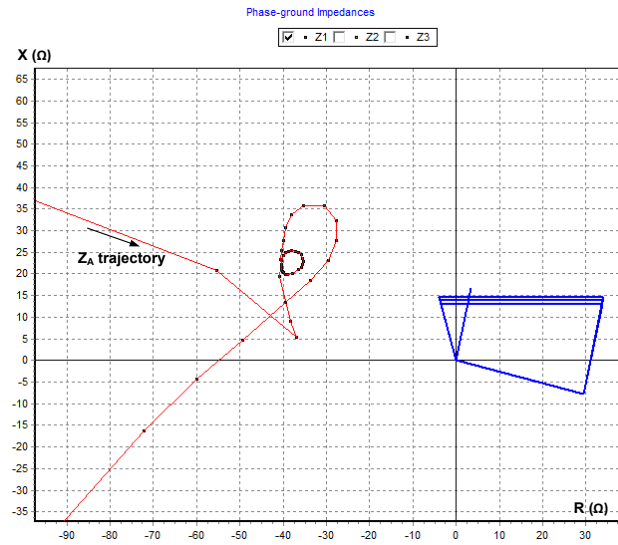


Figure 5.6. Fault impedance phase A ( $Z_A$ ) trajectory at BG side.

Two points obtained in this case are:

- The impedance range for zone 1 setting is increased into  $85\% \cdot Z_L$ .
- In the case of single line circuit without source infeed, the weak infeed signaling scheme is needed to trigger the distance relay and SPAR operation there.

#### 5.4. Radial Double Circuit Case (Keramasan – Mariana)

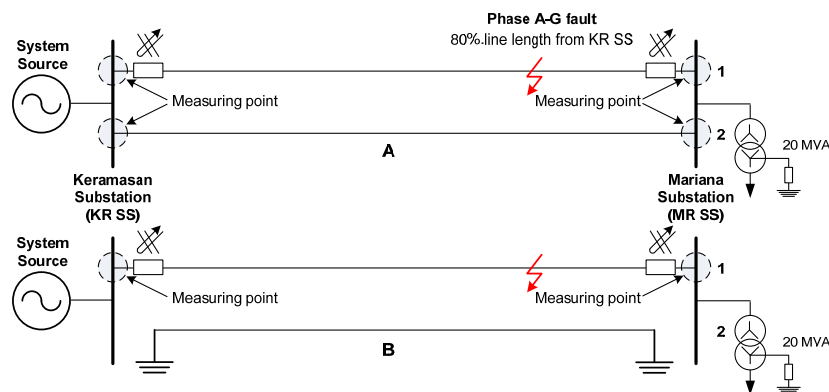


Figure 5.7. Radial double circuit case; Keramasan – Mariana. Double circuit operation (A) and single circuit operation (B).

Keramasan – Mariana section is normally operated with double circuit. At this section, the system source is in KR SS side. While in MR SS side, there is only a power transformer load without source. Two different fault conditions are simulated to see the effect of the total fault impedance ( $Z_T = Z_{ARC} + Z_{EF}$ ) at single infeed, double infeed as well as parallel line mutual inductive coupling to the distance relay performances.

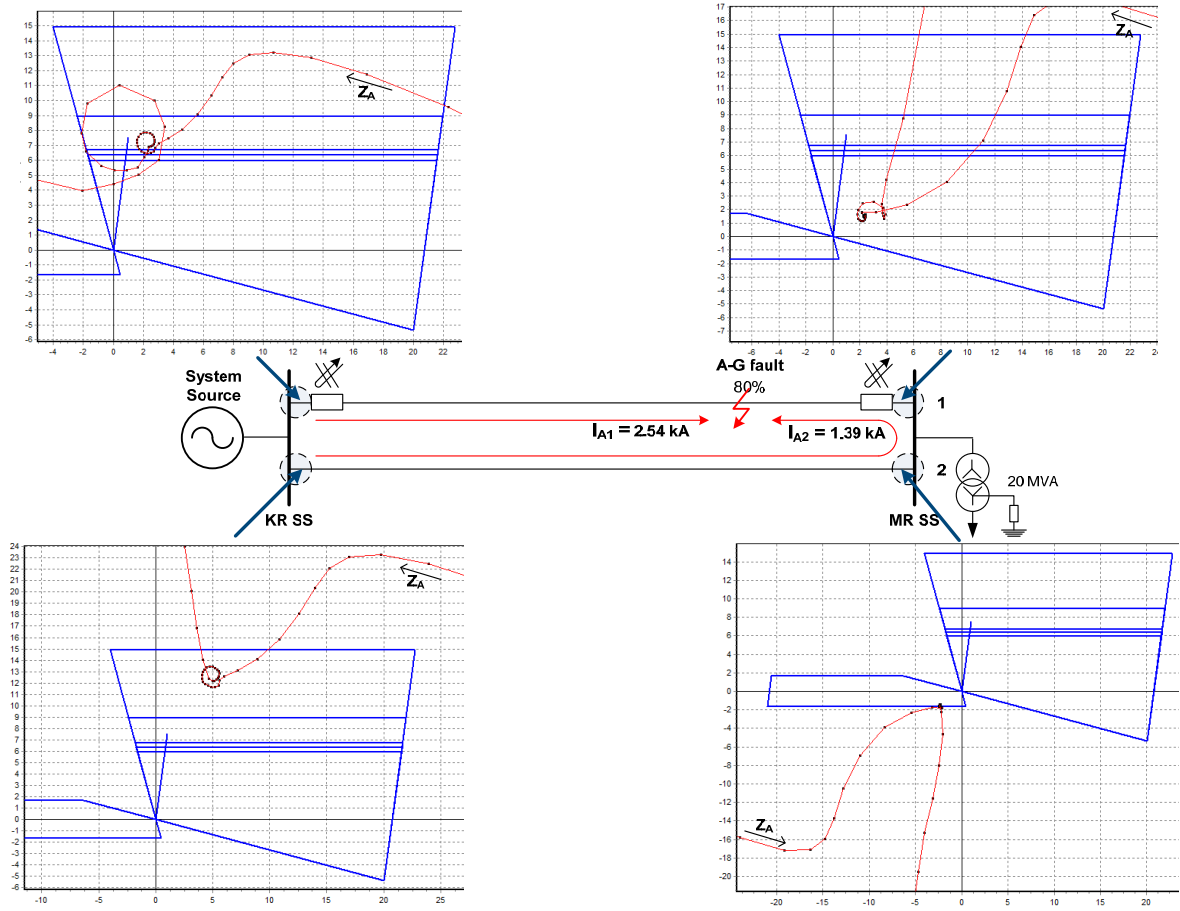


Figure 5.8. Fault impedance phase A ( $Z_A$ ) trajectory at each side of the distance relay; case A.

In the first case (case A), two circuits are operated with fault location at line 1, 80 % from KR SS. The  $Z_A$  trajectory and the distance relay setting in R – X plane at each line side responses to this fault are shown in figure 5.8. In line 2, the KR distance relay sees the fault in front of its position at zone 3 protection area. Whereas the MR distance relay sees the fault behind its position at zone 4 protection area. Both KR side and MR side distance relays at line 2 are used as back up protection when the MR distance relay at line 1 fails to operate.

In line 1, both KR and MR  $Z_A$  trajectories do not come exactly in the line impedance position as described in their R – X plane. The KR  $Z_A$  trajectory is at the right position and higher than  $80\%.Z_L$ . The MR  $Z_A$  trajectory is at the right position of  $20\%.Z_L$ . Those occur because of two reasons:

1. The infeed current from the opposite side of the line (KR side 2.54 kA and MR side 1.39 kA) to  $Z_T$  as explained in section 3.1.5.1. For example in the KR distance relay point of view, the infeed current contribution from MR side increases the measured impedance by the relay and vice versa.
2. The mutual zero sequence impedance  $Z_{0M}$  and the zero sequence current which flows in line 2 (1.39 kA) as explained in section 3.1.5.4.

While the effect of reason number 1 is apparently seen in both KR and MR  $Z_A$  trajectories at line 1, the effect of reason number 2 is more clearly shown in the KR  $Z_A$  trajectory. The short circuit current  $I_{A2}$  in line 2, which has the same direction with the short circuit current  $I_{A1}$ , makes the measuring error in a positive value and increases the measuring impedance. Underreach condition occurs. Because of this effect, the KR distance relay in line 1 senses the fault in zone 2, outside zone 1 protection area. In this situation, increasing zone 1 protection area is not a good solution. There are two possible solutions to cope this underreach condition. Firstly, by using  $I_{A2}$  that flows in line 2 as an analog input to the KR distance relay in line 1. This current is used to compensate the measurement error as explained in 3.1.5.4. Secondly, Permissive Underreach Transfer Trip (PUTT) signaling scheme implementation. In the PUTT scheme, as explained in section 3.1.6.1., when the distance relay detects the fault at zone 2 protection area and at the same time receives signal which is sent by the distance relay zone 1 area from the opposite side, the delay time zone 2 tripping will be accelerated to trip instantaneously and triggered SPAR operation.

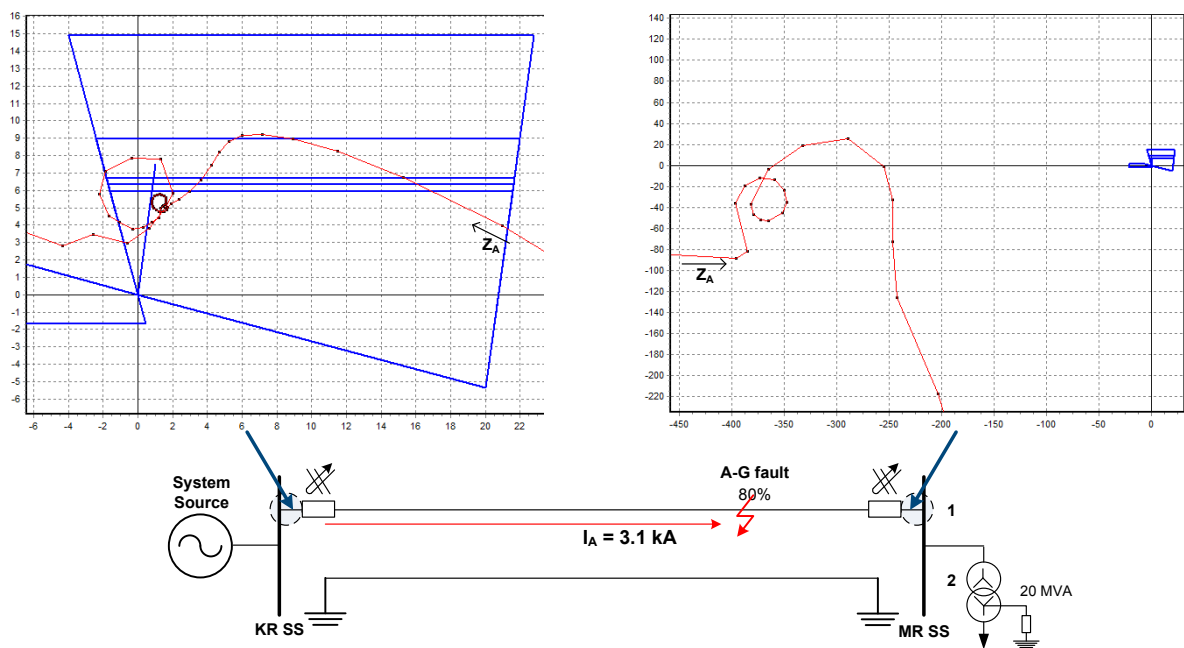


Figure 5.9. Fault impedance phase A ( $Z_A$ ) trajectory at each side of the distance relay; case B.

Another case (case B) is simulated to see how far the infeed current and mutual zero sequence impedance affects the KR – MR line section. In case B, the fault location is still 80 % from KR SS. The line configuration is different now, line 2 is not operated and grounded at each line side. With this configuration, the infeed current and the mutual zero sequence impedance effects are omitted. The  $Z_A$  trajectories in both sides are shown in figure 5.9. From the  $Z_A$  trajectory in KR side, it is clearly shown that the underreach condition vanishes and the measured total fault resistance decreases. Those situations confirm the infeed current and the mutual zero sequence effects.



Case A and B result comparison also asserts dominant resistive identity of  $Z_T$ . Figure 5.10 shows the fundamental frequency  $Z_T$  value. In both cases, the  $Z_T$  value are same  $1.77 + j0.37 \Omega$ . If the  $Z_T$  value in section 5.3 and this section is compared, although built with same arc parameters both  $Z_T$  are different in value. This occurs because the short circuit arcing current is different in both cases. In section 5.3, the short circuit current is 1.79 kA and here is 3.1 kA. It can be concluded that the higher the short circuit arcing current, the lower the fundamental arc impedance. The secondary arc duration for both case A and B are 0.031 and 0.021 s.

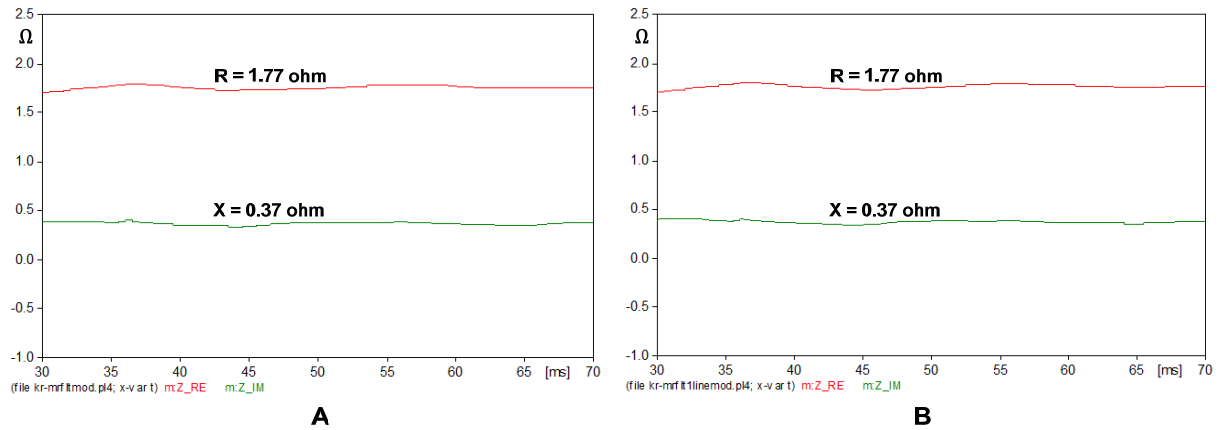


Figure 5.10. Total fault impedance ( $Z_{ARC}$  and  $Z_{EF}$ ) value

Several points obtained from case A and B are:

- Although the system source is only at one section side, the parallel circuit configuration provides a path for the short circuit current to reach the opposite side. This current causes the infeed current and the mutual zero sequence effects.
- Input short circuit current from another line or the PUTT signaling scheme are best ways to overcome underreaching condition caused by the mutual zero sequence effect.
- The total impedance fault  $Z_T$  is same for case A and case B, because at both cases the total short circuit current flows to the arc is same 3.1 kA.
- The arc faults with same arc parameters have fundamental arc impedance that inversely proportional in relation to the short circuit current ( $i_{arc}$ ).

### 5.5. Non-radial Double Source Double Circuit Case (Prabumulih – Bukit Asam)

The last case is the arc fault in non-radial double circuit with double system source. The arc fault is located in express feeder Prabumulih – Bukit Asam, 80 % and 95 % of the line length from PB SS, as illustrated in figure 5.11. This section is surrounded by two big power plants (2x52 MW in GM SS and 4x65 MW in BK SS) and three system sources. Within this situation, a high short circuit current will be expected in the simulation.

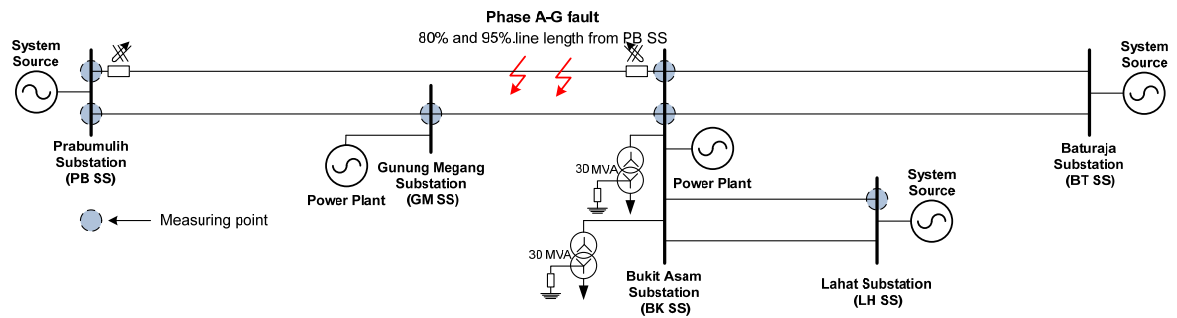


Figure 5.11. Non-radial double source double circuit case; Prabumulih – Bukit Asam.

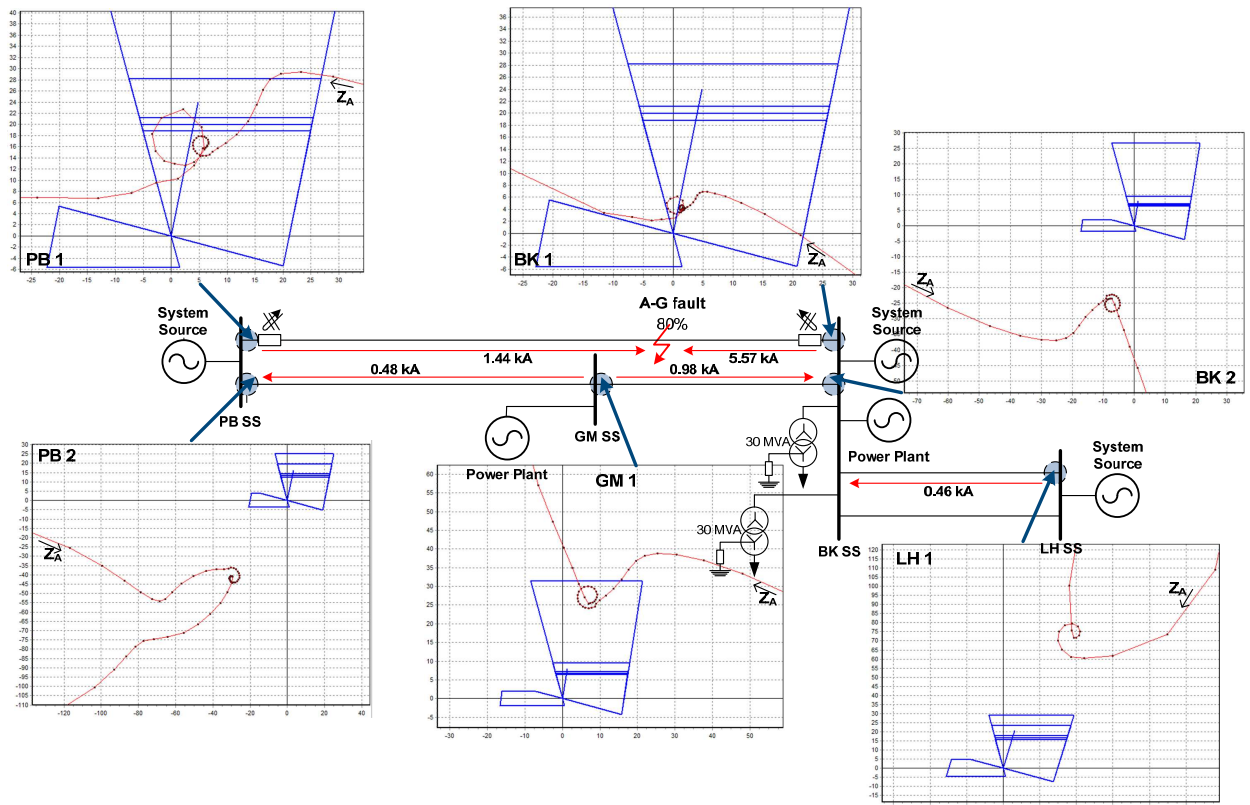


Figure 5.12. Fault impedance phase A ( $Z_A$ ) trajectory at each side of the distance relay; 80% from PB SS

R – X planes that consist of  $Z_A$  trajectory and distance relay setting at each measuring point for 80 % fault location are shown in figure above. At PB SS side, the PB 2 distance relay detects the fault behind its protection area because the short circuit current (0.48 kA) in this line flows to the measuring point. This short circuit current also influences the measured impedance in the PB 1 distance relay. The 0.48 kA short circuit current, which flows in the opposite direction of the 1.44 kA short circuit current, causes the measuring error to a negative value. This makes the total measured reactance in the PB 1 distance relay reduced. This situation does not interfere the PB 1 distance relay operating time because the  $Z_A$  trajectory is still inside zone 1 protection area. In other situation where the fault location is more than zone 1 reactance range (more than 80 %), there is a possibility that overreach condition will occur and influence the distance relay operating

time. Additional analog input current from the parallel line (PB – GM line) to compensate mutual zero sequence effect (in the PB 2 distance relay) is the best way to cope with this situation.

Now the analysis is focused to the BK 1 distance relay. As generally known, there are total of ten possible faults that can be seen by the relay. They are A – G, B – G, C – G, A – B, A – C, B – C, A – B – G, A – C – G, B – C – G and A – B – C. When a disturbance occurs, the distance relay will measure all those related impedances, and then decide which kind of fault occurred in the network. At figure 5.12 fault situation, the BK 1 distance relay does not only sense the fault in phase A – G, but also in phase A – B and A – C as shown in figure 5.13.

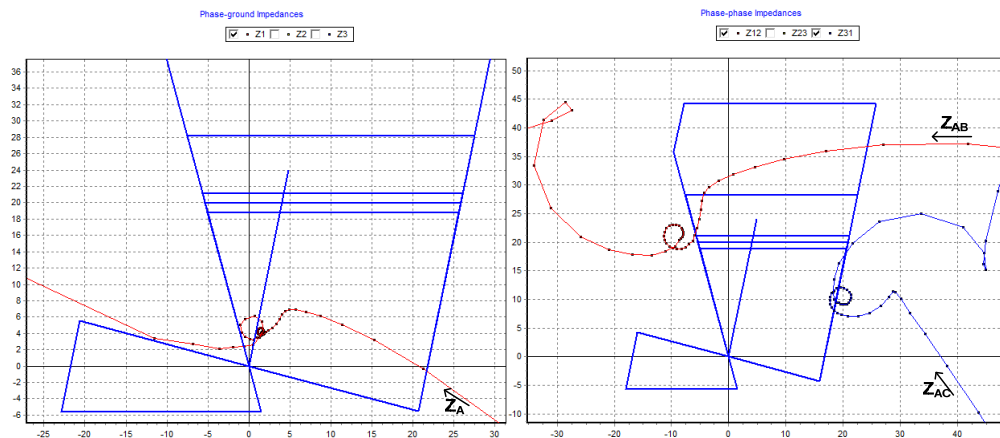


Figure 5.13.  $Z_A$ ,  $Z_{AB}$  and  $Z_{AC}$  trajectories in phase-to-ground and phase-to-phase elements; 80% from PB SS.

In the above figure, it is clearly shown that high short circuit current in phase A at BK 1 measuring point (5.57 kA) causes the measured impedance  $Z_{AB}$  and  $Z_{AC}$  to approach the phase-to-phase element protection area. In this situation, the  $Z_{AC}$  measured impedance is less than 13.3 ms inside the zone 1 protection area. Accordingly, the distance relay does not declare that a fault in phase A – B or A – C occur in the network.

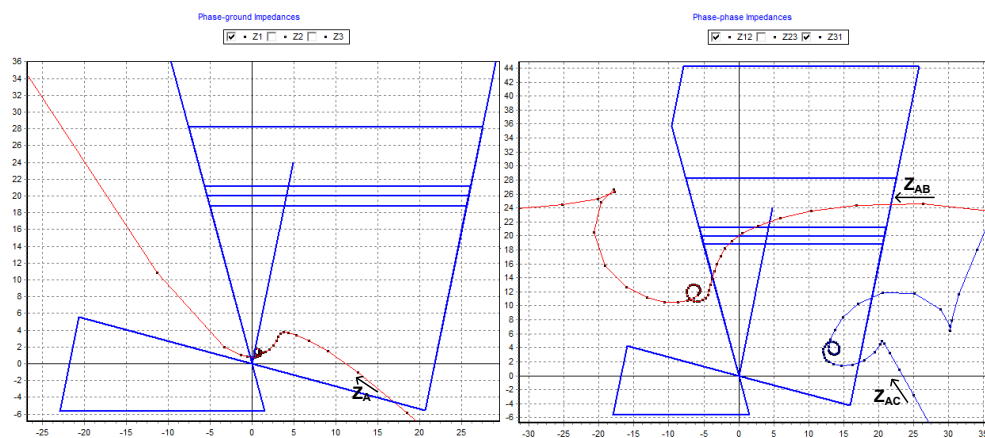


Figure 5.14.  $Z_A$ ,  $Z_{AB}$  and  $Z_{AC}$  trajectories in phase-to-ground and phase-to-phase elements; 95% from PB SS.

On other simulation, the fault point is located 95% from PB SS approaching BK SS. The phase A short circuit current at BK 1 measuring point becomes 8.26 kA. The  $Z_A$ ,  $Z_{AB}$  and  $Z_{AC}$

measured impedances are shown in figure 5.13. The  $Z_A$  measured impedance approaches to the origin point whereas the  $Z_{AB}$  and  $Z_{AC}$  go deeper in the zone 1 phase-to-phase protection area. The  $Z_{AC}$  trajectory is inside the protection area more than 13.3 ms. Consequently, the BK 1 distance relay declares a fault in phase A – G and phase A – C. As mentioned earlier in section 5.1, the SPAR setting operation in South Sumatera system is triggered by zone 1 phase-to-ground element and signaling scheme elements. For this fault condition, the distance relay also declares phase A – C fault in the network. Therefore, the SPAR operation is prohibited. At the end, only the PB 1 circuit breaker will be reclosed and the BK 1 circuit breaker will be tripped 3 poles.

In order to avoid above situation, the phase-to-phase resistive range setting should be evaluated, especially near strong source area where high phase to ground short circuit current is expected. The BK 1 zone 1 resistive range is reduced into  $10.5 \Omega$  in ohm-phase domain. With this new setting, instantaneous zone 1 phase-to-phase tripping (phase A – C) will be avoided as shown in figure below.

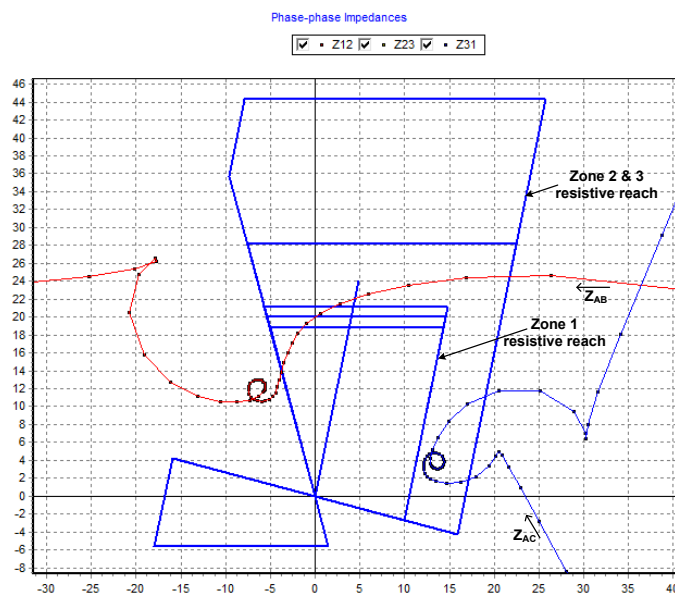


Figure 5.15.  $Z_{AB}$  and  $Z_{AC}$  trajectories with reduced zone 1 resistive range setting; 95% from PB SS.

The secondary arc duration for 80 % and 95 % fault location are 0.223 and 0.214 s.

From this case, it can be concluded that:

- In the parallel line, if the current in both lines flows in the opposite direction, then the distance relay will measure lower total reactance. Input zero sequence current from each parallel line to the distance relay is necessary to avoid this situation.
- The fault arc (phase A-G) near the strong source bus results in high short circuit current that attracts  $Z_{AB}$  and  $Z_{AC}$  trajectories inside phase-to-phase protection element. Therefore, resistive range phase-to-phase element should be evaluated in this area.

## VI. CONCLUSION AND RECOMMENDATION

### 6.1. Conclusion

Conclusions of this study consist of three major parts that have been discussed in detail in the previous chapters. They are:

#### A. Design quadrilateral characteristic

1. Protection engineers should be aware with the distance relay and the testing equipment characteristics domain when they want to implement their setting calculations or to do distance relay testing.
2. In phase-to-phase setting element, the relationships between ohm-loop and ohm-phase domain are:

$$Z_{ml} = 2 \times Z_{mp} \quad (6.1)$$

$$X_{ml} = 2 \times X_{mp} \quad (6.2)$$

$$R_{ml} = 2 \times R_{mp} ; R_{ml} = 2 \cdot R_1 + R_f ; R_{mp} = R_1 + \frac{R_f}{2} \quad (6.3)$$

3. In phase-to-ground setting element, the relationships between ohm-loop and ohm-phase domain are:

$$Z_{ml} = (1 + K_N) \cdot Z_{mp} \quad (6.4)$$

$$X_{ml} = \left( 1 + \frac{X_N}{X_1} \right) \cdot X_{mp} \quad (6.5)$$

$$R_{ml} = \left( 1 + \frac{R_N}{R_1} \right) \cdot R_{mp} ; R_{ml} = R_1 \cdot \left( 1 + \frac{R_N}{R_1} \right) + R_f ; R_{mp} = R_1 + \frac{R_f}{1 + \frac{R_N}{R_1}} \quad (6.6)$$

#### B. Arc model and parameters in 150 kV system

1. The arc model developed using MODELS language fits with the actual fault arc situation developed by synthetic power arc test.
2. For the fundamental frequency, it is proven that the arc impedance has also inductive behavior and is more or less constant at its primary arc stage.
3. The fault arc occurrences which have been investigated do not have reignition condition in its secondary arc state. It is in agreement with the developed arc model where subsequent dielectric reignition is not taken into account and the secondary arc length has linear relationship in time.

4. Correlation between  $I_0$  versus  $u$  and  $I_0$  versus  $r$  for different voltage levels as proposed in [8] is only valid for arc occurrence in string insulator which is equipped with arcing horn. While for arc occurrence in string insulator without arcing horn those relationships cannot be used as a reference.
5. The arc parameters in 150 kV voltage level based on two cases of arc occurrences in South Sumatera system are:

Table 6.1. Arc parameters, fault arc 15 February 2007 and 3 March 2006

ARC PARAMETER	CASE 1 LINE 1	CASE 1 LINE 2	CASE 2
String insulator	Type A	Type A	Type B
$I_0$ (cm)	120	120	215
$u$ (kV)	1.38	1.38	0.9
$r$ (m $\Omega$ )	53	53	40
$\tau_0$ (ms)	0.5	0.5	0.9
$v_l$ (cm/ms)	45	35	22
$v_r$ (ms/cm)	0.833	0.833	0.466
final arc length (cm)	294.4	333.7	1407.5
primary arc duration (ms)	88.98	89.1	58.6
secondary arc duration (ms)	30.63	50.88	251.5

6. The relationship between the arc parameters and the arc voltage are: the characteristic voltage and resistance ( $u$  and  $r$ ) are proportional to the primary and secondary arc voltage magnitude; the time constant ( $\tau_0$ ) parameter is proportional to the secondary arc duration; the speed of arc elongation ( $v_l$ ) is proportional to the secondary arc voltage magnitude but inversely proportional with the secondary arc duration.
  7. The arc current ( $i_{arc}$ ) is inversely proportional to the primary arc impedance in the fundamental frequency.
  8. The string insulator without arcing horn has higher secondary arc duration (0.2 – 0.3 s) compare with the string insulator which is equipped with arcing horn (less than 0.1 s).
  9. Although the secondary arc parameter is impossible to be estimated, 22 cm/s seems reasonable to represent speed of arc elongation ( $v_l$ ). In this condition, dead time SPAR setting 0.5 – 0.7 s are more than sufficient to wait until the arc eventually extinguished.
- C. Existing setting distance protection evaluation
1. It is better to increase zone 1 impedance range setting into 85 % of  $Z_L$  in order to increase zone 1 reactance range coverage.
  2. At weak infeed source side in single line circuit configuration, the weak infeed signaling scheme is a must to provide tripping and SPAR operation there.
  3. The infeed current from opposite side of the distance relay tends to increase the measured resistance and moves the measured impedance to the right position of  $Z_L$  in R – X plane.

4. The zero-sequence current which flows in the opposite direction in the parallel line tends to decrease the measured reactance and moves the measured impedance lower than the fault point in  $R-X$  plane. The zero-sequence compensation factor which occupies input zero current from the parallel line is a way out for this situation.
5. The zero-sequence current which flows in the same direction in the parallel line tends to increase the measured reactance and moves the measured impedance higher than the fault point in  $R-X$  plane. The zero-sequence compensation factor or PUTT signaling scheme are solutions at this situation.
6. The fault arc near the strong source bus results in high phase-to-ground short circuit current that attracts  $Z_{AB}$  and  $Z_{AC}$  trajectories inside the phase-to-phase protection element. Therefore, resistive range phase-to-phase element should be evaluated by simulating fault arc incident near the bus.

## 6.2. Recommendation

It is recommended to do further study about high fault arc resistance behavior and its impact on the performance of distance protection. Hence, the resistive range setting for phase-to-phase and phase-to-ground elements can be coordinated in such a way that they will embrace both, the low fault and the high fault resistance.

## REFERENCE

- [1] Dube, L; Bonfanti, I *"MODELS: A New Simulation Tool in the EMTP"* European Transactions on Electrical Power, ETEP, vol. 2, no. 1, pp. 45-50, January/February 1992.
- [2] Kreuger, F.H *"Industrial High Voltage: Electric Fields, Dielectrics and Constructions"* Delft University Press, 1992.
- [3] Kreuger, F.H *"Industrial High Voltage: Coordinating, Measuring and Testing"* Delft University Press, 1992.
- [4] Goda, Y; Iwata, M; Ikeda, K; Tanaka, S *"Arc Voltage Characteristic of High Current Fault Arcs in Long Gaps"* IEEE Transaction on Power Delivery, vol. 15, no. 2, pp. 791-795, April 2000.
- [5] Johns, A.T; Salman, S.K; *"Digital Protection for Power System"* Peter Peregrinus Ltd, 1995.
- [6] Kizilcay, M *"Evaluation of Existing Secondary Arc Models"* EEUG Meeting Budapest, 1996.
- [7] Kizilcay, M; Dube, L *"Post Processing Measured Transient Data using MODELS in the ATP-EMTP"* EEUG News, May 1997.
- [8] Kizilcay, M; Koch, K.H *"Numerical Fault Arc Simulation Based on Power Arc Tests"* European Transactions on Electrical Power, ETEP, vol. 4, no. 3, pp. 177-185, May/June 1994.
- [9] Kizilcay, M; Pniok, T *"Digital Simulation of Fault Arcs in Power Systems"* European Transactions on Electrical Power, ETEP, vol. 1, no. 1, pp. 55-60, January/February 1991.
- [10] Phadke, A.G; Thorp, J.S *"Numerical Distance Protection: Principles and Applications"* Research Studies Press Ltd and John Wiley & Sons Inc, 1988.
- [11] Popov, M; van der Sluis, L; Paap, G.C *"Investigation of the Circuit Breaker Reignition Overvoltages Caused by No-load Transformer Switching Surges"* European Transactions on Electrical Power, ETEP, vol. 11, no. 6, pp. 413-422, November/December 2001.
- [12] Terzija, V; Koglin, H-J *"On the Modeling of Long Arc in Still Air and Arc Resistance Calculation"* IEEE Transaction on Power Delivery, vol. 19, no. 3, pp. 1012-1017, July 2004.
- [13] Van der Sluis, L *"Transient in Power Systems"* John Wiley & Sons Ltd, 2001.



- [14] Watson, N; Arrillaga, J *"Power Systems Electromagnetic Transients Simulation"* The Institution of Electrical Engineers, 2003.
- [15] Ziegler, G *"Numerical Distance Protection: Principles and Applications"* Siemens AG, 1999.
- [16] "Network Protection and Automation" Areva, 2002.
- [17] "Technical Reference Manual: REL 511-C1" ABB, 2003.

## Acknowledgement

Thanks and praise to God Almighty who makes everything possible to me and always guides my way. This thesis research mainly depends on individual effort, but I owe much gratitude to persons who participate in this research. First, I would like to thank my daily supervisor, Dr. ir. Marjan Popov for guiding me well during my project and giving me freedom to be more creative exploring this research. Thanks for the discussions and helped dealing with EMTP software. Many thanks to other thesis committee members: Prof. ir. L. van der Sluis, Prof. Dr. J. J. Smit and Prof. Dr. V. Terzija for taking effort to read and evaluate my thesis report. I also remember and grateful to “Guru-guru” senior protection specialists in Perusahaan Listrik Negara (PLN), who introduced and taught me about power system protection theoretically and practically.

Two years achieving master degree in TU Delft was a wonderful time for me. Special thanks to PLN for providing me great opportunity to study in Delft. To my classmates and Indonesian friends in Delft (Firman, Jarot, Albert, Himmel, Didik, Credo and others), thanks for the friendship. I will miss the moments when we learned together, made jokes each other and did incredible journey. Remembering my father who passed away 5 years ago, thanks for your encouraging advice, I really experience what you said now. To my mother and other family members who I believe always mention my name in their prayers, thanks for your love and support.

Handy Wihartady  
(Delft, 9 June 2009)